Functional mechanics of concavo-convex articulations and neurocentral sutures in the vertebral column of sauropod dinosaurs

by

John Alexander Fronimos

A dissertation submitted in partial fulfillment
of the requirements for the degree of
Doctor of Philosophy
(Geology)
in the University of Michigan
2016

Doctoral Committee:

Associate Professor Jeffrey A. Wilson, Chair
Professor Tomasz K. Baumiller
Professor Daniel C. Fisher
Professor Philip D. Gingerich
Professor Laura M. MacLatchy

ACKNOWLEDGMENTS

This dissertation would not have been possible without the opportunities and guidance provided by my advisor, Jeff Wilson. I thank Jeff for challenging me to operate outside my comfort zone in asking new questions, applying new methods, and traveling the world to visit museum collections. Tom Baumiller provided invaluable insights on biomechanics and experimental approaches, particularly with regard to Chapter 3. I also thank my other dissertation committee members, Dan Fisher, Philip Gingerich, and Laura MacLatchy, for their feedback and conversation. Bill Sanders has been a source of rewarding discussion and instruction in molding and casting, specimen conservation, and many other techniques. Adam Rountrey, Linda Garcia, and Cindy Stauch were indispensable for the logistics of my work and did not object to receiving an alligator in the mail. I have learned a great deal about visual design from Carol Abraczinskas, which is reflected throughout the figures of this dissertation. Chapters 2 and 3 were submitted to Paleobiology, the former co-authored with Jeff Wilson, the latter with Jeff Wilson and Tom Baumiller. Chapter 4 was submitted to Ameghiniana with Jeff Wilson as co-author.

Each phase of my research depended upon the advice and contributions of many individuals. Allan Woodward, Cameron Carter, and Justin Touchstone (Florida Fish and Wildlife Research Institute) kindly donated the alligator used in Chapter 2. Rex Miller, Tony Pease, Nate Nelson, and Meg Willis-Redfern, RT (Michigan State University College of Veterinary Medicine, Department of Radiology) conducted CT scans and provided data processing. Shawn

O’Grady and Stephanie O’Malley (UM 3D Lab) were deeply knowledgeable and helpful in working with digital models and 3D printing. Numerous individuals assisted me on my travels and in museum collections, including, but not limited to: Matt Lamanna, Amy Henrici, Dan Pickering, Alan Tabrum, and Norm Wuerthele (Carnegie Museum of Natural History); Bill Simpson and Alan Resetar (Field Museum of Natural History); José Manuel Marín Ferrer and Ainara Rodríguez (Museo Paleontológico de Elche); Diogenes Campos, Rodrigo Machado, and Irma Yamamoto (Museu de Ciências da Terra); Daniela Schwarz and Thomas Schossleitner (Museum für Naturkunde); Matt Carrano and Mark Florence (National Museum of Natural History, Smithsonian Institution); Paul Sereno and Bob Masek (University of Chicago); and Greg Schneider (University of Michigan Museum of Zoology). M. Langer (Universidade de São Paulo, Riberão Preto) provided JAW with access to *Saturnalia*. Travel to South America was made possible by a grant from STEPPE, a research consortium that is supported by the National Science Foundation. I also thank Francisco “Pachy” Ortega and Pedro Mocho for the opportunity to examine specimens under study, and Hussam Zaher for advice on traveling to Brazil. Chris Brochu, Thiago Marinho, Julia Molnar, and Steve Salisbury provided discussion and insight into crocodylomorph diversity and evolution. Advice on data analysis was provided by Michael Doube and Miriam Zelditch. Literature access was possible thanks to the tireless efforts of the UM Library staff, especially the Interlibrary Loan service and the Buhr Remote Shelving Facility, as well as the HathiTrust Digital Library and the Biodiversity Heritage Library. I thank Will Downs (He et al. 1998) and Gerhard Meijer (Janensch 1950) for translations made available through the Polyglot Paleontologist website (http://www.paleoglot.org). Color schemes used in figures were developed with ColorBrewer v2.0.

I am deeply indebted to the UM Department of Earth and Environmental Sciences for accepting me as a graduate student and for all the support I have received, both material and intellectual. Anne Hudon, Brandi Berg, and Nancy Kingsbury have provided bottomless reserves of patience and kindness in making sure I met all degree requirements and was reimbursed for all expenses. Funding from the Scott Turner Award and the Rackham Graduate Student Research Grant made possible many of the analyses performed. I have enjoyed the opportunity to teach for Sarah Aciego, Tom Baumiller, Greg Dick, John Geissman, Jamie Gleason, Kacey Lohmann, Nathan Niemi, Nathan Sheldon, Rob van der Voo, and Jeff Wilson, as well as the support of Chris Malvica and everyone at Camp Davis (thanks for the great meals!). The experience was enriched by many excellent students, and I owe special thanks to my volunteer helpers Sydney Foote and Abijah Simon. I can't wait to see the great things you all accomplish.

In my time at Michigan, I have been privileged to be part of a vibrant and supportive student community. I am grateful to my fellow Wilson Lab members, Lucas Joel, Emile Moacdieh, Keegan Melstrom, Taryn O'Connell, and David Hunt, as well as my predecessors Mike D'Emic, Takehito Ikejiri, and John Whitlock, for their advice and conversation. I shall be watching your careers with great interest. My annex friends Tara Smiley, Katie Loughney, and Sole Domingo provided a lot of support, conversation, and laughs; I wish you all the best. To Meg Veitch, my de facto biomechanics lab mate, thanks for maintaining a presence. I thank my other friends in paleontology, Mike Cherney, Joe El Adli, Julia Fahlke, Kris Purens, and Valerie Syverson, for so much over the years. To all my friends in Earth and Environmental Sciences, past and present, you have made my years in Ann Arbor truly rewarding, and I will always be grateful for the opportunity to get to know you.

Finally, and most importantly, I dedicate this work to my family, whose love, support, and encouragement make everything possible. Your reward for listening to me talk about dinosaurs all this time is more of the same, forever.

TABLE OF CONTENTS

LIST OF FIGURES

LIST OF TABLES

ABSTRACT

Sauropod dinosaurs achieved the largest body sizes and the most elongate necks and tails of any terrestrial vertebrate. Their necks and tails were held aloft as cantilevers, beams supported at one end and free at the other. Synovial joints between vertebrae provide mobility, and synchondrosial joints within vertebrae facilitate growth. These requirements come at a cost, as the joints are potential sites of dislocation, with deleterious consequences for the living animal. Morphological specializations of sauropod inter- and intravertebral joints provided stability without compromising other functional demands.

Sauropod intervertebral joints were characterized by concavo-convex morphology, which has been hypothesized to confer greater flexibility or to stabilize joints against dislocation by translation. Examination of joint mobility in an extant analog, *Alligator*, reveals that concavo-convex joints do not confer greater flexibility than do planar joints, nor do they inherently limit mobility. Convexity is greatest in regions of the greatest shear, consistent with a stabilizing function.

Sauropod intervertebral joints have a consistent polarity in which the concave articular surface faces the body (i.e., cervical opisthocoely, caudal procoely). Physical modeling reveals that this polarity is more stable than its opposite because it inhibits the convex articulation from rotating out of joint. The advantage of the sauropod polarity is enhanced by greater joint mobility, distal loading, and mechanically advantageous ligament insertion sites. This provided stabilization without compromising other functions.

The intravertebral (i.e., neurocentral) joints of archosaurs such as sauropods remain unfused to a later age than in most other vertebrates, permitting rapid, sustained growth to large body sizes. The greater susceptibility of the joints to dislocation compared to fused bone may be compensated for by complex, interdigitated sutures that resist compression, rotation, and translation. In the sauropod *Spinophorosaurus*, variation in sutural complexity along the vertebral column is consistent with the expected stress distribution. Large-scale morphological structures in the sutures are oriented to resist specific regional stresses.

The integration of fossil data with studies of extant taxa and model experiments provides a means to answer functional questions about extinct organisms. The results offer insights into skeletal biomechanics that are widely applicable to other vertebrates.

CHAPTER 1

INTRODUCTION

The axial skeleton of Diplodocus *is a marvel of construction.*
It is a mechanical triumph of great size, lightness, and strength.
– H. F. Osborn, 1899

Sauropod dinosaurs were walking backbones,
as anyone who has collected a skeleton in the field can attest.
– J. A. Wilson and K. Curry Rogers, 2012

Sauropod dinosaurs are among the most immediately recognizable extinct organisms by virtue of their distinctive body plan, a long neck and tail coupled with an elephantine frame. To the public, sauropods are often symbols of obsolescence, their gigantism contrasting sharply with the small and dynamic mammals that succeeded them. This widespread conception regards the sauropod body plan itself as intrinsically maladaptive and destined for extinction. The evidence in the fossil record reveals a quite different story, one of diversity, vitality, and biological innovation. Sauropods first appeared in the Late Triassic (Buffetaut et al. 2000) and soon became the dominant megaherbivores in most terrestrial ecosystems, a role not relinquished until their extinction at the end of the Cretaceous. The length of their tenure on Earth exceeds 135 Ma, more than twice the interval since their extinction. Sauropods were widespread, occurring on every continent (Weishampel et al. 2004; Cerda et al. 2012), and diverse, numbering more than 100 genera when last tallied a decade ago (Upchurch et al. 2004) and attaining a standing diversity of 24 genera in the Late Jurassic (Kimmeridgian-Tithonian; Mannion et al. 2011). The

rate of description of new species shows no sign of declining (D'Emic 2012), suggesting that many more species remain to be discovered. The story of sauropods is not a cautionary tale; it is a story of the supreme adaptability of the vertebrate form.

Sauropod gigantism presents an informative case study in how the vertebrate skeleton accommodates extreme stress and how the need for strength and stability is balanced against potentially competing functional demands. Sauropods achieved the largest body sizes (Alexander 1989) and longest necks (Taylor and Wedel 2013) of any terrestrial vertebrate. Some species are estimated to have reached masses as high as 50 tons, and even the smallest exceeded a ton in adult mass (Carrano 2005). Their long necks and tails were held aloft (Coombs 1975), as indicated by the lack of tail drag marks in fossil trackways (e.g., Bird 1941), and so functioned as cantilevers, beams supported at one end and free at the other. Anatomically, these beams were segmented into bony elements, the vertebrae, which were joined by soft tissues such as ligaments, muscle, and cartilage. Joints between vertebrae are necessary for mobility, and joints within vertebrae permit growth (Vital et al. 1989). However, these requirements come at a cost, as the joints also represent potential points of failure by dislocation, which has deleterious consequences for the living animal.

This dissertation considers several morphological features of sauropod vertebrae that may have served to stabilize the intervertebral and intravertebral joints, facilitating the evolution of long, heavy necks and tails. Functional hypotheses concerning extinct organisms, such as those discussed here, are commonly generated by analogy to modern taxa or to other types of mechanical systems. It is not possible to test functional hypotheses in vivo for extinct taxa. Experimentation is nonetheless possible using data from a variety of sources, including analogous taxa, physical or computational models, phylogeny, ichnology, and taphonomy

(Plotnick and Baumiller 2000). The underlying assumptions are uniformitarian: if physical laws operate consistently across time and space, then mechanical comparisons are possible among organisms and between organisms and man-made machines. The intent of such paleobiomechanical studies is not to identify the precise function of a structure in the living organism, nor is it to identify a particular solution to a mechanical problem as optimal. Instead, the objective is to determine whether a structure has the faculty or capability to perform a proposed function (Fisher 1985; Plotnick and Baumiller 2000). Additionally, competing functional hypotheses that make different predictions can be compared to determine which is best supported by data from the chosen study system; this approach also carries no assumptions regarding optimality (Fisher 1985). The biomechanical investigations described here use a variety of sources of data, including fossil specimens, extant analog taxa, and physical models, to test hypotheses concerning the function of vertebral structures in sauropods. The results illuminate how sauropods were able to support elongated necks and tails at very large body sizes, and also provide a framework for understanding the functional significance of joint morphology in other vertebrates, including humans.

Chapters 2 and 3 investigate the mechanics of the joints between vertebral centra in sauropods. Ancestrally, the intercentral joints of sauropodomorph dinosaurs are planar (e.g., *Plateosaurus*, Huene 1907-8). Among sauropods, concavo-convex intercentral joints evolved multiple times in different regions of the vertebral column. In all but the earliest sauropods, the cervical centra are opisthocoelous, meaning the anterior articular surface is convex and the posterior one is concave (e.g., *Shunosaurus*, Zhang 1988). In several lineages, the caudal centra are procoelous, that is, anteriorly concave and posteriorly convex (e.g., McIntosh 1990). The early evolution and consistent retention of cervical opisthocoely, together with the repeated

evolution of caudal procoely, suggests that this pattern conferred some advantage in the context of the sauropod neck and tail.

Chapter 2 examines the functional significance of concavo-convex intervertebral joints relative to planar joints. This is done using *Alligator mississippiensis*, an animal with procoelous vertebrae, as an extant analog. To determine whether a concavo-convex morphology increases intervertebral joint mobility relative to the ancestral planar condition, joint range of motion is measured in situ in an alligator using X-ray CT scanning and compared to joint convexity measurements from the same individual. Serial variation in convexity is also qualitatively compared to the expected distribution of shear stress in the alligator vertebral column.

Chapter 3 explores why concavo-convex joints in the sauropod neck and tail have a consistent mechanical polarity. In cervical opisthocoely and caudal procoely, the concave articular surface faces towards the body and the convex one faces away from the body. Physical models of concavo-convex centra loaded as cantilevers are used to compare the sauropod-type polarity to its theoretical opposite (i.e., cervical procoely or caudal opisthocoely). Photoelastic strain visualization is used to assess whether the stress distribution on the joint surfaces differs between polarities. To determine whether the two polarities differ in stability, the model joints are loaded to the point of failure under a range of biologically plausible conditions. Implications for concavo-convex joints in other vertebrates, including those of the appendicular skeleton, are discussed.

Chapter 4 concerns the mechanics of the neurocentral suture, the intravertebral joint between the separately ossified neural arch and centrum. This suture is an important zone of growth during ontogeny in vertebrates (Vital et al. 1989), and the late fusion of the suture in archosaurs may have enabled the rapid, sustained growth necessary for gigantism (Ikejiri 2010).

The complex, interdigitated sutures present in archosaurs may represent an adaptation to strengthen joints against compression and shear (Ikejiri 2010), as studies of cranial sutures have found a correspondence between the degree of interdigitation and the magnitude and orientation of stress (e.g., Herring and Mucci 1991). To evaluate whether this relationship holds true in sauropods, sutural complexity is quantified in the presacral vertebral column of the sauropod *Spinophorosaurus* using the length-ratio and fractal dimension metrics. Observed serial patterns are linked to regional variation in the loading of the neurocentral junction.

Chapter 5 summarizes the above research and presents some of the outstanding questions raised by the results.

Literature Cited

Alexander, R. M. 1989. Dynamics of dinosaurs and other extinct giants. Columbia University Press, New York.

Bird, R. T. 1941. A dinosaur walks into the museum. Natural History 47:74–81.

Buffetaut, E., V. Suteethorn, G. Cuny, H. Tong, J. Le Loeuff, S. Khansubha, and S. Jongautchariyakul. 2000. The earliest known sauropod dinosaur. Nature 407:72–74.

Carrano, M. T. 2005. The evolution of sauropod locomotion: morphological diversity of a secondarily quadrupedal radiation. Pp. 229–251 *in* K. A. Curry Rogers and J. A. Wilson, eds. The sauropods: evolution and paleobiology. University of California Press, Berkeley.

Cerda, I. A., A. P. Carabajal, L. Salgado, R. A. Coria, M. A. Reguero, C. P. Tambussi, and J. J. Moly. 2012. The first record of a sauropod dinosaur from Antarctica. Naturwissenschaften 99:83–87.

Coombs, W. P. 1975. Sauropod habits and habitats. Palaeogeography, Palaeoclimatology, Palaeoecology 17:1–33.

D'Emic, M. D. 2012. The early evolution of titanosauriform sauropod dinosaurs. Zoological Journal of the Linnean Society 166:624–671.

Fisher, D. C. 1985. Evolutionary morphology: beyond the analogous, the anecdotal, and the ad hoc. Paleobiology 11:120–138.

Herring, S. W., and R. J. Mucci. 1991. In vivo strain in cranial sutures: the zygomatic arch. Journal of Morphology 207:225–239.

Huene, F. v. 1907-1908. Die Dinosaurier der Europäischen Triasformation mit Berücksichtigung der aussereuropäischen Vorkommnisse. Geologische und Palæontologische Abhandlungen (Suppl. 1):1–419.

Ikejiri, T. 2010. Morphology of the neurocentral junction during postnatal growth of *Alligator* (Reptilia, Crocodylia). Doctoral thesis, Department of Geological Sciences, University of Michigan, Ann Arbor, 182 p. Unpublished.

Mannion, P. D., P. Upchurch, M. T. Carrano, and P. M. Barrett. 2011. Testing the effect of the rock record on diversity: a multidisciplinary approach to elucidating the generic richness of sauropodomorph dinosaurs through time. Biological Reviews 86:157–181.

McIntosh, J. S. 1990. Species determination in sauropod dinosaurs with tentative suggestions for their classification. Pp. 53–69 *in* K. Carpenter and P. J. Currie, eds. Dinosaur systematics: approaches and perspectives. Cambridge University Press, U.K.

Osborn, H. F. 1899. A skeleton of *Diplodocus*. Memoirs of the American Museum of Natural History 1:189–214.

Plotnick, R. E., and T. K. Baumiller. 2000. Invention by evolution: functional analysis in paleobiology. Paleobiology 26:305–323.

Taylor, M. P., and M. J. Wedel. 2013. Why sauropods had long necks; and why giraffes have short necks. PeerJ 1:e36.

Upchurch, P., P. M. Barrett, and P. Dodson. 2004. Sauropoda. Pp. 259–322 *in* P. Dodson, and H. Osmólska, eds. The Dinosauria, 2nd ed. University of California Press, Berkeley.

Vital, J. M., Beguiristain, J. L., Algara, C., Villas, C., Lavignolle, B., Grenier, N., and Sénégas, J. 1989. The neurocentral vertebral cartilage: anatomy, physiology and physiopathology. Surgical and Radiologic Anatomy 11:323–328.

Weishampel, D. B., P. M. Barrett, R. A. Coria, J. Le Loeuff, X. Xu, X. Zhao, A. Sahni, E. M. P. Gomani, C. R. Noto. 2004. Dinosaur distribution. Pp. 517–606 *in* P. Dodson, and H. Osmólska, eds. The Dinosauria, 2nd ed. University of California Press, Berkeley.

Wilson, J. A., and K. Curry Rogers. 2012. Sauropoda. Pp. 444–481 *in* M. K. Brett-Surman, T. R. Holtz, Jr., and J. O. Farlow, eds. The complete dinosaur, 2nd ed. Indiana University Press, Bloomington.

Zhang, Y. 1988. The Middle Jurassic dinosaur fauna from Dashanpu, Zigong, Szechuan. Vol I. Sauropod dinosaur (I). *Shunosaurus*. Journal of the Chengdu College of Geology 3:1–89.

CHAPTER 2

CONCAVO-CONVEX INTERVERTEBRAL JOINTS STABILIZE THE VERTEBRAL COLUMN IN SAUROPOD DINOSAURS AND CROCODYLIANS

Abstract.—Sauropod dinosaurs achieved the largest body sizes and the most elongate necks and tails of any terrestrial vertebrate. The highly elongate, cantilevered necks of sauropods were composed of opisthocoelous vertebrae joined at concavo-convex joints. Opisthocoelous centra also occurred in the dorsal region of sauropods and procoelous centra in the tails of certain lineages. Concavo-convex joints have been hypothesized to increase the flexibility of the spine or to stabilize the intervertebral joints against shear stresses. Using the American alligator (*Alligator mississippiensis*) as an extant analog, the relationship between centrum articular convexity and flexibility was tested. Condyle convexity and range of motion were measured at every intervertebral joint in an alligator, with the range of motion measured in situ. Results reveal that strongly convex condyles occur in the alligator presacral column where flexibility is low, and amphiplatyan vertebrae occur in the distal caudal region where flexibility is highest. The negative relationship between joint convexity and flexibility is not significant, indicating that flexibility is independent of centrum articular morphology. The most strongly convex condyles occur in regions in which high shear stresses are predicted to result from terrestrial locomotion and tail flexion. The evolution of opisthocoelous cervical vertebrae by early sauropods likely strengthened the increasingly long and massive neck against catastrophic dislocations without compromising joint mobility. The stabilization provided by dorsal

opisthocoely and caudal procoely may relate to clade-specific specializations such as the "whiplash" tails of flagellicaudatans and the "wide-gauge" limb stance in titanosaurs. The study of opisthocoely and procoely provides a means to understand the loading regimes acting on the vertebral column in sauropods and other vertebrates, which may, in the future, lead to new insights into the posture, behavior, and ecology of fossil taxa.

Introduction

Sauropod dinosaurs achieved the largest body sizes (Alexander 1998) and the most elongate necks and tails of any terrestrial vertebrate (Müller et al. 2010). The long necks and tails were held aloft (Coombs 1975), as indicated by the lack of tail drag marks in trackways (Bird 1941), and so functioned as cantilevers, beams supported at one end and free at the other. As a result, the considerable weights of the neck and tail were transferred proximally to the body. This would have been experienced as compression of the vertebral centra and extension of the ligaments and muscles of the neural arches, as in mammals (Slijper 1946) and extant reptiles (Hoffstetter and Gasc 1969), as well as shear stress on the intervertebral joints (Salisbury and Frey 2001). Resisting the large magnitude of these forces would have been essential for sauropods to support long necks and tails without sustaining potentially life-threatening injuries.

One avenue for stabilizing the vertebral column against these forces is modification of the centrum articular surface morphology. Sauropod centra commonly exhibit a specialized concavo-convex form (e.g., opisthocoely, procoely). Although the presence of opisthocoely in particular has long been recognized as characteristic of sauropods (Owen 1859b), the biomechanical consequences for the flexibility and stability of the sauropod vertebral column have not previously been investigated in detail. Such investigation is enabled by the existence of

concavo-convex intervertebral joints in a variety of modern vertebrates (Table 2.1), in particular crocodylians, which, along with birds, make up the sauropod extant phylogenetic bracket. Reconstructing joint function based on extant analogs is a necessary step toward understanding how sauropods supported their large bodies and hyperelongated necks and tails, as well as a means to interpret posture and behavior in specific taxa.

Terminology.—The nomenclature used in this paper to describe intervertebral joints and vertebral centra is summarized in Table 2.2. The term "concavo-convex intervertebral joint" is here used to refer to articulations between vertebral centra in which one articular surface is convex (i.e., the condyle) and the other is concave (i.e., the cotyle). This terminology resembles that of Hay (1908: p. 5), who referred to them as "concavo-convex" and "convexo-concave" joints, and of Nopcsa (1930: p. 1), who did likewise in German. However, the use of "convexo-concave" and "concavo-convex" by these authors to describe opposite anatomical polarities is not followed here, because it is generally redundant with the terms "opisthocoely" and "procoely." Concavo-convex intervertebral joints are often referred to as "ball-and-socket joints" (e.g., Owen 1859b; Troxell 1925; Romer 1956), drawing an analogy to the better-known joints of the appendicular skeleton, such as the glenohumeral joint, in which a hemispherical condyle rotates in the cotyle with a substantial range of motion. As described in the Discussion below, extensive rotational mobility cannot be assumed a priori in vertebrae with concavo-convex joints. The alternative term "semi-spheroidal articulations" favored by Salisbury and Frey (2001) is equivalent to "concavo-convex joints."

By convention, the term "opisthocoelous" ("opistho" = back, "coel" = hollow) refers only to centra that are both posteriorly concave and anteriorly convex, and "procoelous" ("pro" =

front) refers to centra with the converse polarity. Virchow (1914: p. 114) developed a set of terms to describe vertebral central morphology that specify both ends of the concavo-convex centra. A centrum that is anteriorly convex and posteriorly concave would be described as opisthocoelous and prokyrt, and a centrum that is anteriorly concave and posteriorly convex would be both procoelous and opisthokyrt ("kyrt" = convex). In conventional usage, vertebrae that are concave at both ends are termed "amphicoelous" or "platycoelous" depending on the strength of concavity (Romer 1956), not "biconcave," and those that are planar at both ends are "amphiplatyan," not "biplanar." Those that are convex at both ends are "biconvex," not "amphikyrt," the term favored by Virchow (1914: p. 114), or "convexo-convex" (Hay 1908). Several authors (e.g., Williams 1950; Hoffstetter and Gasc 1969) have used "opisthocoelous" to describe not only centra, but also joints between centra in which the anterior of the two articular surfaces participating in the joint is the concave one (and "procoelous" for the opposite configuration). This usage creates some confusing scenarios (for instance, an amphicoelous vertebra and a biconvex one could combine to create an "opisthocoelous" joint) and is not adopted here.

Concavo-convex Intervertebral Joints in Sauropods.—Among sauropodomorph dinosaurs, concavo-convex joints between vertebral centra occur uniquely within sauropods. In all other sauropodomorphs, all postaxial vertebrae except those fused in the sacrum are amphicoelous or amphiplatyan (e.g., *Eoraptor*, Sereno et al. 2012; *Plateosaurus*, Huene 1907-8; *Melanorosaurus*, van Heerden 1979; Fig. 2.1A). The universality of this condition in non-sauropod sauropodomorphs indicates that amphicoely or amphiplaty was the plesiomorphic condition from which the opisthocoelous and procoelous vertebrae of sauropods were eventually

derived. The definition of Sauropoda and the associated node have shifted in a more inclusive direction in recent years, and as a result, concavo-convex intervertebral joints are presently recovered as a synapomorphy of a slightly more exclusive clade than Sauropoda. Three of the most basally diverging sauropods included in the phylogeny of Yates (2007), *Antetonitrus* (Yates and Kitching 2003), *Lessemsaurus* (Pol and Powell 2007), and *Gongxianosaurus* (He et al. 1998), are represented by amphicoelous to amphiplatyan vertebrae, although the complete vertebral series is not known for these species. Optimization of the presence of concavo-convex intervertebral joints remains ambiguous near the base of Sauropoda due to uncertainty in the anatomy and phylogenetic placement of these taxa.

Concavo-convex joints were acquired by sauropods in different regions of the vertebral column at different times (Fig. 2.2). In all but the earliest sauropods (see above), the postaxial cervical vertebrae are opisthocoelous (Fig. 2.1B). The earliest example of this is the Late Triassic *Isanosaurus* (Buffetaut et al. 2000), for which only one of the cervical centra is known. In later basal sauropods (e.g., *Tazoudasaurus*, Allain et al. 2004; *Kotasaurus*, Yadagiri 1988) and all eusauropods the pattern is invariant, representing a time span of at least 135 Ma.

The acquisition of cervical opisthocoely by sauropods was accompanied or followed by a spread into the adjacent anterior dorsal region as that region became increasingly "cervicalized," with the extension of opisthocoely into the posterior dorsal region occurring later and only in certain lineages. The presence of opisthocoelous dorsal vertebrae in sauropods was sufficiently distinctive that Owen (1859b) used it as the basis for placing all sauropods then known together in a new suborder he named Opisthocoelia; the name has priority over Sauropoda, but has fallen into disuse (see discussion in Hatcher 1903; Riggs 1903). The timing of the appearance of dorsal opisthocoely is uncertain due to the incomplete preservation of some early sauropods (e.g.,

Isanosaurus, Buffetaut et al. 2000; *Vulcanodon*, Raath 1972). In most lineages, opisthocoely in the dorsal region remained restricted to the anteriormost vertebrae (Fig. 2.2), as in *Tazoudasaurus* (Allain and Aquesbi 2008) and *Shunosaurus* (Zhang 1988). Two sauropod lineages independently acquired opisthocoely in the middle and posterior dorsal vertebrae: the basal eusauropod *Mamenchisaurus* (Ouyang and Ye 2002; Xing et al. 2015) and the neosauropod clade Macronaria (Salgado et al. 1997; Wilson 2002).

In the caudal region, many sauropods retain the ancestral amphicoelous condition (e.g., *Limaysaurus*, Calvo and Salgado 1995; *Camarasaurus*, Osborn and Mook 1921). Procoelous anterior caudal vertebrae (Fig. 2.1C) evolved independently three or four times, according to our current understanding of sauropod interrelationships (Fig. 2.2): (1) in the Late Jurassic basal eusauropod *Mamenchisaurus* (Young 1954); (2) in the diplodocoid clade Flagellicaudata (Calvo and Salgado 1995); (3) in the titanosaur clade Lithostrotia (McIntosh 1990; Wilson and Sereno 1998; Upchurch et al. 2004); and (4) in a tail of uncertain taxonomic position once referred to the Late Jurassic *Janenschia* (Bonaparte et al. 2000). In some Late Cretaceous lithostrotians, middle and distal caudal vertebrae are also procoelous (McIntosh 1990; Wilson 2002; Upchurch et al. 2004). In several lithostrotian taxa, the transition from posteriorly concave dorsal and sacral vertebrae to anteriorly concave caudal vertebrae occurs via a biconvex first caudal vertebra (see D'Emic and Wilson 2011: Table 1). The general pattern of caudal procoely is reversed in the lithostrotian *Opisthocoelicaudia* (Borsuk-Bialynicka 1977), in which the anterior caudal centra are opisthocoelous and the middle and posterior caudal centra are amphiplatyan. Other variants occur in the distal caudal region. In flagellicaudatans, some titanosaurs, and *Cetiosauriscus*, the distal caudal vertebrae are biconvex (Wilson and Sereno 1998; Wilson et al. 1999). More complex arrangements of centrum types, including opisthocoelous, procoelous, amphicoelous,

and biconvex centra, are found in the distal caudal regions of the titanosaur *Rinconsaurus* (Calvo and González Riga 2003) and the euhelopodid *Tangvayosaurus* (pers. obs., JAW).

Functional Hypotheses.—All sauropods with long necks and large body size also have opisthocoelous cervical centra, suggesting that opisthocoely had a functional role in enabling the characteristic sauropod body plan. Many forms also exhibit concavo-convex joints between vertebral centra in the dorsal and caudal regions of the spine, indicating that further advantages were derived for certain taxa by increasing the serial extent of opisthocoely and procoely. The functional consequences of these centrum articular morphologies have not been assessed in detail for sauropods, so comparison to other vertebrates is necessary. Concavo-convex joints between centra occur in a variety of vertebrate lineages besides Sauropoda (Table 2.1). Among these, the procoelous centra of crocodylians have received the most attention in biomechanical studies. The hypotheses generated by those studies are discussed below.

Concavo-convex joints have two major mechanical properties that may explain their evolution in vertebrates. The first property is that concavo-convex joints permit rotation without impingement of one articular surface on the other; a close contact is maintained over the joint surface throughout rotation, unlike in planar joints (Fig. 2.3A, B). This property has led to the hypothesis that opisthocoely and procoely evolved to provide a greater range of motion on each intervertebral joint relative to the ancestral amphiplatyan condition, resulting in an overall more flexible vertebral column. Cope (1896) was one of the earliest to provide evidence in favor of this hypothesis, noting that concavo-convex joints occur throughout the vertebral column in laterally undulating animals, such as lizards and snakes, and are restricted to the cervical region in upright animals, such as mammals and (to the extent of his knowledge) dinosaurs (see Table

2.1). He believed it was the action of flexing the joint that caused the concavo-convex form to develop. Referencing earlier work by Marsh, he declared, “the ball-and-socket vertebral articulation has been produced by constant flexures of the column in all directions” (Cope 1896: p. 304). Troxell (1925) proposed the opposite causal relationship, in which the presence of a concavo-convex joint form is what allows increased flexibility. In a study of the procoelous vertebrae of crocodylians he suggested that, when a concavo-convex intervertebral joint is rotated, “throughout the movement one segment glides with ease on the other,” resulting in “great pliability in the tail and body of the crocodile” (Troxell 1925: p. 606). The assumption that opisthocoely and procoely are linked to increased flexibility was applied to sauropods by Osborn and Mook (1921: p. 323), Wilson and Carrano (1999: p. 264), and Powell (2003: p. 67), the latter of whom cited Troxell (1925) in support.

The second property of concavo-convex articulations pertinent to their biological function is that they restrict translation perpendicular to the axis of the vertebral column (e.g., laterally, dorsoventrally), unlike planar joints, in which the bones provide no obstacle to translation (Fig. 2.3C, D). This is because concavo-convex joints have one articular surface nested within another, creating a physical barrier to translation as well as increasing the area of contact between articular surfaces. This stabilizing characteristic was noted by Sullivan (1922) and Barnett (1954) and implied by Cope (1887: p. 337, “this strong kind of articulation”) and Romer (1956: p. 224), who attributed to it “a strengthening of the column.” This principle is applied in the design of prosthetic intervertebral discs in humans, in which a concavo-convex structure is used to prevent translation and reduce shear loads acting on the zygapophyses (Huang et al. 2003). In a study of the procoelous vertebrae of crocodylians, Salisbury and Frey (2001) proposed that concavo-convex intervertebral joints evolved to stabilize the vertebral

column against shear loading, and not to increase flexibility beyond that present in ancestral forms with amphicoelous vertebrae. Salisbury and Frey (2001: p. 87) predicted that, if the flexibility hypothesis were true, there would be a consistent relationship between "the extent to which procoely is developed" and flexibility throughout the vertebral column in the crocodylians they studied. They rejected this hypothesis as inconsistent with their observations but did not present descriptions or measurements of serial variation in articular morphology to support that decision. Further evaluation of their prediction is needed.

Test of Functional Hypotheses.—The present work aims to assess explicitly the two hypotheses of concavo-convex intervertebral joint function using data collected from an extant model organism, the American alligator (*Alligator mississippiensis*). Intracolumnar variation in flexibility was measured in situ in a representative alligator with all soft tissues intact, and then the defleshed, disarticulated vertebrae of the same individual were measured to quantify the shape of the condyles. If the hypothesis that the joints increase flexibility is correct, then the most strongly convex condyles should occur in the most flexible regions of the vertebral column. If the joints instead stabilized the vertebral column, then convexity and flexibility should show an inverse relationship or no relationship, depending on whether the restriction of translation is linked to a restriction of rotation. The results permit a reassessment of the function of concavo-convex intervertebral joints in sauropods and other vertebrates. The functional significance of differences in articular polarity (opisthocoely vs. procoely) is the subject of another work; here only the function of concavo-convex joints irrespective of polarity will be addressed.

Institutional Abbreviations.—**FMNH**: Field Museum of Natural History, Chicago, USA; **MCT**: Museu de Ciências da Terra, Rio de Janeiro, Brazil; **MLP**: Museo de La Plata, La Plata,

Argentina; **UMMP**: University of Michigan Museum of Paleontology, Ann Arbor, USA; **USNM**: National Museum of Natural History, Smithsonian Institution, Washington, D.C., USA.

Materials and Methods

The direct observation of concavo-convex intervertebral joint mechanics within a complete animal can be achieved by examining an extant analog that is comparable to sauropods. *Alligator mississippiensis* was chosen for study because crocodylians are the closest living relatives of sauropods that also exhibit concavo-convex (in this case, procoelous) joints throughout the vertebral column. As in all crocodylians, the first caudal centrum in *A. mississippiensis* is biconvex, resembling the condition in titanosaur sauropods (e.g., *Alamosaurus*, Gilmore 1946). American alligators are also readily available and of sufficient size for articular surfaces to be easily examined. A 3.5-year-old female alligator (snout-vent length = 31.7 cm; total length = 65.2 cm) that had previously died in captivity was provided by the Florida Fish and Wildlife Research Institute (UMMP R1720). The specimen was excused from institutional review by the University of Michigan University Committee on Use and Care of Animals because it was not sacrificed for this project. The alligator was frozen and stored in a right laterally flexed position for six to eight months prior to shipping and two and a half months between receipt and scanning. The left side of the ribcage exhibited signs of crushing, possibly sustained in transit, although the ribs and gastralia were unbroken. Left lateral flexion was restricted as a result. Right lateral flexion was unimpeded. The specimen remained pliable in all other directions. To verify that the specimen approximated the range of motion achieved in life, comparisons were made to images of swimming crocodylians taken for kinematic study by Frey and Salisbury (2001) and Fish et al. (2007) and to previously published measurements from

cadaveric specimens (Virchow 1914; Molnar et al. 2014). These comparisons were also used to validate that the studied specimen was representative of crocodylians generally.

Measurements of the range of motion on each intervertebral joint were made in situ, that is, in the animal with all soft tissues intact, via X-ray Computed Tomography. The specimen was scanned at the Department of Radiology of the Michigan State University College of Veterinary Medicine on a GE Brightspeed 16 slice CT system at 120 kV and 325–350 MA, with a slice thickness of 0.625 mm and an imaging matrix of 512 pixels x 512 pixels x 16 bit depth. Scans were made of the animal in a straight baseline pose and at maximum right lateral flexion, ventral flexion, and dorsal hyperextension (Fig 2.4A). For each flexed/extended pose, the specimen was manually curved with gentle force until the point at which the joints became rigid and could not be rotated further without a considerable increase in force. Although it is possible the animal could, in life, have applied greater forces, this criterion is easily applied across the entire vertebral column and is sufficient for determining variation in the relative flexibility of different regions. Once this pose had been determined, the specimen was secured in position against a pegboard for scanning, using wooden pegs, string, zip ties, and surgical tape to prevent shifting during the scans.

The scans were processed by the Michigan State University College of Veterinary Medicine using Mimics software by Materialise to produce 3D reconstructions of the skeleton in each pose (Fig. 2.4A); these were imported into the CAD software package 3-matic by Materialise to be aligned for measurement. Flexibility was measured at each intervertebral joint by first creating a datum plane passing sagittally (for dorsoventral flexion/extension) or horizontally (for lateral flexion) through the two vertebrae. The sagittal plane was defined by the tips of the neural spines and the midpoint of the ventral surface of the centrum articulation. The

horizontal plane was defined by the dorsalmost points of the overlapping zygapophyses of the adjacent joints anterior and posterior to the joint being studied. A screen capture was taken orthogonal to each plane so that angle measurements could be taken within the plane. This process was repeated for every joint to account for the three-dimensional curvature of the specimen.

For dorsoventral flexion, the angle between the vertebrae was defined as the intersection of the horizontal axes. Horizontal axes were defined by the floor of the neural canal, which is functionally constant throughout the vertebral column, or by the long axis of the centrum when the neural canal was insufficiently resolved (i.e., in distal caudal vertebrae). The endpoints of the neural canal or centrum were marked on the model in 3-matic before screen capture so that the points could be recognized even if obscured in some views. For lateral flexion, the angle between vertebrae was defined as the intersection of the midlines of the vertebrae, which were found using the midpoints between the left and right pre- and postzygapophyses. The images were imported into Adobe Photoshop, in which lines were drawn to connect the ends of the neural canal or the midpoints of each vertebra (Fig. 2.4B). The angle measurement tool was used to find the angle of intersection of these lines. The line drawing and angle measurement procedures were repeated three times for each image to assess measurement error, with the results averaged. Dorsoventral flexibility was calculated as the angle between the greatest dorsal and greatest ventral flexion, lateral flexibility as the greatest right lateral flexion doubled (assuming bilateral symmetry in flexibility). Similar methods of angular measurement were applied to turtles by Werneburg et al. (2014).

Convexity measurements were acquired from the same specimen after defleshing, permitting the comparison of convexity and flexibility values without the influence of

intraspecific variation. Prior to defleshing, the specimen was dissected. During the dissection, observations were made of the relationship between soft tissue structures, such as epaxial muscles, and vertebral morphology. Joint capsules between vertebral centra were opened to document the soft tissue configuration of the joints. Regional identities were validated at this time. Defleshing was accomplished by boiling the specimen slowly for about an hour, after which remaining muscle and other tissue was picked off. Joint capsules were carefully severed with a scalpel and probe.

Measurements of condyle length, width, and height, cotyle depth, and total centrum length were collected using digital calipers with a precision of 0.01 mm. The measurements were taken three times each to assess the magnitude of measurement error and the results were averaged. As before, the floor of the neural canal was used to determine the horizontal axis of the specimen, to which all lengths are parallel and widths and heights are orthogonal. Condyle width and height were measured using the entire articular surface, including the flattened rim, if present. Convexity was defined by the ratio of condyle anteroposterior length to condyle transverse width (lateral convexity) and condyle anteroposterior length to condyle height (dorsoventral convexity). A perfectly hemispherical condyle would have a length equal to the radius of a sphere and a height and width equal to the diameter, resulting in a convexity ratio of 0.5. A planar articular surface would have a length of zero, and therefore a convexity ratio of zero. These measurements were compared to measurements taken from additional specimens of *Alligator mississippiensis*, as well as the crocodylians *Melanosuchus niger*, *Caiman crocodilus*, and *Crocodylus acutus*, to verify the representative character of the studied specimen (UMMP R1720).

The data were plotted against the cumulative functional length of the centra, beginning at the anterior end of the axis, as a measure of position along the length of the animal. Functional length is here defined as the centrum length (including the condyle) minus the cotyle depth to approximate the overlap of one centrum on another, cotyle depth being consistently less than condyle length. This calculation of functional length does not take into consideration the cartilage thickness between centra but provides a useful first approximation of position in the spine, which is sufficient for visualizing serial variation in flexibility and convexity. Linear regression of flexibility on convexity was used to determine the relationship between and correlation of the variables.

Results

Soft Tissue Morphology of Intervertebral Centrum Joints.—Dissection of the alligator specimen confirmed that the joints between vertebral centra are synovial, as described by Salisbury and Frey (2001). Each synovial cavity is surrounded by a ring of fibrous cartilage, the annulus fibrosus. The condyle of each vertebra consists of a restricted convexity in the middle of the articular surface, surrounded by a flattened periphery to which the annulus fibrosus attaches (Fig. 2.5A). On planar articular surfaces, the annulus fibrosus persists but is not indicated on the bone by any osteological correlate. The presence of a septum dividing the synovial cavity transversely (septum intercorporale, Salisbury and Frey 2001: p. 93) is attested to on several condyles by the presence of a fovea (fovea condyli, Salisbury and Frey 2001: p. 94; Fig. 2.5A) to which the septum would have attached. On several other vertebrae, a fragment of the septum remained attached to the condyle after separation of the vertebrae, indicating the same connection. Unlike the specimens described by Salisbury and Frey (2001: p. 94), in UMMP

R1720 the fovea does not expand into a concavity in distal caudal vertebrae; instead, the condyles give way to flat articular surfaces.

Regional Identities.—The American alligator studied has 64 vertebrae. There are nine cervical vertebrae, defined by whether or not the ribs articulate with the sternum (following Romer 1956). The ninth cervical vertebra has an elongate free rib resembling a dorsal rib that does not contact the sternum. There are ten thoracic vertebrae, five lumbar vertebrae (defined by the absence of ribs, following Romer 1956), two sacral vertebrae, and 40 caudal vertebrae. These values are consistent with previously described vertebral counts for *Alligator mississippiensis* (9:10:5:2:39; Reese 1915) and *A. sinensis* (9:10:5:2:36; Cong et al. 1998); slight variations in caudal vertebral count are known in crocodylians (Reese 1915). Caudal vertebrae 36–40 were not resolved in the CT scans of the specimen in dorsal and ventral flexion, and 39–40 were not resolved in the scan of lateral flexion, due to the small size of these elements relative to the slice thickness of the scans.

Several major subregional morphological transitions were documented in the specimen (Figs. 2.6, 2.7). Hypapophyses are present from the axis to the fourth dorsal vertebra. The scapula overlies the eighth and ninth cervical and first dorsal vertebrae, with the glenoid positioned adjacent to the ninth cervical vertebra. All thoracic vertebrae have free ribs. The ninth and tenth thoracic ribs are “floating ribs” that do not contact the sternum. Chevrons occur from caudal intervertebral joint 2/3 to joint 34/35; the chevrons are greatly reduced beginning with joint 31/32. The last transverse processes are present on the right side of the 16th caudal vertebra and the left side of the 17th caudal vertebra. The caudofemoralis longus muscle originates on the first, second, or third caudal vertebra to the 13th caudal vertebra in UMMP R1720, but tendons or

fascia likely persisted to the last of the transverse processes. This coincides approximately with the transition from a double to a single dorsal scale row, which occurs at the 18th caudal vertebra. Zygapophyses do not appear to overlap posterior to caudal joint 31/32. Neural spines and prezygapophyses disappear after caudal vertebra 36. The remainder of the neural arch, including the postzygapophyses, persists until caudal vertebra 39.

Range of Motion (ROM).—The measured angles on each intervertebral joint, beginning with cervical joint 2/3 (hereafter Cv2/3), are presented in Figure 2.6, and the total range of motion on each joint in Figure 2.7. The raw measurements are provided in Table 2.3. Measurement error is sufficiently low that it does not obscure patterns within and between regions, remaining below 0.6° for dorsoventral measurements and rarely exceeding 4° for lateral measurements (Fig. 2.6). The joint between the two sacral vertebrae provides an additional test for error within the data collection process. On this joint, a range of motion of 4.2° dorsoventrally and 1.6° laterally was measured. If the sacral joint is assumed to be fully immobile, this result suggests that a margin of error of about 4° should be considered for all measurements, which does not obscure the prevailing patterns. However, the joint between the sacral vertebrae in this individual remains unfused, and the possibility of a few degrees of flexibility between sacral vertebrae at this ontogenetic stage cannot be excluded.

The raw measurements of intervertebral angles (Fig. 2.6; Table 2.3) reveal an intrinsic dorsoventral curvature of the presacral spine. The cervical and anterior thoracic regions exhibit a dorsal curvature even at the maximum ventral flexion of the specimen; the neck cannot be flexed below the horizontal except at joint Cv2/3 and at the cervico-thoracic joint. The result is a permanent “S”-curvature of the neck. The greatest dorsoventral curvature of the neck occurs at

Cv7/8; at maximum dorsal extension, this joint makes an angle of 25° dorsal to the horizontal, the greatest dorsoventral angle measured anywhere in the vertebral column. Throughout the rest of the spine, the baseline dorsoventral curvature remains within 5° of horizontal, indicating a nearly straight resting pose.

A slight lateral curvature of the spine can be attributed to postmortem crushing. There should be no intrinsic curvature in the lateral direction due to the bilateral symmetry of the animal. An intrinsic right lateral curvature is observed in the anterior cervical and thoracic regions, and left lateral curvature occurs in the posterior cervical and lumbar regions. This pattern could result from the crushing that affected the specimen while it was transported in a right laterally flexed position. The crushing of the ribcage restricted left lateral flexion of the thorax, which likely prevented the specimen from being completely straightened during the scans. The baseline curvature at any given joint does not exceed 5° in either direction and does not significantly alter the overall pattern of the data.

The raw angle measurements were used to compute the total possible range of motion (ROM) in both the dorsoventral and lateral directions (Fig. 2.7; Table 2.3). The dorsoventral range of motion (dvROM) shows only a small amount of variability throughout the vertebral column and seldom exceeds 20°. The dvROM is greatest in the posterior cervical (maximum of 18.2°), posterior lumbar (13.3°), and middle to distal caudal regions (26.9°). It is lowest in the thoracic, anterior lumbar, and anterior caudal regions, as well as adjacent to the sacrum; in each of these regions, values typically range from 0–10°. A variation in dvROM of at least 10° between adjacent joints is common throughout the series, with the exception of the posterior thoracic, anterior lumbar, and middle caudal regions, where variation is limited to only a few degrees from one joint to the next. The greatest variation in dvROM occurs among the distal

caudal vertebrae, with a change of 21.4° between caudal joint 25/26 (Ca25/26) and Ca26/27. Caudal vertebrae 36–40 were not resolved in the scans of dorsal extension and ventral flexion, so no data is available on the dvROM of those joints. Significant changes in dvROM do not appear to coincide with anatomical transitions with the exception of those occurring around the sacrum.

The lateral range of motion (latROM) shows a much greater magnitude of regional variation than does the dvROM, with modest presacral and anterior caudal values typically less than 20° and middle and distal caudal values that increase to a maximum greater than 70°. The presacral vertebrae predominately range between 10 and 20° of latROM (maximum = 22.9° at Cv4/5) except adjacent to the appendicular girdles, at which values are less than 5°. LatROM is reduced in the posterior cervical and anterior thoracic vertebrae, reaching its lowest (2.8°) at the cervico-thoracic joint, which is also the approximate position of the glenoid. By thoracic vertebra 3 (T3), values are once again high (> 20°), coinciding with the loss of the hypapophyses. LatROM is especially low adjacent to the sacrum (3.2° at L5/S1; 1.9° at S2/Ca1). The anterior caudal intervertebral joints from Ca1/2 to Ca7/8 exhibit a modest latROM of less than or equal to 15°. The middle caudal joints from Ca8/9 to Ca28/29 predominately range from 20–40° of latROM, with a much lower value for Ca15/16 (6.4°). This local anomaly does not correlate to any anatomical transition or visible pathology; manipulation of the defleshed skeleton indicates the low latROM to be a genuine feature and not an experimental artifact. The distal tail exhibits the greatest latROM in the series, reaching a maximum of 76.5° at Ca34/35. The abrupt decrease in latROM to 33° at Ca37/38 can be explained as an experimental artifact due to the difficulty of restraining very small distalmost caudal vertebrae in a flexed pose during scanning. Caudal vertebrae 39 and 40 were not resolved in the scan of lateral flexion.

Convexity.—Convexity variation along the vertebral column of *Alligator mississippiensis* is displayed in Figure 2.7. The raw measurements and calculated ratios are provided in Table 2.4. Dorsoventral and lateral convexity show closely similar patterns. Dorsoventral convexity is greater than lateral convexity by an average of six percentage points. The highest convexity measured is 0.53, consistent with the model of vertebral condyles as hemispheres. The lowest measured values were indistinguishable from zero; those vertebrae are considered to be amphiplatyan. No amphicoelous vertebrae were observed.

Convexity values are highest in the presacral and anterior caudal regions, apart from the low values adjacent to the sacrum, and diminish posteriorly along the tail, becoming abruptly amphiplatyan near mid-length coincident with several other anatomical changes. In the cervical region, convexity values are generally high, ranging between 0.41 and 0.47 dorsoventrally and between 0.32 and 0.42 laterally, with the lowest values at the cervico-thoracic joint. Similar values occur in the thoracic region (0.41 to 0.53 dorsoventrally; 0.32 to 0.42 laterally) with a greater magnitude of variation between adjacent vertebrae, up to 11 percentage points. Although the cause of such large changes remains unknown, comparable differences in convexity between adjacent vertebrae are seen in other crocodylians, sauropods, and snakes (pers. obs., JAF). The first four lumbar joints are within the range of variation of the thoracic region. Convexity decreases precipitously at the lumbo-sacral joint to values much lower than those observed elsewhere in the presacral column (0.22 dorsoventrally; 0.13 laterally). This decrease is mirrored in the biconvex first caudal centrum, which has a lower convexity anteriorly than posteriorly, although the magnitude of the difference is much less (0.42 vs. 0.51 dorsoventrally; 0.30 vs. 0.35 laterally). The first five caudal joints all exhibit convexities within the range of the presacral column (excluding L5/S1). From Ca5/6 to Ca18/19 the convexities are more modest, ranging

between 0.15 and 0.29 laterally and between 0.19 and 0.36 dorsoventrally, with a general declining trend. Throughout the tail to this point, changes in convexity between adjacent joints can be as great as 16 percentage points. All centra posterior to the joint Ca18/19 are amphiplatyan. This occurs very close to the end of the transverse processes.

Relationship of Convexity to Flexibility.—In general, the areas of greatest convexity in the alligator vertebral column (the presacral and anterior caudal regions) are the regions for which flexibility is lowest (Fig. 2.7). The amphiplatyan distal caudal vertebrae show the greatest range of motion. The two variables show a moderate inverse correlation, with a stronger correlation in the lateral dimension than in the dorsoventral dimension (Fig. 2.8). This pattern is driven strongly by the amphiplatyan distal caudal vertebrae. When the distal caudal vertebrae are excluded, convexity and flexibility continue to show a weak inverse relationship, but the correlation is negligible (Fig. 2.8).

The pattern observed here is not confounded by other anatomical variables. For instance, changes in the presence of structures that are predicted to influence the total ROM, such as ribs and overlapping zygapophyses, are not linked to major shifts in ROM or convexity. Instead, the same pattern can be observed across all body regions.

Discussion

Representative Nature of Alligator *Specimen*.—The flexibility measured here is consistent with the range of motion of living crocodylians, as seen in kinematic studies of swimming animals (Frey and Salisbury 2001; Fish et al. 2007) and in cadaveric specimens

(Virchow 1914; Molnar et al. 2014). The maximum flexibility achieved in dorsal extension is closely comparable to that documented by Fish et al. (2007) for *Alligator mississippiensis*. Maximum lateral flexion is slightly greater than that observed by Frey and Salisbury (2001) for *Osteolaemus tetraspis*, but not unrealistically so. The flexibility of the cervical region is consistent with that described by Virchow (1914) from a cadaveric specimen of *Alligator mississippiensis* in varying states of defleshing. Virchow (1914) also noted that the intrinsic curvature of this region can be explained by the wedge-like shape of the centra. The pattern of posteriorly-decreasing lateral flexibility in the lumbar region matches that described by Molnar et al. (2014) from cadaveric specimens of *Crocodylus niloticus*. Thus, the specimen under study (UMMP R1720) retains a lifelike range of motion that is representative of crocodylians generally. The convexity measurements for this specimen are generally consistent with those of other crocodylians, apart from the interspecific differences noted below.

Functional Interpretation of Concavo-convex Joint Function in Alligator.—The flexibility hypothesis predicts a strong positive correlation between convexity and ROM at a joint. The results for *Alligator mississippiensis* show the opposite pattern: the most strongly convex vertebral condyles occur in regions of the vertebral column that demonstrated the least flexibility. On this basis, the hypothesis that procoely in crocodylians provides greater flexibility to the spine can be rejected. A negative correlation between convexity and flexibility is only moderately well-supported when amphiplatyan distal caudal vertebrae are included in the analysis and essentially uncorrelated when distal caudal vertebrae 19–40 are excluded. This indicates that, for the majority of the vertebral column, the degree of convexity is not a significant controlling factor for ROM. Strongly convex articulations neither enhance nor restrict

flexibility. Instead, it may be that zygapophyses, ribs, muscles, and ligaments are the most important factors, as suggested by Molnar et al. (2014). This relationship may hold true beyond Crocodylia, as Werneburg et al. (2015) found the cervical mobility of turtles to be better correlated with other factors, such as vertebral height and width, than with centrum articular morphology.

The results of our analysis are consistent with the stability hypothesis proposed by Salisbury and Frey (2001). The convexity measured in the American alligator was greatest in the mid-cervical, mid-thoracic, and anterior caudal regions, all of which would have experienced substantial shear stress, particularly during terrestrial locomotion. Below, we discuss our expectations for the regionalization of shear stress on the basis of anatomy and behavior. Then, we assess the concordance of this interpretation with the fossil record of the evolution of procoely in crocodylians.

Shear stresses in the tail are generated actively, by muscular retraction of the hind limbs by the caudofemoralis longus muscle (CFL) during terrestrial locomotion, as well as passively by the force of gravity acting on the tail. In both cases, it is expected that shear stresses will decrease distally in the tail, abruptly in the case of the CFL. Convexity values in the tail are high (procoelous) proximally, in those caudal vertebrae that have the transverse processes for origin of the CFL (Gatesy 1991), and low (amphiplatyan) in the more distal portion of the tail that lacks these processes. In addition to retracting the hind limb, the CFL also flexes the tail laterally (Gatesy 1991). The role in lateral flexion indicates that the CFL is also important to the tail-driven swimming of crocodylians. During each of these behaviors, the region of the tail from which the CFL originates is subject to much greater shear stresses than the region distal to the end of the transverse processes. In addition, the distal tail of crocodylians drags on the ground

during walking, eliminating shear stresses associated with supporting a cantilevered extremity. As a result, there should be little to no functional advantage for procoely over amphiplaty in the distal caudal centra of crocodylians.

Shear stresses experienced during semi-erect or sprawling terrestrial locomotion explain the high convexity values observed in the alligator presacral spine. The cervical region experiences increased shear stresses because it supports the large and heavy skull up off the ground. Although the dorsal region is not cantilevered like the neck and tail, it nonetheless experiences shear stresses that result from bending of the trunk while walking or running. Crocodylians exhibit a range of locomotor styles, including a sprawling "low-walk," a semi-erect "high-walk," and, in some taxa, multiple forms of gallop (Renous et al. 2002). With the limbs sprawled or semi-erect, a symmetrical walk cycle introduces shear stresses via the mediolateral component of the limb propulsive forces (Carrier 1990; Schilling 2011) and through the balance of forces between the braced and suspended limbs, which also produce axial torsion (Carrier 1990; Salisbury and Frey 2001). Although asymmetric locomotion (i.e., galloping) also generates these shear stresses, this behavior is restricted among crocodylians (i.e., not alligatorids; Allen et al. 2014) and therefore does not explain the universality of dorsal procoely within Crocodylia. Concavo-convex joints contribute passive stabilization against the lateral component of the propulsive force, supplementing the active stabilization provided by contralateral contractions of the hypaxial muscles (Carrier 1990, 1993). Although both terrestrial and aquatic locomotion create shear stresses in the tail, in the trunk it is only terrestrial locomotion that creates shear stress (e.g., Carrier 1993).

An apparent exception to the correspondence between shear stress and convexity is presented by the vertebrae adjacent to the pelvic girdle. There, significant shear stresses should

be generated by the actions of the limbs and the CFL, and thus high convexity values would be expected. Instead, convexity values in the lumbo-sacral and sacri-caudal joints are lower than those of adjacent joints. The absence of strong convexity in these regions may be compensated by additional bracing not present elsewhere in the presacral column. In the alligator observed in our study (UMMP R1720), the condyle of the fifth lumbar vertebra exhibits lateral facets that articulate with the first sacral ribs, suggesting that this vertebra is partially sacralized (see also Reese 1915). The morphology described here is observed in another, slightly larger specimen of *Alligator mississippiensis* (UMMP R1185), but other crocodylian taxa show no comparable decrease in convexity. Elevated convexity values in the lumbo-sacral joint are present in *Crocodylus acutus* (convexity = 0.52 dorsoventrally, 0.31 laterally; FMNH 22030), *Caiman crocodilus* (0.53 dorsoventrally, 0.39 laterally; FMNH 217159), and an intermediate result in *Melanosuchus niger* (0.44 dorsoventrally, 0.25 laterally; FMNH 218507).

As in the lumbo-sacral centra, the diminished anterior convexity of the biconvex first caudal centrum may be attributed to partially sacralization. As above, the pattern described here is not universal within Crocodylia. The anterior convexity is even less strongly developed in *Caiman crocodilus* (0.16 dorsoventrally, 0.16 laterally; FMNH 217159), whereas the anterior convexity exceeds the posterior convexity in *Melanosuchus niger* (0.43 dorsoventrally, 0.33 laterally at anterior end; 0.35 dorsoventrally, 0.26 laterally at posterior end; FMNH 218507) and *Crocodylus acutus* (0.50 dorsoventrally, 0.34 laterally at anterior end; 0.38 dorsoventrally, 0.28 laterally at posterior end; FMNH 22030). The differences observed between crocodylian taxa do not differentiate alligatorids from crocodylids and therefore cannot be attributed to additional shear stress generation during galloping in the latter (Allen et al. 2014). Broader study of axial biomechanics across Crocodylia is necessary to explain these patterns.

The fossil record of crocodylomorphs provides further evidence that crocodylian procoely evolved to stabilize the spine against shear stresses. Fossil crocodylomorphs that possessed an unsegmented osteodermal shield, which would have provided dorsal bracing, lack procoely (Salisbury and Frey 2001). Although the presence of dorsal procoely in taxa that possessed a segmented osteodermal shield is most consistent with the creation of shear stresses during terrestrial locomotion, the evidence is unclear as to whether the locomotor regime of key fossil taxa was fully terrestrial or partially aquatic. The basal eusuchian *Isisfordia* exhibits what Salisbury et al. (2006: Fig. 5) described as "incipiently procoelous vertebrae" (dorsoventral convexity values for figured vertebrae are less than 0.25) along with a segmented osteodermal shield. Salisbury et al. (2006) interpreted *Isisfordia* as capable of both swimming and terrestrial high-walking. The basal eusuchian *Pietraroiasuchus* also has weakly procoelous vertebrae and a segmented osteodermal shield, and it was interpreted to be semi-aquatic to fully marine (Buscalioni et al. 2011). Swimming alone cannot account for the acquisition of procoely, as the marine-adapted thalattosuchian crocodyliforms universally exhibit amphicoelous vertebrae despite including forms with and without osteoderms providing bracing (see review in Delfino and Dal Sasso 2006). The non-crocodyliform crocodylomorph *Junggarsuchus* represents a fully terrestrial, erect-limbed cursorial form that possesses procoelous vertebrae and lacks osteoderms (Clark et al. 2004). In contrast, similarly cursorial lineages of notosuchian crocodyliforms with reduced osteodermal shields do not have procoelous vertebrae (e.g., *Notosuchus*, Pol 2005; *Baurusuchus*, Nascimento and Zaher 2010; *Mariliasuchus*, Nobre and Carvalho 2013). Future discoveries of basal eusuchians and related crocodyliforms should provide clarity as to the biomechanical regime under which procoely evolved.

Intervertebral Joint Structure in Sauropods.—The nature of soft tissues associated with the intervertebral joints in sauropod dinosaurs can be inferred based on correspondence between hard and soft tissues in their nearest extant relatives (Bryant and Russell 1992; Witmer 1995), which are birds and crocodylians. Living crocodylians have synovial joints between presacral and postsacral vertebrae, as described by Salisbury and Frey (2001) and observed in UMMP R1720. In living birds, joints of the cervical and sometimes thoracic spine are also synovial (Baumel and Raikow 1993). Osteological correlates of these synovial joint structures include a flattened rim around the periphery of the condyle to which the annulus fibrosus attaches, as well as the fovea condyli near the center of the condyle, to which the septum intercorporale attaches.

Both of these osteological structures are observed in sauropods. The flattened peripheral rim around the condyle can be seen in many sauropod specimens (e.g., Diplodocidae, Dicraeosauridae, Schwarz et al. 2007; *Giraffatitan*, *Baurutitan*; see Fig. 2.5B). It is generally thin and inconsistently expressed except in the caudal vertebrae of titanosaurs, where the rim is broad, surrounding a centrally-restricted condyle (e.g., *Alamosaurus*, *Trigonosaurus*). This closely resembles the pattern in *Alligator*. The same feature is seen in some theropods (e.g., *Aerosteon*, Sereno et al. 2008; see also Carrano et al. 2012: character 175), supporting the phylogenetic bracketing. Numerous sauropod specimens also exhibit the fovea condyli (e.g., Dicraeosauridae, Diplodocidae, Schwarz et al. 2007; *Camarasaurus*, *Giraffatitan*, *Rukwatitan*; see Fig. 2.5B). Further discussion of the inference of synovial joints between vertebral centra in fossil taxa is provided by Schwarz et al. (2007) with regard to sauropods and by Witzmann et al. (2014) regarding phytosaurs and other fossil archosaurs.

Functional Significance of Concavo-convex Joints in Sauropods.—The close morphological correspondence between the concavo-convex intervertebral joints present in crocodylians and sauropod dinosaurs, together with the observed and inferred presence of synovial joints in each, respectively, suggests that inferences we have drawn about the functional role of the joints in crocodylians can be applied to sauropods. The results of our study of joint mobility and articular surface convexity in *Alligator mississippiensis* suggest that concavo-convex joints evolved to stabilize the spine against shear stresses, not to confer flexibility beyond that present in the ancestral condition. Concavo-convex joints are nearly universally present in the cervical region and commonly present in the anterior trunk and anterior tail regions as well (see Fig. 2.2). Below we discuss potential regional loading regimes that may have influenced the evolution of these features in sauropods.

Neck elongation not only increases mass and stress magnitudes, but also the lever arm for gravitational forces acting on the neck. The opisthocoelous cervical centra characterizing all but the earliest sauropods acted to prevent dislocation of the neck vertebrae. In all sauropods for which sufficient material is known, opisthocoely extends from the cervical region into the anteriormost dorsal vertebrae, which would have borne the full weight of the neck and served as the origin for the dorsal extensor and ventral flexor muscles inserting on the neck (e.g., the longus colli dorsalis and ventralis; see Cong et al. 1998, crocodylians, and Wedel and Sanders 2002, birds). The action of these muscle groups in bending the neck would generate shear stresses more like those of the cervical region than the rest of the dorsal region. The increase in stability offered by opisthocoelous centra did not intrinsically require a reduction in neck flexibility, because convexity and flexibility are uncorrelated. In contrast, other solutions for stabilizing intervertebral joints, such as hyposphene-hypantrum accessory articulations and

vertebral fusion, are more restrictive of joint mobility. As more discoveries of early sauropods are made, it will be possible to more completely characterize the association between cervical opisthocoely, neck length, and body size.

There is a fairly abrupt change from opisthocoelous to amphiplatyan or platycoelous articular surfaces starting at about the fourth or fifth dorsal vertebra in non-macronarian sauropods (see Fig. 2.2). In most cases, the loss of dorsal opisthocoely is accompanied by the appearance of hyposphene-hypantrum articulations, which are typically present throughout the dorsal series of saurischians (Gauthier 1986). These hyposphene-hypantrum articulations on the neural arch may have provided some stabilization against shear. In macronarians (Salgado et al. 1997; Wilson and Sereno 1998) and in *Mamenchisaurus* (Ouyang and Ye 2002), opisthocoelous centra continue straight through from the cervical region to the sacrum. In many macronarians, the acquisition of mid- to posterior dorsal opisthocoely is accompanied by loss of the dorsal bracing provided by the hyposphene-hypantrum articulations (Wilson 2002). This may signal a change in the loading regime of the trunk associated with the acquisition of a "wide-gauge" limb posture in which the propulsive force has a strong mediolateral component (Wilson and Carrano 1999). Complicating this picture, however, in some macronarians (e.g., *Camarasaurus*, Osborn and Mook 1921; *Giraffatitan*, Janensch 1950) and in *Mamenchisaurus* (Ouyang and Ye 2002) opisthocoely and hyposphene-hypantrum articulations co-occur in middle and posterior dorsal vertebrae. It is possible that other aspects of the paleobiology of these animals explain this pattern, but further reconstruction of the stress regime of the sauropod trunk is necessary before any conclusions can be drawn.

Procoelous caudal vertebrae in sauropods are mechanically equivalent to opisthocoelous cervical vertebrae, because in both cases the concave articular surface is oriented towards the

body (i.e., the supported end of the cantilever). Evolution of caudal procoely independently in several sauropod lineages (Fig. 2.2) likely indicates changes in the shear stresses acting on the spine, but these are probably not a function of size alone because the ancestral amphiplatyan condition is retained in sauropods spanning a broad size range. Instead, the greater amount of variation in caudal articular surface morphology suggests that the tail did not require the same degree of "safe mobility" as the neck, possibly due to the greater number of intervertebral joints present (maximum > 80 in the tail vs. 18–19 in the neck) and lighter terminal load.

The phylogenetic and serial distributions of procoely in the sauropod tail are more complex than those of opisthocoely in the neck; no single satisfactory explanation for the acquisition of caudal procoely seems to apply to all taxa. The serial distribution of procoely does not match any particular anatomical transition, such as the end of the transverse processes and associated CFL (e.g., *Diplodocus*, Hatcher 1901; *Andesaurus*, Mannion and Calvo 2011, although the convexity in this taxon is quite weak). The independent evolution of procoelous anterior caudal vertebrae in several lineages does suggest an important functional role, but differences in caudal anatomy between these lineages prevent the identification of a single factor necessitating the evolution of procoely. It may, instead, be the case that procoely evolved in different clades in response to different functional or structural adaptations, such as the "whiplash" tail and "wide-gauge" limb posture. In flagellicaudatans, the long "whiplash" tail may have been sufficiently massive to necessitate the evolution of procoely, perhaps in concert with swinging the tail laterally for defense. The absence of procoely in *Shunosaurus*, which has a tail club that may have been wielded defensively and a much shorter tail than flagellicaudatans have (Zhang 1988), suggests that tail length might be more important to the evolution of procoely than lateral mobility. In contrast, titanosaurs, particularly lithostrotians, typically have

relatively short tails (Wilson et al. 1999; Wilson 2002). Titanosaur caudal procoely is more likely a result of having a "wide-gauge" limb posture in which the femoral shaft is angled laterally relative to the femoral head (Wilson and Carrano 1999). This created a more mediolateral orientation of the CFL comparable to that in crocodylians, generating similar transverse shear stresses. Another possibility is that titanosaurs habitually browsed in bipedal or tripodal postures, utilizing the short tail for additional stability (e.g., Borsuk-Bialynicka 1977; Wilson and Carrano 1999; Powell 2003). In this posture, the majority of the body weight would be borne by the caudal vertebrae and their joints, greatly increasing the shear stresses and the need for strongly procoelous centra.

Functional Significance of Biconvex Caudal Vertebrae in Sauropods.—The biconvex first caudal centrum present in some titanosaurs, such as *Alamosaurus*, *Baurutitan*, and *Saltasaurus*, is quite similar to that of crocodylians, a resemblance that has long been recognized (e.g., Lydekker 1893). As in *Alligator*, the first caudal centrum has a lower convexity anteriorly than posteriorly in *Alamosaurus* (0.22 dorsoventrally at the anterior end; 0.39 dorsoventrally at the posterior end; USNM 15560) and *Baurutitan* (0.30 dorsoventrally, 0.27 laterally at the anterior end; 0.40 dorsoventrally, 0.33 laterally at the posterior end; MCT 1490-R). These resemblances indicate that the sacri-caudal joint in some titanosaurs was a site of very low mobility and that the first caudal vertebra was in the process of becoming sacralized. This is consistent with the observation by D'Emic and Wilson (2011) that the biconvex "first caudal" vertebra of *Neuquensaurus*, which is also less strongly convex anteriorly (approximately 0.14 dorsoventrally, 0.15 laterally at the anterior end; 0.34 dorsoventrally, 0.27 laterally at the posterior end; MLP Ly1), is actually a seventh sacral vertebra. Thus, titanosaurs show a pattern

of increasing stabilization of the proximal tail from the ancestral amphiplatyan condition to procoelous centra with increasing convexity to an incipiently or completely sacralized first caudal vertebra. We hypothesize this indicates increasing shear stresses possibly associated with the acquisition of "wide-gauge posture," and perhaps also an increasing utilization of tripodal posture. The question of why the incipient sacral vertebra is biconvex rather than procoelous is the subject of future research.

The presence of series of biconvex centra in the distal caudal region of flagellicaudatans, titanosaurs, and *Cetiosauriscus* indicates comparatively low shear stresses. Whereas concavo-convex joints between centra confer resistance to dislocation by shear stresses, the articulation of one condyle with another provides no overlap and a very low area of contact (Sullivan 1922). It is logical that these joints would be restricted to the end of the tail where the mass to be supported is minimal and muscular attachments are few. It seems plausible that convex-to-convex articulations would be permissive of a wide range of motion (Sullivan 1922), resulting in flexible tail tips, particularly in the "whiplash" tails of flagellicaudatans. A high degree of mobility is already found in the amphiplatyan distal caudal vertebrae of *Alligator*, exceeding 70° at the most flexible joint; it is possible that biconvex distal caudal vertebrae in sauropods conferred hypermobility beyond this.

Conclusions

The study of *Alligator mississippiensis* as an analog for the function of concavo-convex joints between vertebral centra in sauropod dinosaurs reveals that the joints do not confer greater flexibility to the vertebral column relative to planar joints between amphiplatyan vertebrae. Instead, strongly convex condyles occur in the less-flexible presacral column; amphiplatyan

vertebrae occur in the highly flexible distal tail. The correlation between flexibility and convexity is not significant, meaning that centrum articular morphology neither enhances nor restricts flexibility in a predictable fashion. The most strongly convex condyles occur in regions in which high shear stresses are predicted to result from terrestrial locomotion and the action of the caudofemoralis longus muscle. This is consistent with the hypothesis that opisthocoelous and procoelous vertebrae stabilize the spine against dislocation by shear stresses. This mode of stabilization does not intrinsically require any sacrifice of vertebral mobility.

The evolution of opisthocoelous cervical vertebrae by early sauropods likely strengthened the increasingly long and massive neck against catastrophic dislocations. Opisthocoely should therefore be understood as one of the suite of character states that allowed sauropods to dominate terrestrial megaherbivore niches throughout the Jurassic and Cretaceous and to achieve unmatched extremes of body size and neck length. Dorsal opisthocoely appears to be linked anteriorly to the origins of the muscles flexing the neck; transverse shear stresses associated with a “wide-gauge” posture may be responsible for the posterior extension of opisthocoely in titanosaurs. Caudal procoely could have provided stability against shear stresses resulting from multiple causes, including the length and weight of the tail, the lateral flexion of the tail by the caudofemoralis longus muscle, and perhaps the use of the tail to support the body in a tripodal posture. Further work is needed to explain the complexities of these patterns. The study of opisthocoely and procoely provides a means to understand the loading regimes acting on the vertebral column in sauropods and other vertebrates, which may, in the future, provide new insights into the posture, behavior, and ecology of fossil taxa.

Literature Cited

Alexander, R. M. 1998. All-time giants: the largest animals and their problems. Palaeontology 41:1231–1245.
Allain, R., and N. Aquesbi. 2008. Anatomy and phylogenetic relationships of *Tazoudasaurus naimi* (Dinosauria, Sauropoda) from the late Early Jurassic of Morocco. Geodiversitas 30:345–424.
Allain, R., N. Aquesbi, J. Dejax, C. Meyer, M. Monbaron, C. Montenat, P. Richir, M. Rochdy, D. Russell, P. Taquet. 2004. A basal sauropod dinosaur from the Early Jurassic of Morocco. Comptes Rendus Palevol 3:199–208.
Allen, V., J. Molnar, W. Parker, A. Pollard, G. Nolan, and J. R. Hutchinson. 2014. Comparative architectural properties of limb muscles in Crocodylidae and Alligatoridae and their relevance to divergent use of asymmetrical gaits in extant Crocodylia. Journal of Anatomy 225:569–582.
Barnett, C. H. 1954. The structure and functions of fibrocartilages within vertebrate joints. Journal of Anatomy 88:363–368.
Baumel, J. J., and R. J. Raikow. 1993. Arthrologia. *In* J. J. Baumel, A. S. King, J. E. Breazile, H. E. Evans, and J. C. Vanden Berge, eds. Handbook of avian anatomy: nomina anatomica avium, 2nd edition. Publications of the Nuttall Ornithological Club 23: 133–187.
Baumel, J. J., and L. M. Witmer. 1993. Osteologia. *In* J. J. Baumel, A. S. King, J. E. Breazile, H. E. Evans, and J. C. Vanden Berge, eds. Handbook of avian anatomy: nomina anatomica avium, 2nd edition. Publications of the Nuttall Ornithological Club 23: 133–187.
Beddard, F. E. 1898. The structure and classification of birds. Longmans, Green, and Company, London.
Benson, R. B. J. 2010. A description of *Megalosaurus bucklandii* (Dinosauria: Theropoda) from the Bathonian of the UK and the relationships of Middle Jurassic theropods. Zoological Journal of the Linnean Society 158:882–935.
Bird, R. T. 1941. A dinosaur walks into the museum. Natural History 47:74–81.
Bonaparte, J. F., W.-D. Heinrich, and R. Wild. 2000. Review of *Janenschia* Wild, with the description of a new sauropod from the Tendaguru beds of Tanzania and a discussion on the systematic value of procoelous caudal vertebrae in the sauropoda. Palaeontographica Abteilung A 256:25–76.
Borsuk-Bialynicka, M. 1977. A new camarasaurid sauropod *Opisthocoelicaudia skarzynskii* gen. n., sp. n. from the Upper Cretaceous of Mongolia. Palaeontologia Polonica 37:5–64.
Bryant, H. N., and A. P. Russell. 1992. The role of phylogenetic analysis in the inference of unpreserved attributes of extinct taxa. Philosophical Transactions of the Royal Society of London B 337:405–418.
Buffetaut, E., V. Suteethorn, G. Cuny, H. Tong, J. Le Loeuff, S. Khansubha, and S. Jongautchariyakul. 2000. The earliest known sauropod dinosaur. Nature 407:72–74.
Buscalioni, A. D., P. Piras, R. Vullo, M. Signore, and C. Barbera. 2011. Early eusuchia crocodylomorpha from the vertebrate-rich Plattenkalk of Pietraroia (Lower Albian, southern Apennines, Italy). Zoological Journal of the Linnean Society 163:S199–S227.
Calvo, J. O., and B. J. González Riga. 2003. *Rinconsaurus caudamirus* gen. et sp. nov., a new titanosaurid (Dinosauria, Sauropoda) from the Late Cretaceous of Patagonia, Argentina. Revista Geológica de Chile 30:333–353.
Calvo, J. O., and L. Salgado. 1995. *Rebbachisaurus tessonei* sp. nov. a new Sauropoda from the Albian-Cenomanian of Argentina; new evidence on the origin of the Diplodocidae. Gaia 11:13–33.

Cameron, H. U. 1974. The intervertebral joint of the longnose gar, *Lepisosteus osseus.* Canadian Journal of Zoology 52:803–804.
Carrano, M. T., R. B. J. Benson, and S. D. Sampson. 2012. The phylogeny of Tetanurae (Dinosauria: Theropoda). Journal of Systematic Paleontology 10:211–300.
Carrier, D. 1990. Activity of the hypaxial muscles during walking in the lizard *Iguana iguana*. Journal of Experimental Biology 152:453–470.
———. 1993. Action of the hypaxial muscles during walking and swimming in the salamander *Dicamptodon ensatus*. Journal of Experimental Biology 180:75–83.
Chatterjee, S., and Z. Zheng. 2002. Cranial anatomy of *Shunosaurus*, a basal sauropod dinosaur from the Middle Jurassic of China. Zoological Journal of the Linnean Society 136:145–169.
Clark, J. M., X. Xu, C. A. Forster, and Y. Wang. 2004. A Middle Jurassic 'sphenosuchian' from China and the origin of the crocodylian skull. Nature 430:1021–1024.
Cohen, K. M., S. C. Finney, P. L. Gibbard, and J.-X. Fan. 2013. The ICS International Chronostratigraphic Chart. Episodes 36:199–204.
Cong, L., L. Hou, X. Wu, and J. Hou. 1998. The gross anatomy of *Alligator sinensis* Fauvel. China Science and Technology, Beijing.
Coombs, W. P. 1975. Sauropod habits and habitats. Palaeogeography, Palaeoclimatology, Palaeoecology 17:1–33.
Cope. E. D. 1887. The origin of the fittest. D. Appleton and Company, New York.
———. 1896. The primary factors of organic evolution. Open Court Publishing Company, Chicago.
Curry Rogers, K. 2009. The postcranial osteology of *Rapetosaurus krausei* (Sauropoda: Titanosauria) from the Late Cretaceous of Madagascar. Journal of Vertebrate Paleontology 29:1046–1086.
Delfino, M., and C. Dal Sasso. 2006. Marine reptiles (Thalattosuchia) from the Early Jurassic of Lombardy (northern Italy). Geobios 39:346–354.
D'Emic, M. D. 2012. The early evolution of titanosauriform sauropod dinosaurs. Zoological Journal of the Linnean Society 166:624–671.
D'Emic, M. D., and J. A. Wilson. 2011. New remains attributable to the holotype of the sauropod dinosaur *Neuquensaurus australis*, with implications for saltasaurine systematics. Acta Palaeontologica Polonica 56:61–73.
D'Emic, M. D., J. A. Wilson, and R. Thompson. 2010. The end of the sauropod dinosaur hiatus in North America. Palaeogeography, Palaeoclimatology, Palaeoecology 297:486–490.
Fish, F. E., S. A. Bostic, A. J. Nicastro, and J. T. Beneski. 2007. Death roll of the alligator: mechanics of twist feeding in water. Journal of Experimental Biology 210:2811–2818.
Flower, W. H. 1885. An introduction to the osteology of the Mammalia, 3rd edition. MacMillan and Company, London.
Frey, E., and S. Salisbury. 2001. The kinematics of aquatic locomotion in *Osteolaemus tetraspis* Cope. Pp. 165–179 *in* G. C. Grigg, F. Seebacher, and C. E. Franklin, eds. Crocodilian biology and evolution. Surrey Beatty and Sons, Chipping Norton, U.K.
Gaffney, E. S. 1975. A phylogeny and classification of the higher categories of turtles. Bulletin of the American Museum of Natural History 155:387–436.
Gatesy, S. M. 1991. Caudofemoral musculature and the evolution of theropod locomotion. Paleobiology 16:170–186.

Gauthier, J. A. 1986. Saurischian monophyly and the origin of birds. *In* K. Padian, ed. The origin of birds and the evolution of flight. Memoirs of the California Academy of Sciences 8:1–55.
Gilmore, C. W. 1946. Reptilian fauna of the North Horn Formation of central Utah. Geological Survey Professional Paper 210-C:29–51.
Hatcher, J. B. 1901. *Diplodocus* (Marsh): its osteology, taxonomy, and probable habits, with a restoration of the skeleton. Memoirs of the Carnegie Museum 1:1–63.
———. 1903. Osteology of *Haplocanthosaurus*, with description of a new species, and remarks on the probable habits of the Sauropoda and the age and origin of the *Atlantosaurus* beds. Memoirs of the Carnegie Museum 2:1–72.
Hay, O. P. 1908. The fossil turtles of North America. Carnegie Institution of Washington, Publication 75:1–568.
He, X., C. Wang, S. Liu, F. Zhou, T. Liu, K. Cai, and B. Dai. 1998. [A new species of sauropod from the Early Jurassic of Gongxian Co., Sichuan.] Acta Geologica Sichuan 18:1–6.
Hoffstetter, R., and J.-P. Gasc. 1969. Vertebrae and ribs of modern reptiles. Pp. 201–310 *in* C. Gans, ed. Biology of the Reptilia. Academic Press, London.
Horner, J. R., D. B. Weishampel, and C. A. Forster. 2004. Hadrosauridae. Pp. 438–463 *in* Weishampel et al. 2004.
Huang, R. C., F. P. Girardi, F. P. Cammisa, Jr., and T. M. Wright. 2003. The implications of constraint in lumbar total disc replacement. Journal of Spinal Disorders and Techniques 16:412–417.
Huene, F. v. 1907-1908. Die Dinosaurier der Europäischen Triasformation mit Berücksichtigung der aussereuropäischen Vorkommnisse. Geologische und Palæontologische Abhandlungen (Suppl. 1):1–419.
Janensch, W. 1950. Die Wirbelsäule von *Brachiosaurus brancai*. Palaeontographica (Suppl. 7):27–93.
Kellner, A. W. A., and Y. Tomida. 2000. Description of a new species of Anhangueridae (Pterodactyloidea) with comments on the pterosaur fauna from the Santana Formation (Aptian-Albian), northeastern Brazil. National Science Museum Monographs 17:1–135.
Kluge, A. G. 1967. Higher taxonomic categories of gekkonid lizards and their evolution. Bulletin of the American Museum of Natural History 135:1–60.
Lehman, T. M., F. W. McDowell, and J. N. Connelly. 2006. First isotopic (U-Pb) age for the Late Cretaceous *Alamosaurus* vertebrate fauna of west Texas, and its significance as a link between two faunal provinces. Journal of Vertebrate Paleontology 26:922–928.
Lydekker, R. 1893. The dinosaurs of Patagonia. Anales del Museo de La Plata 2:1–14.
Mannion, P. D., and J. O. Calvo. 2011. Anatomy of the basal titanosaur (Dinosauria, Sauropoda) *Andesaurus delgadoi* from the mid-Cretaceous (Albian–early Cenomanian) Río Limay Formation, Neuquén Province, Argentina: implications for titanosaur systematics. Zoological Journal of the Linnean Society 163:155–181.
McIntosh, J. S. 1990. Species determination in sauropod dinosaurs with tentative suggestions for their classification. Pp. 53–69 *in* K. Carpenter and P. J. Currie, eds. Dinosaur systematics: approaches and perspectives. Cambridge University Press, U.K.
McPhee, B. W., A. M. Yates, J. N. Choiniere, and F. Abdala. 2014. The complete anatomy and phylogenetic relationships of *Antetonitrus ingenipes* (Sauropodiformes, Dinosauria): implications for the origins of Sauropoda. Zoological Journal of the Linnean Society 171:151–205.

Molnar, J. L., S. E. Pierce, and J. R. Hutchinson. 2014. An experimental and morphometric test of the relationship between vertebral morphology and joint stiffness in Nile crocodiles (*Crocodylus niloticus*). Journal of Experimental Biology 217:758–768.

Müller, J., T. M. Scheyer, J. J. Head, P. M. Barrett, I. Werneburg, P. G. P. Ericson, D. Pol, and M. R. Sánchez-Villagra. 2010. Homeotic effects, somitogenesis and the evolution of vertebral numbers in recent and fossil amniotes. PNAS 107:2118–2123.

Nascimento, P. M., and H. Zaher. 2010. A new species of *Baurusuchus* (Crocodyliformes, Mesoeucrocodylia) from the Upper Cretaceous of Brazil, with the first complete postcranial skeleton described for the family Baurusuchidae. Papéis Avulsos de Zoologia 50:323–361.

Noble, G. K. 1922. The phylogeny of the Salientia. Bulletin of the American Museum of Natural History 46:1–87.

Nobre, P. H., and I. S. Carvalho. 2013. Postcranial skeleton of *Mariliasuchus amarali* Carvalho and Bertini, 1999 (Mesoeucrocodylia) from the Bauru Basin, Upper Cretaceous of Brazil. Ameghiniana 50:98–113.

Nopcsa, F. 1930. Über prozöle und opisthozöle Wirbel. Anatomische Anzeiger 69:19–25.

Norman, D. B. 2004. Basal Iguanodontia. Pp. 413–437 *in* Weishampel et al. 2004.

Norman, D. B., H.-D. Sues, L. M. Witmer, and R. A. Coria. 2004. Basal Ornithopoda. Pp. 393–412 *in* Weishampel et al. 2004.

Olsen, P. E. 1979. A new aquatic eosuchian from the Newark Supergroup (Late Triassic-Early Jurassic) of North Carolina and Virginia. Postilla 176:1–14.

Osborn, H. F., and C. C. Mook. 1921. *Camarasaurus*, *Amphicœlias*, and other sauropods of Cope. Memoirs of the American Museum of Natural History 3:247–387.

Ouyang, H., and Y. Ye. 2002. The first mamenchisaurian skeleton with complete skull *Mamenchisaurus youngi*. Sichuan Scientific and Technology Publications, Sichuan, China.

Owen, R. 1836. Aves. Pp. 265–357 *in* R. B. Todd, ed. The cyclopædia of anatomy and physiology. Marchant, London.

———. 1859a. Monograph on the fossil Reptilia of the Cretaceous formations. Supplement No. I. Pterosauria (*Pterodactylus*). Paleontographical Society, London:1–19.

———. 1859b. On the orders of fossil and recent Reptilia, and their distribution in time. Report of the British Association for the Advancement of Science 29:153–166.

———. 1866a. On the anatomy of vertebrates. Vol. I. Fishes and reptiles. Longmans, Green, and Co., London.

———. 1866b. On the anatomy of vertebrates. Vol. II. Birds and mammals. Longmans, Green, and Co., London.

Pol, D. 2005. Postcranial remains of *Notosuchus terrestris* Woodward (Archosauria: Crocodyliformes) from the upper Cretaceous of Patagonia, Argentina. Ameghiniana 42:1–36.

Pol, D., and J. E. Powell. 2007. New information on *Lessemsaurus sauropoides* (Dinosauria: Sauropodomorpha) from the Upper Triassic of Argentina. Special Papers in Palaeontology 77:223–243.

Powell, J. E. 1992. Osteologia de *Saltasaurus loricatus* (Sauropoda-Titanosauridae) del Cretácico Superior del Noroeste Argentino. Pp. 166–230 *in* J. L. Sanz and A. D. Buscalioni, eds. Los dinosaurios y su entorno biotico. Instituto “Juan de Valdés”, Cuenca, Spain.

———. 2003. Revision of South American titanosaurid dinosaurs: palaeobiological, palaeobiogeographical and phylogenetic aspects. Records of the Queen Victoria Museum 111:1–173.
Pritchard, A. C., A. H. Turner, S. J. Nesbitt, R. B. Irmis, and N. D. Smith. 2015. Late Triassic tanystropheids (Reptilia, Archosauromorpha) from northern New Mexico (Petrified Forest Member, Chinle Formation) and the biogeography, functional morphology, and evolution of Tanystropheidae. Journal of Vertebrate Paleontology 35:e911186-1–20.
Raath, M. A. 1972. Fossil vertebrate studies in Rhodesia: a new dinosaur (Reptilia: Saurischia) from near the Trias-Jurassic boundary. Arnoldia 5:1–37.
Reese, A. M. 1915. The alligator and its allies. G. P. Putnam's Sons, New York.
Renous, S., J.-P. Gasc, V. L. Bels, and R. Wicker. 2002. Asymmetrical gaits of juvenile *Crocodylus johnstoni*, galloping Australian crocodiles. Journal of Zoology (London) 256:311–325.
Riggs, E. S. 1903. Structure and relationships of opisthocœlian dinosaurs. Part I. *Apatosaurus* Marsh. Field Columbian Museum, Geological Series 2:165–196.
Romer, A. S. 1956. Osteology of the reptiles. University of Chicago Press.
Salgado, L., R. A. Coria, and J. O. Calvo. 1997. Evolution of titanosaurid sauropods I: phylogenetic analysis based on the postcranial evidence. Ameghiniana 34:3–32.
Salisbury, S. W., and E. Frey. 2001. A biomechanical transformation model for the evolution of semi-spheroidal articulations between adjoining vertebral bodies in crocodilians. Pp. 85–134 *in* G. C. Grigg, F. Seebacher, and C. E. Franklin, eds. Crocodilian biology and evolution. Surrey Beatty and Sons, Chipping Norton, U.K.
Salisbury, S. W., R. E. Molnar, E. Frey, and P. M. A. Willis. 2006. The origin of modern crocodyliforms: evidence from the Cretaceous of Australia. Proceedings of the Royal Society B 273:2439–2448.
Schilling, N. 2011. Evolution of the axial system in craniates. Frontiers in Zoology 8:1–19.
Schwarz, D., E. Frey, and C. A. Meyer. 2007. Pneumaticity and soft-tissue reconstructions in the neck of diplodocid and dicraeosaurid sauropods. Acta Palaeontologica Polonica 52:167–188.
Sereno, P. C., R. N. Martinez, J. A. Wilson, D. J. Varricchio, O. A. Alcober, and H. C. E. Larsson. 2008. Evidence for avian intrathoracic air sacs in a new predatory dinosaur from Argentina. PLoS ONE 3:1–20.
Sereno, P. C., R. N. Martínez, and O. A. Alcober. 2012. Osteology of *Eoraptor lunensis* (Dinosauria, Sauropodomorpha). Society of Vertebrate Paleontology Memoir 12:83–179.
Slijper, E. J. 1946. Comparative biologic-anatomical investigations on the vertebral column and spinal musculature of mammals. Verhandelingen der Koninklijke Nederlandsche Akademie van Wetenschappen, Afdeling Natuurkunde 2:1–128.
Smith, D. K. 2015. Craniocervical myology and functional morphology of the small-headed therizinosaurian theropods *Falcarius utahensis* and *Nothronychus mckinleyi*. PLoS ONE 10:1–16.
Sullivan, W. E. 1922. The function of articular discs. The Anatomical Record 24:49–53.
Troxell, E. L. 1925. Mechanics of crocodile vertebræ. Bulletin of the Geological Society of America 36:605–614.
Upchurch, P., P. M. Barrett, and P. Dodson. 2004. Sauropoda. Pp. 259–322 *in* Weishampel et al. 2004.

van Heerden, J. 1979. The morphology and taxonomy of *Euskelosaurus* (Reptilia: Saurischia; Late Triassic) from South Africa. Navorsinge van die Nasionale Museum 4:21–84.
Virchow, H. 1914. Über die Alligatorwirbelsäule. Archiv für Anatomie und Physiologie Anatomische Abteilung 1914:103–142.
Wedel, M. J., and R. K. Sanders. 2002. Osteological correlates of cervical musculature in Aves and Sauropoda (Dinosauria: Saurischia), with comments on the cervical ribs of *Apatosaurus*. PaleoBios 22:1–6.
Weishampel, D. B., P. Dodson, and H. Osmólska, eds. 2004. The Dinosauria, 2nd edition. University of California Press, Berkeley.
Werneburg, I., J. K. Hinz, M. Gumpenburger, V. Volpato, N. Natchev, and W. G. Joyce. 2014. Modeling neck mobility in fossil turtles. Journal of Experimental Zoology Part B: Molecular and Developmental Evolution 324:230–243.
Werneburg, I., L. A. B. Wilson, W. C. H. Parr, and W. G. Joyce. 2015. Evolution of neck vertebral shape and neck retraction at the transition to modern turtles: an integrated geometric morphometric approach. Systematic Biology 64:187–204.
Whitlock, J. A. 2011. A phylogenetic analysis of Diplodocoidea (Saurischia: Sauropoda). Zoological Journal of the Linnean Society 161:872–915.
Williams, E. E. 1950. Variation and selection in the cervical central articulations of living turtles. Bulletin of the American Museum of Natural History 94:505–562.
Wilson, J. A. 2002. Sauropod dinosaur phylogeny: critique and cladistic analysis. Zoological Journal of the Linnean Society 136:217–276.
———. 2006. Anatomical nomenclature of fossil vertebrates: standardized terms or 'lingua franca'? Journal of Vertebrate Paleontology 26:511–518.
Wilson, J. A., and M. T. Carrano. 1999. Titanosaurs and the origin of "wide-gauge" trackways: a biomechanical and systematic perspective on sauropod locomotion. Paleobiology 25:252–267.
Wilson, J. A., and P. C. Sereno. 1998. Early evolution and higher-level phylogeny of sauropod dinosaurs. Society of Vertebrate Paleontology Memoir 5:1–68.
Wilson, J. A., R. N. Martinez, and O. Alcober. 1999. Distal tail segment of a titanosaur (Dinosauria: Sauropoda) from the Upper Cretaceous of Mendoza, Argentina. Journal of Vertebrate Paleontology 19:591–594.
Witmer, L. M. 1995. The extant phylogenetic bracket and the importance of reconstructing soft tissues in fossils. Pp. 19–33 *in* J. Thomason, ed. Functional morphology in vertebrate paleontology. Cambridge University Press, New York.
Witzmann, F., D. Schwarz-Wings, O. Hampe, G. Fritsch, and P. Asbach. 2014. Evidence of spondyloarthropathy in the spine of a phytosaur (Reptilia: Archosauriformes) from the Late Triassic of Halberstadt, Germany. PLoS ONE 9:1–13.
Xing, L., T. Miyashita, J. Zhang, D. Li, Y. Ye, T. Sekiya, F. Wang, and P. Currie. 2015. A new sauropod dinosaur from the Late Jurassic of China and the diversity, distribution, and relationships of mamenchisaurids. Journal of Vertebrate Paleontology 35:e889701-1–17.
Yadagiri, P. 1988. A new sauropod *Kotasaurus yamanpalliensis* from Lower Jurassic Kota Formation of India. Journal of the Geological Society of India 11:102–127.
Yates, A. M. 2007. Solving a dinosaurian puzzle: the identity of *Aliwalia rex* Galton. Historical Biology 19:93–123.

Yates, A. M., and J. W. Kitching. 2003. The earliest known sauropod dinosaur and the first steps towards sauropod locomotion. Proceedings of the Royal Society of London B 270:1753–1758.

Young, C. C. 1954. On a new sauropod from Yiping, Szechuan, China. Scientia Sinica 3:491–504.

Zhang, Y. 1988. The Middle Jurassic sauropod fauna from Dashanpu, Zigong, Sichuan Vol. I: sauropod dinosaur (I): *Shunosaurus*. Sichuan Publishing House of Science and Technology, Chengdu, China.

Zhou, X., W. J. Sanders, and P. D. Gingerich. 1992. Functional and behavioral implications of vertebral structure in *Pachyaena ossifraga* (Mammalia, Mesonychia). Contributions from the Museum of Paleontology, University of Michigan 28:289–319.

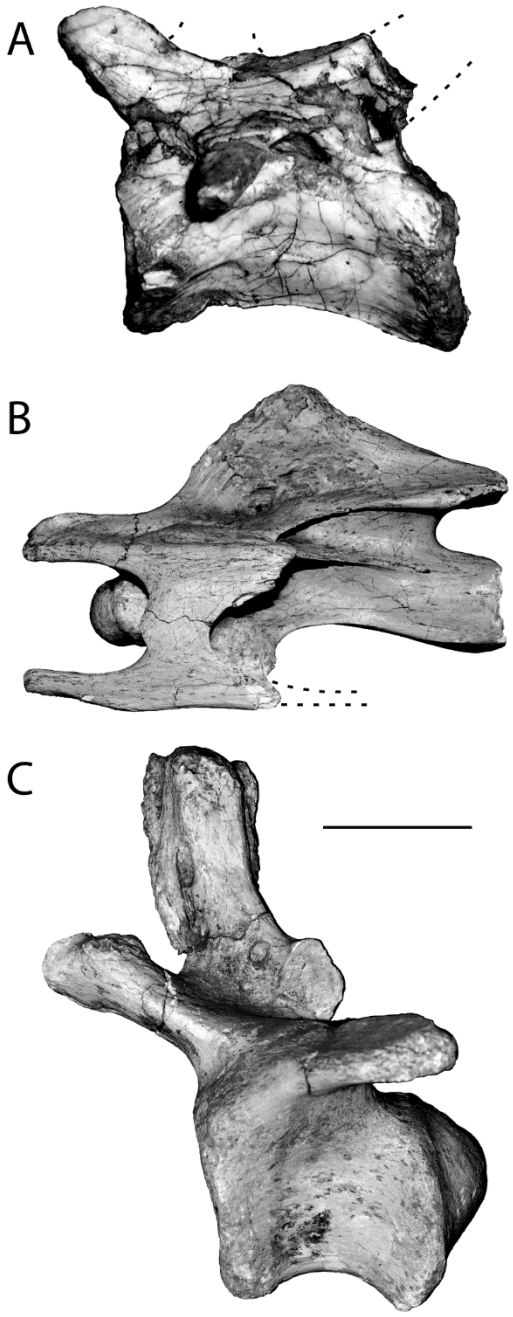

Figure 2.1. Centrum articular morphologies found in sauropodomorph vertebrae. **A**, amphicoelous cervical vertebra of the basal sauropodomorph *Saturnalia*; **B**, opisthocoelous cervical vertebra of the titanosaur sauropod *Trigonosaurus*; **C**, procoelous caudal vertebra of the titanosaur sauropod *Trigonosaurus*. Vertebrae are shown in left lateral view. Dashed lines indicate missing regions of vertebrae. Scale bar equals 1 cm for **A**, 10 cm for **B**, 5 cm for **C**.

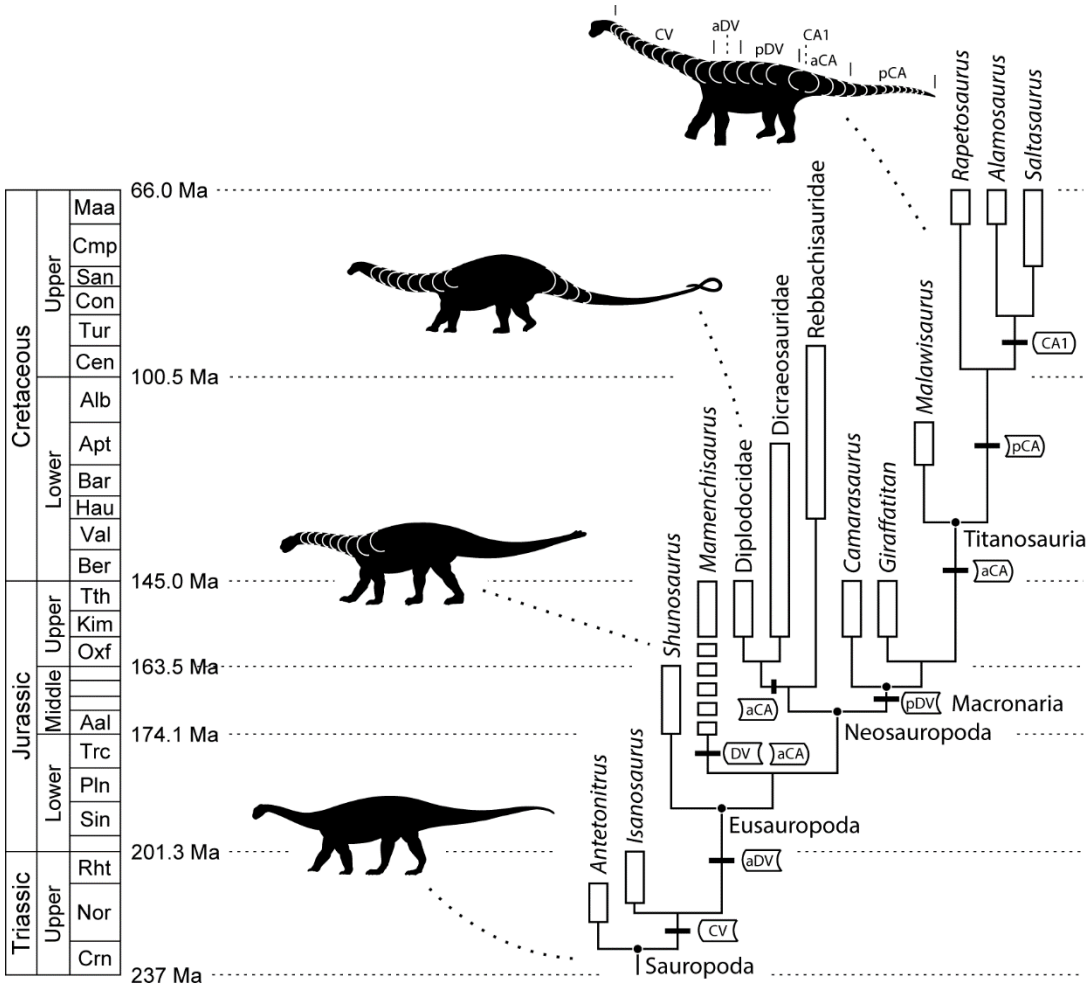

Figure 2.2. Time-calibrated phylogeny of sauropods showing the phylogenetic and serial distribution of opisthocoelous, procoelous, and biconvex centra, depicted as schematic centra in left lateral view. Topology follows the analyses of Wilson (2002) and Yates (2007) and is simplified for clarity. Sauropod silhouettes depict the serial distributions of opisthocoely and procoely for a basal sauropod, a basal eusauropod, a flagellicaudatan diplodocoid, and a lithostrotian titanosaur (outlines modified from Wilson and Sereno 1998). Temporal ranges are based on first and last occurrences reported in McPhee et al. (2014; *Antetonitrus*), Buffetaut et al. (2000; *Isanosaurus*), Chatterjee and Zheng (2002; *Shunosaurus*, *Mamenchisaurus*), Ouyang and Ye (2002; *Mamenchisaurus*), Whitlock (2011; Diplodocidae, Dicraeosauridae, Rebbachisauridae), D'Emic (2012; *Camarasaurus*, *Giraffatitan*, *Malawisaurus*), Curry Rogers (2009; *Rapetosaurus*), Lehman et al. (2006; *Alamosaurus*), D'Emic et al. (2010; *Alamosaurus*), and Powell (1992; *Saltasaurus*). Broken bars for *Mamenchisaurus* indicate uncertainty in the temporal range of the taxon. Time scale follows Cohen et al. (2013) with absolute ages in Ma. Abbreviations: **a**, anterior; **CA**, caudal centra; **CA1**, first caudal centrum; **CV**, cervical centra; **DV**, dorsal centra; **p**, posterior.

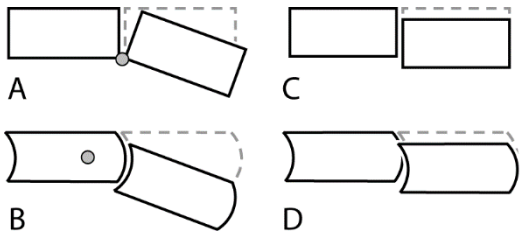

Figure 2.3. Schematic showing the behavior of amphiplatyan (**A**, **C**) and concavo-convex (**B**, **D**) centra in rotation (**A**, **B**) and translation (**C**, **D**). The centrum at left is fixed, and force is applied to the centrum at right. Note the impingement of the cotylar rim on the condyle in **D**. Gray dashed lines indicate the original position of the moving centrum; gray circles in **A** and **B** indicate the approximate position of the center of rotation.

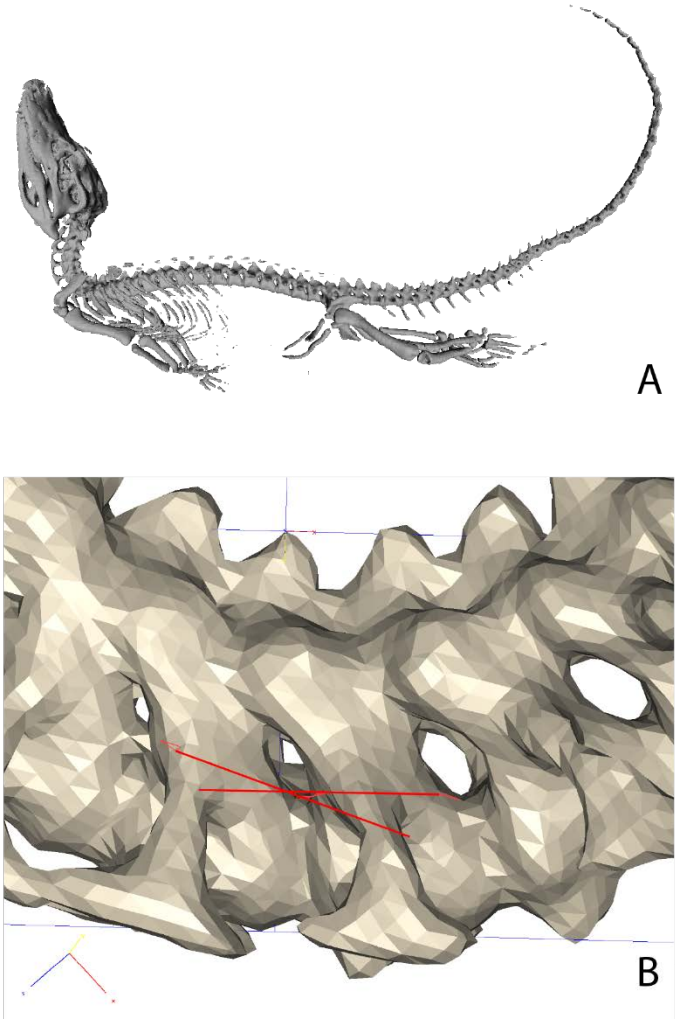

Figure 2.4. CT scans were used to calculate the range of motion on the intervertebral joints of *Alligator mississippiensis* (UMMP R1720). **A**, digital reconstruction of the skeleton of UMMP R1720 segmented from CT scans of the specimen in left lateral view at maximum dorsal hyperextension. **B**, detail of 6th and 7th cervical vertebrae in left lateral view showing how the angle between vertebrae was measured. Red lines indicate the floor of the neural canal, used as a consistent reference line.

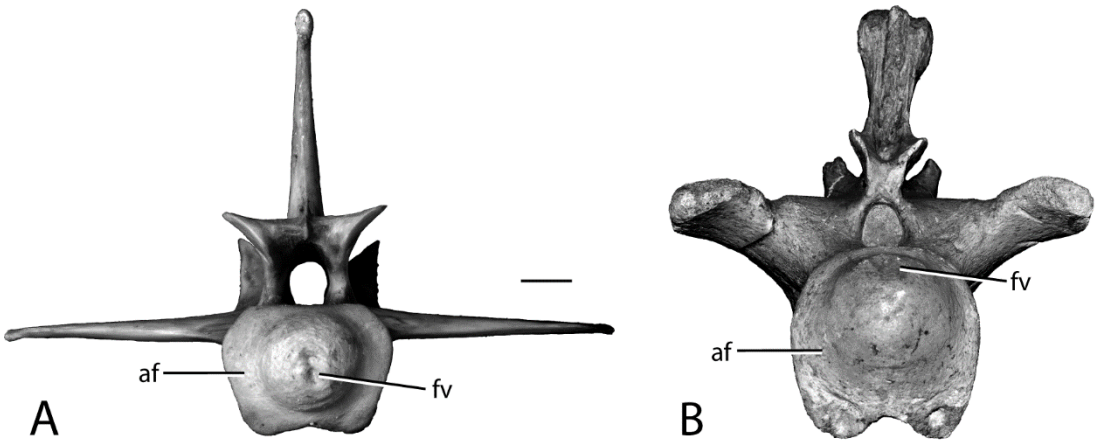

Figure 2.5. Osteological correlates of synovial intercentral joints in a crocodylian (**A**) and a sauropod (**B**) caudal vertebra. Note the flattened condylar margin for attachment of the annulus fibrosus (**af**) and the fovea condyli for attachment of the septum intercorporale (**fv**). **A**, 7th caudal vertebra of *Crocodylus acutus* (FMNH 22030) in posterior view. **B**, 6th caudal vertebra of the titanosaur *Baurutitan britoi* (MCT 1490-R) in posterior view. Scale bar equals 1 cm for **A**, 2 cm for **B**.

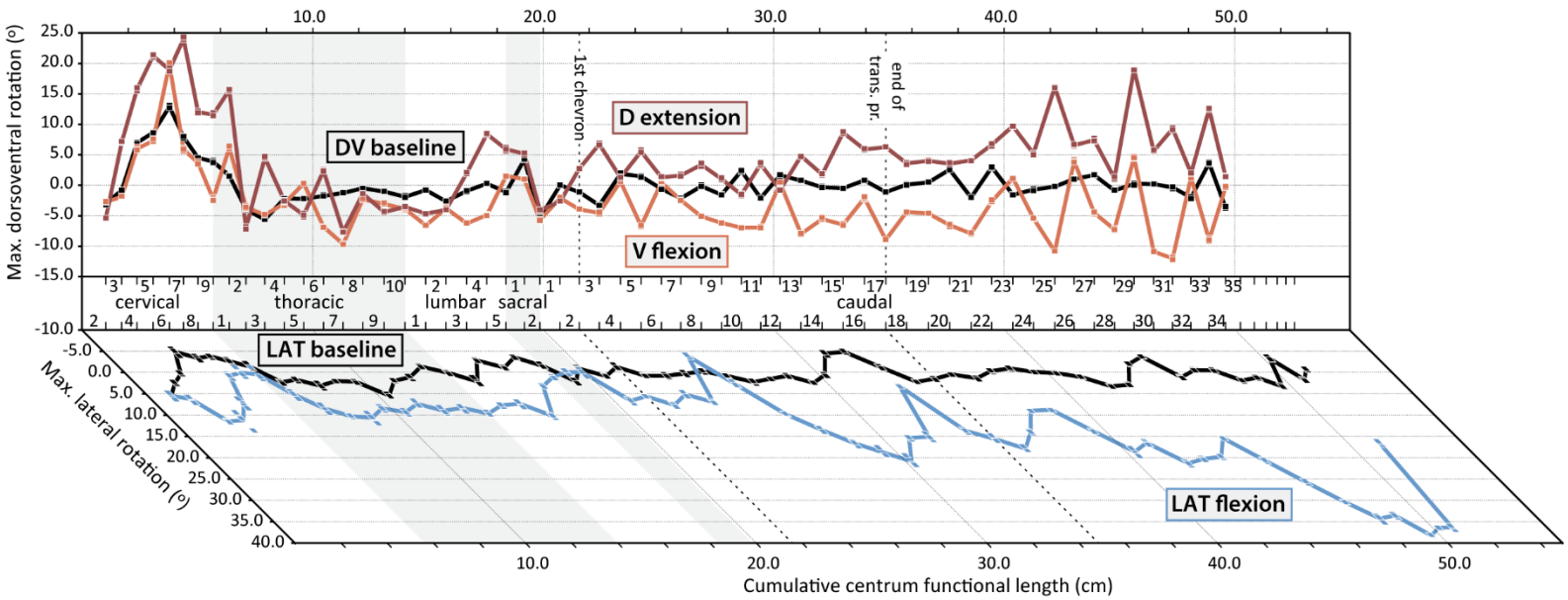

Figure 2.6. Measured intervertebral angles in *Alligator mississippiensis* (UMMP R1720) under dorsoventral (upper panel) and lateral (lower panel) rotation. The lower panel has been angled to give the illusion that it is extending out of the plane of the page, orthogonal to the upper panel. Note that the range of motion (indicated by the difference between the greatest and least angles of rotation for a given intervertebral joint) is greatest in the posterior caudal region. The black lines represent the baseline condition, before force was applied to the carcass, to which can be compared maximum dorsiflexion (dark red), ventriflexion (light red), and lateral flexion (blue). Lateral flexion represents a one-sided value (i.e., flexion to the right side). Squares represent three replicates for each measurement; trend lines connect mean values among replicates. The x-axis depicts both serial position along the column (shown as scaled boxes) and absolute length (tick marks). Abbreviations: **D**, dorsal; **DV**, dorsoventral; **LAT**, lateral; **V**, ventral.

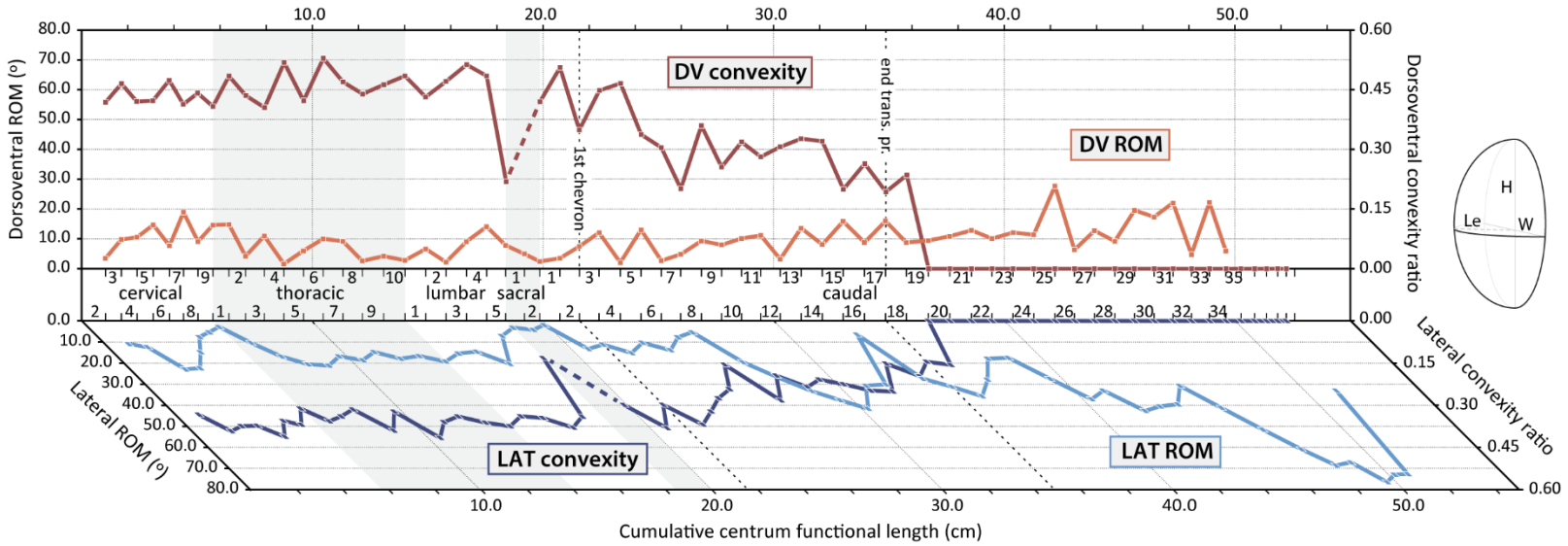

Figure 2.7. Measured range of motion and vertebral condyle convexity of the intervertebral joints of *Alligator mississippiensis* (UMMP R1720) in dorsoventral (upper panel) and lateral (lower panel) planes. The lower panel has been angled to give the illusion that it is extending out of the plane of the page, orthogonal to the upper panel. Note that convexity values are highest in regions where flexibility is low, and they are lowest in the region of greatest flexibility. The x-axis depicts both serial position along the column (shown as scaled boxes) and absolute length (tick marks). Dashed lines in sacral region indicate a fused intervertebral joint for which convexity is not applicable. Schematic at right depicts measurements used to calculate convexity. Dorsoventral convexity = length (**Le**) / height (**H**); lateral convexity = length (**Le**) / width (**W**). Abbreviations: **DV**, dorsoventral; **H**, height; **LAT**, lateral; **Le**, length; **W**, width.

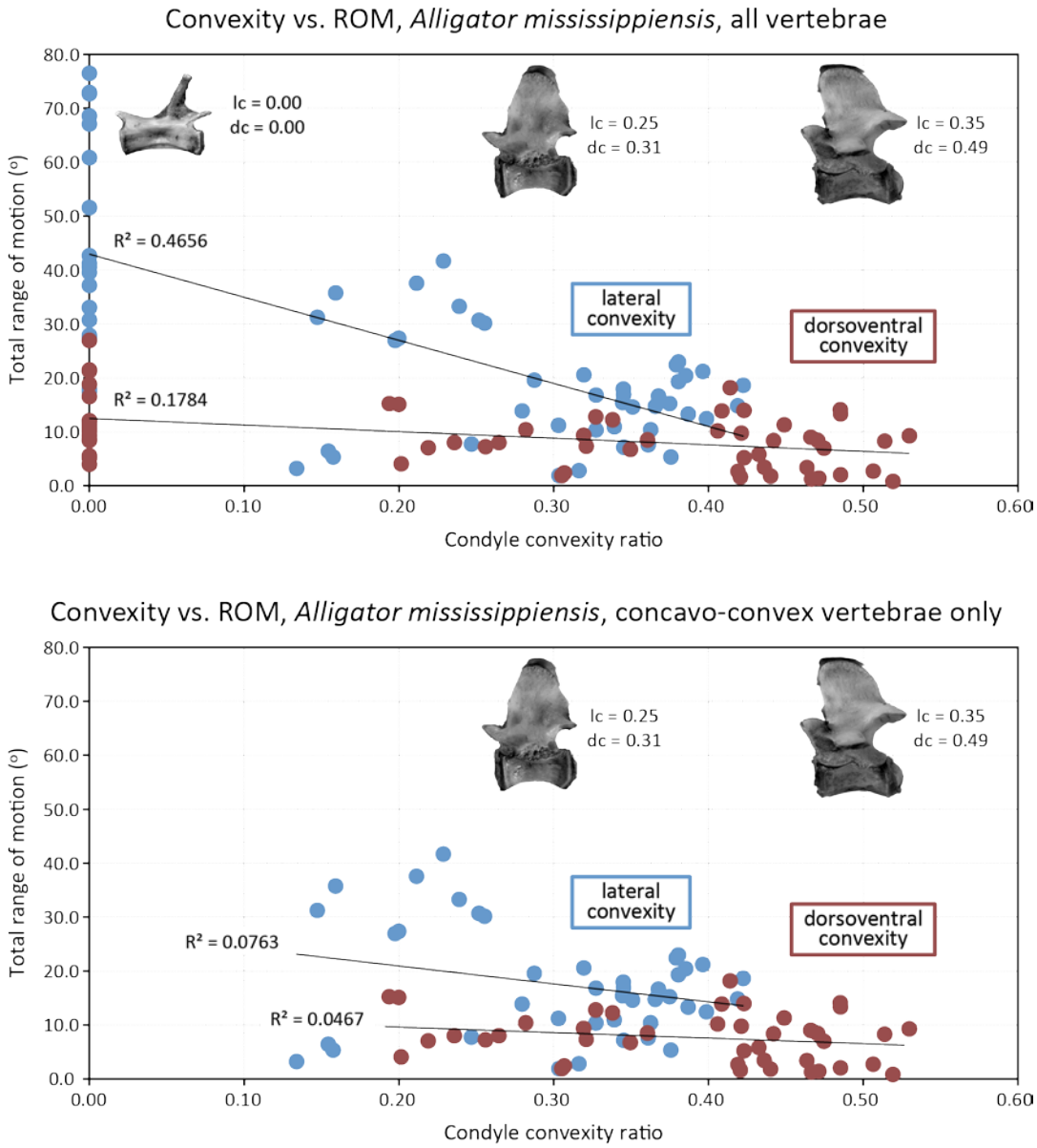

Figure 2.8. Relationship between convexity and range of motion in *Alligator mississippiensis* (UMMP R1720) for the dorsoventral (red) and lateral (blue) dimensions. Black lines show linear regressions for each dimension. With amphiplatyan distal caudal vertebrae 19–40 included (upper panel), a negative relationship is observed that is strongest in the lateral direction. When the amphiplatyan distal caudal vertebrae are excluded (lower panel), the relationship is negligible. Vertebrae depicted are the 26th caudal vertebra (left), the 6th caudal vertebra (middle), and the 4th lumbar vertebra (right) of UMMP R1720 shown in left lateral view, not to scale. Abbreviations: **dc**, dorsoventral convexity; **lc**, lateral convexity.

Table 2.1. Vertebrate clades other than Sauropoda exhibiting concavo-convex vertebral centra. Distribution of opisthocoely and procoely are indicated by vertebral region. Expanded from Nopcsa (1930). The listing is not intended to be exhaustive. Abbreviations: **amph**, amphiplatyan.

TAXON			**Cervical**	**Dorsal**
Osteichthyes				
	Holostei			
		Lepisosteus	N/A	Opisthocoelous
Lissamphibia				
	Anura			
		Most	Procoelous	Procoelous
		Discoglossidae	Opisthocoelous	Opisthocoelous
		Pipa	Opisthocoelous	Opisthocoelous
	Urodeles			
		Salamandrina	Opisthocoelous	Opisthocoelous
Sauropsida				
	Testudines		Opisthocoelous, biconvex, procoelous	Fused, procoelous
	Protorosauria			
		Some tanystropheids	Procoelous	Procoelous
	Squamata		Procoelous	Procoelous
	Pterosauria		Procoelous	Procoelous
	Crocodylomorpha			
		Junggarsuchus	Procoelous	Procoelous
	Crocodyliformes			
		Isisfordia	Procoelous	Procoelous
		Pietraroiasuchus	Procoelous	Procoelous
		Crocodylia	Procoelous	Procoelous
	Ornithischia			
		Basal ornithopods	Opisthocoelous to amphiplatyan	Amphiplatyan
		Basal iguanodontia	Opisthocoelous	Opisthocoelous to amph.
		Hadrosauridae	Opisthocoelous	1st opisthocoelous, amph.
	Theropoda			
		Tetanurae	Opisthocoelous	Opisthocoelous to amph.
		Aves	Heterocoelous	Opisthocoelous to amph.
Mammalia				
	Cetartiodactyla			
		Non-cetaceans	Opisthocoelous	Amphiplatyan
	Perissodactyla		Opisthocoelous	Amphiplatyan
	Mesonychia			
		Pachyaena	Opisthocoelous	Amphiplatyan
	Carnivora			
		Canidae	Opisthocoelous	Amphiplatyan

Table 2.1. (cont.)

Caudal	Additional references	Comments
Opisthocoelous	Cameron 1974	Ginglymode condyles
N/A	Noble 1922	
N/A	Noble 1922	
N/A	Owen 1866a	
Opisthocoelous	Owen 1866a	
Procoelous	Williams 1950; Hoffstetter & Gasc 1969	absent in basal forms, e.g., Gaffney 1975
Procoelous	Olsen 1979; Pritchard et al., 2015	*Tanytrachelos* + *Langobardisaurus* clade
Procoelous	Romer 1956; Kluge 1967	Variable presence in gekkonids
Amph. to procoelous	Owen 1859a; Romer 1956; Kellner and Tomida 2000	
Unknown	Clark et al. 2004	
Procoelous	Salisbury et al. 2006	Weakly procoelous
Procoelous	Buscalioni et al. 2011	Biconvex first caudal centrum
Procoelous	Owen 1859b	Biconvex first caudal centrum
Amphiplatyan	Norman et al. 2004	Weakly opisthocoelous
Amphiplatyan	Norman 2004	Weakly to strongly opisthocoelous
Amphiplatyan	Horner et al. 2004	
Amphiplatyan	Benson 2010; Carrano et al. 2012	Opisthocoely may be lost, e.g., Smith 2015
Amph. to procoelous	Owen 1836; Beddard 1898; Baumel & Witmer 1993	
Amphiplatyan	Owen 1866b; Flower 1885	Weak in Suina, Hippopotamidae, Flower 1885
Amphiplatyan	Owen 1866b; Flower 1885	
Amphiplatyan	Zhou et al. 1992	
Amphiplatyan	pers obs, JAF	Weakly opisthocoelous

Table 2.2. Systems of nomenclature for concavo-convex intervertebral joints and vertebral centra. Terms in bold are those used in this paper. Symbols composed of parentheses represent schematic vertebra centra in left lateral view, such that **((** indicates a centrum that is anteriorly convex and posteriorly concave.

	Concavo-convex vertebral centrum types				
Name for concavo-convex joints	((	))	) (	( )	Author
Concavo-convex	**Opisthocoelous**	**Procoelous**	**Amphicoelous**	**Biconvex**	**Conventional "Romerian" terminology (sensu Wilson 2006)**
Ball-and-socket	"	"	"	"	e.g., Owen 1859; Troxell 1925; Romer 1956
Semispheroidal	"	"	"	"	Salisbury and Frey 2001
-	Convexo-concave	Concavo-convex	Concavo-concave	Convexo-convex	Hay 1908
-	Opisthocoelous, Prokyrt	Procoelous, Opisthokyrt	-	Amphikyrt	Virchow 1914
Konkavo-konvexen; konvexo-konkaven	Opisthozöl	Prozöl	-	Bikonvexer	Nopcsa 1930

Table 2.3. Measured angles and range of motion (ROM) between vertebral centra, *Alligator mississippiensis* (UMMP R1720). All measurements are in degrees. Positive values indicate angles dorsal to or right lateral to the baseline. Negative values indicate angles ventral to or left lateral to the baseline. Abbreviations: **Ca**, caudal; **Cv**, cervical; **L**, lumbar; **Meas**, replicate measurement; **ROM**, range of motion; **S**, sacral; **T**, thoracic.

	Ventral flexion				Dorsal hyperextension			
Joint	Meas 1	Meas 2	Meas 3	**Average**	Meas 1	Meas 2	Meas 3	**Average**
Cv2/3	-2.7	-2.8	-2.7	-2.7	-5.4	-5.4	-5.4	-5.4
Cv3/4	-2.0	-1.9	-1.8	-1.9	7.0	7.1	7.2	7.1
Cv4/5	6.3	5.9	5.8	6.0	15.8	15.5	16.0	15.8
Cv5/6	7.1	7.2	7.6	7.3	21.0	21.3	21.4	21.2
Cv6/7	19.5	19.9	20.1	19.8	18.9	19.2	18.7	18.9
Cv7/8	5.6	6.1	5.9	5.9	23.9	23.9	24.3	24.0
Cv8/9	3.6	3.9	3.5	3.7	12.2	11.9	11.9	12.0
Cv9/T1	-2.0	-2.3	-2.5	-2.3	11.5	11.9	11.4	11.6
T1/2	6.2	6.0	6.4	6.2	15.4	15.8	15.7	15.6
T2/3	-3.4	-3.8	-3.6	-3.6	-7.0	-6.8	-7.2	-7.0
T3/4	-4.9	-4.9	-4.8	-4.9	4.5	4.4	4.7	4.5
T4/5	-3.3	-2.9	-2.7	-3.0	-2.5	-2.6	-2.6	-2.6
T5/6	0.3	0.3	0.3	0.3	-5.2	-4.6	-4.9	-4.9
T6/7	-6.8	-6.8	-6.9	-6.8	2.4	2.5	2.3	2.4
T7/8	-9.6	-9.7	-9.7	-9.7	-7.6	-7.8	-7.7	-7.7
T8/9	-2.3	-2.4	-2.2	-2.3	-1.3	-1.4	-1.4	-1.4
T9/10	-3.2	-3.1	-2.9	-3.1	-4.4	-4.5	-4.3	-4.4
T10/L1	-3.9	-4.0	-3.8	-3.9	-3.6	-3.6	-3.5	-3.6
L1/2	-6.6	-6.6	-6.6	-6.6	-4.6	-4.6	-4.7	-4.6
L2/3	-3.9	-3.6	-3.8	-3.8	-4.1	-4.0	-4.0	-4.0
L3/4	-6.3	-6.3	-6.2	-6.3	2.0	1.9	2.1	2.0
L4/5	-4.8	-4.9	-5.0	-4.9	8.4	8.3	8.5	8.4
L5/S1	1.6	1.5	1.5	1.5	5.6	6.2	5.9	5.9
S1/S2	1.1	0.9	1.0	1.0	5.2	5.0	5.3	5.2
S2/Ca1	-5.7	-5.6	-5.8	-5.7	-4.0	-4.2	-4.0	-4.1
Ca1/2	-2.2	-2.1	-2.0	-2.1	-2.8	-2.7	-2.6	-2.7
Ca2/3	-4.0	-4.0	-3.9	-4.0	2.8	2.7	2.7	2.7
Ca3/4	-4.5	-4.7	-4.4	-4.5	6.7	6.9	6.6	6.7
Ca4/5	0.6	0.7	0.6	0.6	1.4	1.1	1.3	1.3
Ca5/6	-6.7	-6.8	-6.6	-6.7	5.8	5.4	5.4	5.5
Ca6/7	0.3	0.5	0.6	0.5	1.2	1.3	1.4	1.3
Ca7/8	-2.4	-2.4	-2.5	-2.4	1.8	1.5	1.5	1.6
Ca8/9	-5.2	-5.1	-5.1	-5.1	3.4	3.1	3.6	3.4
Ca9/10	-6.2	-6.1	-6.2	-6.2	1.0	0.9	1.2	1.0
Ca10/11	-7.0	-6.9	-7.0	-7.0	-1.4	-1.7	-1.5	-1.5
Ca11/12	-7.0	-6.8	-7.0	-6.9	3.2	3.4	3.7	3.4

Table 2.3. (cont.)

	Ventral flexion				Dorsal hyperextension			
Joint	Meas 1	Meas 2	Meas 3	**Average**	Meas 1	Meas 2	Meas 3	**Average**
Ca12/13	0.1	0.4	0.5	0.3	-0.7	-0.8	-0.8	-0.8
Ca13/14	-7.9	-8.1	-7.9	-8.0	4.9	4.8	4.7	4.8
Ca14/15	-5.7	-5.6	-5.3	-5.5	1.6	1.8	1.9	1.8
Ca15/16	-6.5	-6.3	-6.6	-6.5	8.6	8.5	8.8	8.6
Ca16/17	-2.3	-2.1	-1.9	-2.1	5.8	5.8	6.0	5.9
Ca17/18	-9.0	-8.9	-8.9	-8.9	6.3	6.2	6.3	6.3
Ca18/19	-4.4	-4.3	-4.4	-4.4	3.7	3.7	3.4	3.6
Ca19/20	-4.6	-4.7	-4.6	-4.6	4.0	4.1	3.9	4.0
Ca20/21	-6.4	-6.8	-6.4	-6.5	3.5	3.4	3.7	3.5
Ca21/22	-8.0	-8.0	-7.8	-7.9	4.2	4.1	4.0	4.1
Ca22/23	-2.8	-2.7	-2.4	-2.6	6.4	6.8	6.8	6.7
Ca23/24	1.2	1.2	1.1	1.2	9.8	9.6	9.7	9.7
Ca24/25	-5.5	-5.4	-5.4	-5.4	5.3	5.3	5.0	5.2
Ca25/26	-10.8	-10.9	-10.8	-10.8	16.2	16.1	16.0	16.1
Ca26/27	4.2	3.9	3.8	4.0	6.4	6.6	6.7	6.6
Ca27/28	-4.7	-4.5	-4.4	-4.5	7.2	7.7	7.3	7.4
Ca28/29	-7.4	-7.1	-7.3	-7.3	0.9	1.1	1.4	1.1
Ca29/30	4.7	4.4	4.5	4.5	19.1	19.0	18.9	19.0
Ca30/31	-10.9	-10.9	-10.9	-10.9	5.5	5.6	5.8	5.6
Ca31/32	-12.0	-11.8	-12.2	-12.0	9.3	9.4	9.1	9.3
Ca32/33	1.3	1.4	1.2	1.3	1.9	2.0	2.0	2.0
Ca33/34	-9.2	-8.7	-9.0	-9.0	12.4	12.4	12.6	12.5
Ca34/35	-0.4	-0.4	-0.2	-0.3	1.5	1.4	1.4	1.4
Ca35/36*				N/A				N/A
Ca36/37*				N/A				N/A
Ca37/38*				N/A				N/A
Ca38/39**				N/A				N/A
Ca39/40**				N/A				N/A

*Not resolved in scans of dorsal hyperextension and ventral flexion

**Not resolved in any scans

Table 2.3. (cont.)

	Baseline (dorsoventral)				Lateral flexion			
Joint	Meas 1	Meas 2	Meas 3	**Average**	Meas 1	Meas 2	Meas 3	**Average**
Cv2/3	-2.8	-3.1	-3.2	-3.0	5.4	6.3	4.7	5.5
Cv3/4	-0.8	-0.8	-0.8	-0.8	5.8	7.1	5.7	6.2
Cv4/5	7.1	7.0	6.8	7.0	11.3	11.4	11.7	11.5
Cv5/6	8.7	8.6	8.6	8.6	9.3	13.6	10.7	11.2
Cv6/7	12.9	13.1	12.7	12.9	7.7	8.4	6.1	7.4
Cv7/8	8.1	7.7	8.0	7.9	0.3	1.4	0.7	0.8
Cv8/9	4.5	4.5	4.5	4.5	1.0	-1.3	0.4	0.0
Cv9/T1	4.1	3.9	3.7	3.9	-1.3	1.5	1.0	0.4
T1/2	1.6	1.6	1.5	1.6	6.2	4.4	5.0	5.2
T2/3	-3.9	-4.1	-3.9	-4.0	8.3	7.5	9.5	8.4
T3/4	-5.7	-5.6	-5.6	-5.6	10.3	10.4	10.1	10.3
T4/5	-2.1	-2.2	-2.2	-2.2	9.5	11.9	10.4	10.6
T5/6	-2.2	-2.3	-2.2	-2.2	8.9	7.9	8.4	8.4
T6/7	-1.9	-1.6	-1.8	-1.8	9.8	8.8	9.3	9.3
T7/8	-1.3	-1.3	-1.2	-1.3	6.6	7.8	7.7	7.4
T8/9	-0.5	-0.5	-0.5	-0.5	9.6	8.1	9.2	9.0
T9/10	-1.0	-1.1	-1.0	-1.0	7.9	7.9	9.1	8.3
T10/L1	-1.7	-2.0	-2.0	-1.9	9.2	9.9	9.8	9.6
L1/2	-0.7	-0.9	-0.8	-0.8	7.6	8.0	7.5	7.7
L2/3	-2.6	-2.7	-2.6	-2.6	7.0	6.8	8.1	7.3
L3/4	-0.8	-1.1	-0.9	-0.9	10.6	9.9	10.1	10.2
L4/5	0.3	0.2	0.3	0.3	3.0	3.3	3.3	3.2
L5/S1	-1.2	-1.0	-1.2	-1.1	0.8	0.9	1.3	1.0
S1/S2	4.1	4.3	4.3	4.2	0.0	0.3	-0.5	-0.1
S2/Ca1	-5.5	-5.2	-5.4	-5.4	-0.8	-0.2	0.9	0.0
Ca1/2	0.0	0.0	0.0	0.0	7.2	6.2	6.5	6.6
Ca2/3	-1.1	-1.2	-1.1	-1.1	5.5	5.7	5.6	5.6
Ca3/4	-3.2	-3.4	-3.3	-3.3	7.3	7.5	8.0	7.6
Ca4/5	1.8	1.8	2.0	1.9	5.3	4.6	5.6	5.2
Ca5/6	1.6	1.5	1.3	1.5	6.7	7.0	7.1	6.9
Ca6/7	-0.6	-0.5	-0.7	-0.6	-3.8	-3.6	-4.2	-3.9
Ca7/8	-2.2	-2.1	-2.1	-2.1	2.0	3.1	2.9	2.7
Ca8/9	0.0	-0.3	-0.2	-0.2	9.9	9.8	9.6	9.8
Ca9/10	-1.6	-1.5	-1.6	-1.6	13.5	13.0	13.9	13.5
Ca10/11	2.5	2.2	2.4	2.4	16.2	17.3	16.4	16.6
Ca11/12	-2.1	-2.1	-2.1	-2.1	19.5	17.5	19.3	18.8

Table 2.3. (cont.)

	Baseline (dorsoventral)				Lateral flexion			
Joint	Meas 1	Meas 2	Meas 3	**Average**	Meas 1	Meas 2	Meas 3	**Average**
Ca12/13	1.5	1.7	1.7	1.6	19.4	21.4	21.7	20.8
Ca13/14	0.8	0.7	0.8	0.8	15.1	15.7	15.2	15.3
Ca14/15	-0.2	-0.4	-0.4	-0.3	15.8	14.2	15.2	15.1
Ca15/16	-0.5	-0.4	-0.5	-0.5	3.2	3.1	3.3	3.2
Ca16/17	0.8	0.8	0.8	0.8	13.3	14.1	13.6	13.7
Ca17/18	-1.2	-1.1	-1.1	-1.1	16.1	14.7	16.0	15.6
Ca18/19	0.1	0.2	0.0	0.1	18.2	18.1	17.3	17.9
Ca19/20	0.4	0.5	0.5	0.5	13.7	14.2	13.9	13.9
Ca20/21	2.7	2.5	2.5	2.6	9.0	8.9	9.0	9.0
Ca21/22	-2.0	-2.0	-2.0	-2.0	8.7	8.7	8.8	8.7
Ca22/23	3.1	2.8	3.0	3.0	13.6	13.6	13.9	13.7
Ca23/24	-1.5	-1.6	-1.6	-1.6	18.4	17.7	19.6	18.6
Ca24/25	-0.7	-0.6	-0.9	-0.7	16.1	16.5	16.9	16.5
Ca25/26	-0.3	-0.2	-0.2	-0.2	20.9	21.8	21.3	21.3
Ca26/27	1.0	1.1	1.0	1.0	20.0	20.3	20.5	20.3
Ca27/28	1.6	1.7	1.7	1.7	19.7	20.0	19.6	19.8
Ca28/29	-0.9	-0.9	-0.8	-0.9	15.3	15.3	15.5	15.4
Ca29/30	0.4	0.3	0.0	0.2	20.9	20.4	20.5	20.6
Ca30/31	0.2	0.2	0.2	0.2	25.9	26.0	25.4	25.8
Ca31/32	-0.2	-0.6	-0.3	-0.4	30.5	30.3	30.4	30.4
Ca32/33	-1.9	-1.9	-2.2	-2.0	35.2	33.6	34.0	34.3
Ca33/34	3.5	3.8	3.6	3.6	33.1	34.0	33.5	33.5
Ca34/35	-3.8	-3.8	-3.5	-3.7	38.4	38.2	38.1	38.2
Ca35/36*	-1.9	-1.9	-1.8	-1.9	36.6	36.3	36.4	36.4
Ca36/37*	2.3	2.3	2.3	2.3	36.9	36.2	35.9	36.3
Ca37/38*	6.5	6.6	6.7	6.6	17.0	16.4	16.1	16.5
Ca38/39**				N/A				N/A
Ca39/40**				N/A				N/A

*Not resolved in scans of dorsal hyperextension and ventral flexion

**Not resolved in any scans

Table 2.3. (cont.)

	Baseline (lateral)					
Joint	Meas 1	Meas 2	Meas 3	**Average**	**Dorsoventral ROM**	**Lateral ROM**
Cv2/3	5.1	5.7	5.4	5.4	2.7	10.9
Cv3/4	2.8	2.6	2.2	2.5	9.0	12.4
Cv4/5	0.5	0.4	0.0	0.3	9.8	22.9
Cv5/6	-5.6	-3.9	-5.1	-4.9	13.9	22.4
Cv6/7	-3.9	-3.4	-2.9	-3.4	6.9	14.8
Cv7/8	-3.5	-4.0	-3.9	-3.8	18.2	7.6
Cv8/9	-3.1	-2.2	-2.7	-2.7	8.3	5.3
Cv9/T1	-1.0	-2.2	-1.0	-1.4	13.9	2.8
T1/2	2.0	2.3	2.6	2.3	14.1	10.4
T2/3	1.6	2.0	1.5	1.7	3.4	16.9
T3/4	3.7	2.4	3.2	3.1	10.2	20.5
T4/5	2.1	2.0	2.0	2.0	0.8	21.2
T5/6	2.0	2.0	2.4	2.1	5.2	8.4
T6/7	5.6	5.0	5.6	5.4	9.2	18.6
T7/8	2.1	2.0	1.8	2.0	8.4	14.7
T8/9	1.5	1.0	0.8	1.1	1.8	17.9
T9/10	-1.6	-1.3	-1.3	-1.4	3.4	16.6
T10/L1	-0.2	0.0	0.3	0.0	2.0	19.3
L1/2	1.1	2.6	2.7	2.1	5.8	15.4
L2/3	-2.8	-3.0	-2.7	-2.8	1.4	14.6
L3/4	-1.2	-1.3	-1.0	-1.2	8.3	20.4
L4/5	-3.8	-3.4	-3.5	-3.6	13.3	7.1
L5/S1	-2.1	-1.3	-1.4	-1.6	7.0	3.2
S1/S2	2.1	1.7	2.5	2.1	4.2	4.2
S2/Ca1	-1.3	-1.0	-0.5	-0.9	1.6	1.9
Ca1/2	0.9	0.7	0.9	0.8	2.7	13.3
Ca2/3	-0.9	-1.9	-1.1	-1.3	6.7	11.2
Ca3/4	0.9	0.7	0.8	0.8	11.3	15.2
Ca4/5	1.1	0.4	0.8	0.8	1.2	10.3
Ca5/6	0.3	-0.1	0.6	0.3	12.2	13.9
Ca6/7	-0.2	0.0	-0.5	-0.2	1.9	7.7
Ca7/8	0.9	0.8	0.7	0.8	4.0	5.3
Ca8/9	2.6	2.2	1.9	2.2	8.5	19.5
Ca9/10	1.4	1.5	1.5	1.5	7.2	26.9
Ca10/11	0.8	0.6	1.0	0.8	9.3	33.3
Ca11/12	2.4	2.5	2.4	2.4	10.4	37.5

Table 2.3. (cont.)

	Baseline (lateral)					
Joint	Meas 1	Meas 2	Meas 3	**Average**	**Dorsoventral ROM**	**Lateral ROM**
Ca12/13	0.3	0.4	0.8	0.5	2.4	41.7
Ca13/14	-4.5	-4.0	-4.8	-4.4	12.8	30.7
Ca14/15	-4.8	-4.7	-5.1	-4.9	7.3	30.1
Ca15/16	-1.3	-1.5	-1.0	-1.3	15.1	6.4
Ca16/17	2.3	2.1	2.2	2.2	8.0	27.3
Ca17/18	1.4	1.3	1.7	1.5	15.2	31.2
Ca18/19	0.3	0.5	0.5	0.4	8.0	35.7
Ca19/20	1.2	1.2	1.6	1.3	8.6	27.9
Ca20/21	-0.1	-0.4	-0.5	-0.3	10.1	17.9
Ca21/22	-1.0	-0.8	-1.1	-1.0	12.0	17.5
Ca22/23	-0.1	-0.2	-0.1	-0.1	9.3	27.4
Ca23/24	0.3	0.0	0.2	0.2	11.3	37.1
Ca24/25	1.0	1.1	1.0	1.0	10.6	33.0
Ca25/26	3.3	3.1	3.3	3.2	26.9	42.7
Ca26/27	3.0	2.7	2.9	2.9	5.5	40.5
Ca27/28	-1.9	-1.9	-2.1	-2.0	11.9	39.5
Ca28/29	-3.7	-3.7	-3.8	-3.7	8.4	30.7
Ca29/30	0.9	1.1	1.3	1.1	18.8	41.2
Ca30/31	-0.5	-0.7	-0.5	-0.6	16.5	51.5
Ca31/32	-0.4	-0.7	-0.4	-0.5	21.3	60.8
Ca32/33	2.1	1.8	1.8	1.9	4.0	68.5
Ca33/34	1.0	1.4	1.2	1.2	21.4	67.1
Ca34/35	3.5	3.0	3.3	3.3	5.1	76.5
Ca35/36*	-3.8	-3.0	-3.1	-3.3	N/A	72.9
Ca36/37*	1.5	1.6	1.9	1.7	N/A	72.7
Ca37/38*	-0.7	-0.5	-0.9	-0.7	N/A	33.0
Ca38/39**				N/A	N/A	N/A
Ca39/40**				N/A	N/A	N/A

*Not resolved in scans of dorsal hyperextension and ventral flexion

**Not resolved in any scans

Table 2.4. Vertebral centrum dimensions and calculated condylar convexity values, *Alligator mississippiensis*. All measurements are in cm except for convexity ratios, which are unitless. Abbreviations: **ant**, anterior; **Ca**, caudal; **cuml**, cumulative; **Cv**, cervical; **DV**, dorsoventral; **func**, functional; **L**, lumbar; **LAT**, lateral; **post**, posterior; **S**, sacral; **T**, thoracic.

Position	Centrum length	Cotyle depth	Condyle length	Condyle width	Condyle height
Cv2	1.12	N/A	0.19	0.56	0.45
Cv3	0.77	0.09	0.23	0.58	0.49
Cv4	0.77	0.08	0.22	0.59	0.53
Cv5	0.78	0.10	0.22	0.58	0.52
Cv6	0.77	0.08	0.25	0.60	0.53
Cv7	0.71	0.07	0.22	0.60	0.52
Cv8	0.75	0.10	0.22	0.58	0.49
Cv9	0.78	0.12	0.19	0.59	0.46
T1	0.83	0.12	0.22	0.61	0.45
T2	0.88	0.14	0.19	0.56	0.44
T3	0.95	0.15	0.18	0.56	0.44
T4	0.96	0.13	0.22	0.56	0.43
T5	0.93	0.11	0.18	0.56	0.43
T6	0.97	0.09	0.24	0.56	0.45
T7	0.97	0.11	0.21	0.58	0.45
T8	0.98	0.12	0.20	0.57	0.45
T9	1.02	0.13	0.21	0.58	0.46
T10	1.00	0.10	0.22	0.59	0.46
L1	0.99	0.09	0.20	0.59	0.47
L2	0.99	0.09	0.22	0.63	0.47
L3	1.00	0.11	0.25	0.64	0.48
L4	0.98	0.10	0.22	0.65	0.46
L5	0.87	0.11	0.10	0.75	0.46
S1	0.79	0.03	N/A	N/A	N/A
S2	0.78	0.10	N/A	N/A	N/A
Ca1(ant)		N/A	0.20	0.67	0.48
Ca1(post)	0.98	N/A	0.26	0.66	0.51
Ca2	0.91	0.11	0.19	0.63	0.54
Ca3	0.94	0.07	0.22	0.59	0.49
Ca4	1.00	0.08	0.19	0.57	0.40
Ca5	0.95	0.08	0.16	0.56	0.46
Ca6	0.92	0.06	0.13	0.54	0.44
Ca7	0.92	0.04	0.09	0.55	0.43
Ca8	0.93	0.08	0.15	0.51	0.41
Ca9	0.89	0.03	0.11	0.54	0.42
Ca10	0.88	0.02	0.13	0.53	0.40
Ca11	0.88	0.02	0.11	0.52	0.39
Ca12	0.89	0.05	0.12	0.51	0.38

Table 2.4. (cont.)

Position	Centrum length	Cotyle depth	Condyle length	Condyle width	Condyle height
Ca13	0.93	0.04	0.12	0.48	0.37
Ca14	0.94	0.02	0.12	0.46	0.36
Ca15	0.91	0.00	0.07	0.45	0.35
Ca16	0.93	0.00	0.09	0.45	0.34
Ca17	0.92	0.00	0.06	0.43	0.33
Ca18	0.91	0.00	0.07	0.44	0.30
Ca19	0.95	0.00	0.00	0.42	0.32
Ca20	0.92	0.00	0.00	0.40	0.32
Ca21	0.93	0.00	0.00	0.40	0.31
Ca22	0.90	0.00	0.00	0.39	0.31
Ca23	0.91	0.00	0.00	0.37	0.29
Ca24	0.89	0.00	0.00	0.36	0.27
Ca25	0.92	0.00	0.00	0.35	0.26
Ca26	0.84	0.00	0.00	0.33	0.25
Ca27	0.87	0.00	0.00	0.32	0.24
Ca28	0.88	0.00	0.00	0.31	0.25
Ca29	0.85	0.00	0.00	0.28	0.22
Ca30	0.85	0.00	0.00	0.28	0.21
Ca31	0.82	0.00	0.00	0.25	0.20
Ca32	0.80	0.00	0.00	0.25	0.17
Ca33	0.78	0.00	0.00	0.22	0.18
Ca34	0.72	0.00	0.00	0.20	0.17
Ca35	0.65	0.00	0.00	0.16	0.15
Ca36	0.60	0.00	0.00	0.14	0.12
Ca37	0.51	0.00	0.00	0.12	0.12
Ca38	0.47	0.00	0.00	0.09	0.04
Ca39	0.38	0.00	0.00	0.08	0.09
Ca40	0.37	0.00	N/A	N/A	N/A

Table 2.4. (cont.)

Position	Func centrum length	Cuml func centrum length	LAT convexity	DV convexity
Cv2	1.12	1.12	0.34	0.42
Cv3	0.69	1.81	0.40	0.47
Cv4	0.68	2.49	0.38	0.42
Cv5	0.68	3.17	0.38	0.42
Cv6	0.69	3.86	0.42	0.47
Cv7	0.64	4.51	0.36	0.41
Cv8	0.65	5.15	0.38	0.44
Cv9	0.66	5.81	0.32	0.41
T1	0.72	6.53	0.36	0.49
T2	0.74	7.27	0.35	0.44
T3	0.79	8.06	0.32	0.41
T4	0.82	8.89	0.40	0.52
T5	0.83	9.71	0.33	0.42
T6	0.87	10.59	0.42	0.53
T7	0.86	11.45	0.37	0.47
T8	0.86	12.31	0.35	0.44
T9	0.89	13.20	0.37	0.46
T10	0.90	14.10	0.38	0.49
L1	0.91	15.01	0.34	0.43
L2	0.89	15.90	0.35	0.47
L3	0.89	16.79	0.39	0.51
L4	0.88	17.67	0.35	0.49
L5	0.76	18.43	0.13	0.22
S1	0.76	19.19	N/A	N/A
S2	0.67	19.87	N/A	N/A
Ca1(ant)		19.87	0.30	0.42
Ca1(post)	0.98	20.84	0.39	0.51
Ca2	0.81	21.65	0.30	0.35
Ca3	0.87	22.52	0.38	0.45
Ca4	0.92	23.44	0.33	0.47
Ca5	0.87	24.31	0.28	0.34
Ca6	0.87	25.18	0.25	0.31
Ca7	0.87	26.05	0.16	0.20
Ca8	0.85	26.90	0.29	0.36
Ca9	0.86	27.76	0.20	0.26
Ca10	0.86	28.63	0.24	0.32
Ca11	0.86	29.49	0.21	0.28
Ca12	0.84	30.33	0.23	0.31

Table 2.4. (cont.)

Position	Func centrum length	Cuml func centrum length	LAT convexity	DV convexity
Ca13	0.89	31.22	0.25	0.33
Ca14	0.92	32.13	0.26	0.32
Ca15	0.91	33.04	0.15	0.20
Ca16	0.93	33.97	0.20	0.26
Ca17	0.92	34.89	0.15	0.19
Ca18	0.91	35.80	0.16	0.24
Ca19	0.95	36.75	0.00	0.00
Ca20	0.92	37.66	0.00	0.00
Ca21	0.93	38.60	0.00	0.00
Ca22	0.90	39.49	0.00	0.00
Ca23	0.91	40.40	0.00	0.00
Ca24	0.89	41.30	0.00	0.00
Ca25	0.92	42.22	0.00	0.00
Ca26	0.84	43.06	0.00	0.00
Ca27	0.87	43.93	0.00	0.00
Ca28	0.88	44.81	0.00	0.00
Ca29	0.85	45.66	0.00	0.00
Ca30	0.85	46.51	0.00	0.00
Ca31	0.82	47.33	0.00	0.00
Ca32	0.80	48.13	0.00	0.00
Ca33	0.78	48.91	0.00	0.00
Ca34	0.72	49.63	0.00	0.00
Ca35	0.65	50.28	0.00	0.00
Ca36	0.60	50.88	0.00	0.00
Ca37	0.51	51.39	0.00	0.00
Ca38	0.47	51.86	0.00	0.00
Ca39	0.38	52.24	0.00	0.00
Ca40	0.37	52.61	N/A	N/A

CHAPTER 3

POLARITY OF CONCAVO-CONVEX INTERVERTEBRAL JOINTS IN THE NECKS AND TAILS OF SAUROPOD DINOSAURS

Abstract.—The highly elongated necks, and often tails, of sauropod dinosaurs are composed of concavo-convex vertebrae that provided stability without compromising mobility. Polarities of these concavo-convex joints in the neck and tail are anatomically opposite one another but mechanically equivalent. Opisthocoelous cervical vertebrae and procoelous caudal vertebrae have the convex articular face directed away from the body and the concave articular face directed towards the body. This "sauropod-type" polarity is hypothesized to be (1) more resistant to fracturing of the cotylar rim and (2) better stabilized against joint failure by rotation than the opposite polarity. We used physical models to test these two functional hypotheses. Photoelastic analysis of model centra loaded as cantilevers reveals that neither polarity better resists fracture of the cotylar rim; strain magnitude and localization are similar in both polarities. We assessed the rotational stability of concavo-convex joints using pairs of concavo-convex centra loaded near the joint. "Sauropod-type" joints withstood significantly greater weight before failure occurred, a pattern we interpret to be dependent on the position of the center of rotation, which is always within the convex part of the concavo-convex joint. In "sauropod-type" joints, the free centrum rotates about a center of rotation that lies within the more stable proximal centrum. In contrast, the opposite polarity results in a free centrum that rotates about an internal point; when the condyle rotates down and out of joint, the distal end rotates back toward the body, unopposed by ligamentous support. "Sauropod-type" joints remained stable with greater mobility, more mechanically-advantageous tensile element insertions, and greater distal loads than the opposite

polarity. The advantages conferred by this joint polarity may have facilitated the evolution of hyperelongated necks and tails by sauropods. Polarity of concavo-convex joints of the appendicular skeleton (e.g., hip, shoulder) may also be explained by rotational stability.

Introduction

Sauropod dinosaurs achieved the largest body sizes (Alexander 1989) and the longest necks of any terrestrial vertebrate (Taylor and Wedel 2013). The long necks and tails are hypothesized to have been held aloft (Coombs 1975) because trackways lack tail drag marks (e.g., Bird 1941). Sauropod necks and tails were loaded like cantilevers, beams supported at only one end (i.e., the body) and free at the other end. As a result, the forces of weight support were likely experienced as compression of the vertebral centra and tension of the muscles, tendons, and ligaments attaching to the neural arches, as in mammals (Slijper 1946) and extant reptiles (Hoffstetter and Gasc 1969). Unlike a rigid cantilevered beam, however, necks and tails are segmented, with joints between vertebrae held together in life by muscles, tendons, ligaments, and cartilage. Intervertebral joints permit mobility but are also potential sites of catastrophic dislocation. In order for sauropods to achieve their characteristic large body sizes and long necks, the intervertebral joints required stabilization against increasingly large stresses without compromising the extent of mobility required for survival. One way in which sauropod intervertebral joints may have been stabilized without compromising flexibility is by the evolution of concavo-convex centra (e.g., opisthocoely, procoely) in the neck and, in some lineages, in the tail (Fronimos and Wilson in review). Previous research on concavo-convex intervertebral joint function in crocodylians has suggested they resist dislocation by shear due to

the nesting of one centrum in another and the increased surface area of contact relative to planar joints (Salisbury and Frey 2001; Fronimos and Wilson in review).

The concavo-convex joints of the sauropod neck and tail show strong, conservative patterns in the polarization of the articular surfaces. Most vertebrae can be classified into two polarities, depending upon which end of the centrum bears the convex articulation (i.e., the condyle) and which the concave articulation (i.e., the cotyle). Opisthocoelous centra (Fig. 3.1A) have the condyle at the anterior end and the cotyle at the posterior end. Procoelous centra (Fig. 3.1B) have the reverse anatomical orientation, with the cotyle facing forward and the condyle facing backward. In sauropods, opisthocoely is characteristic of the presacral spine (Fig. 3.1C). Only the most basally diverging sauropods (i.e., *Antetonitrus*, *Lessemsaurus*, *Gongxianosaurus*) retain the ancestral condition of amphiplatyan (flat-ended) cervical centra, and these taxa are not known from complete cervical series. In all other sauropods, all postaxial cervical centra are invariantly opisthocoelous, as are at least some centra in the pectoral region (e.g., *Tazoudasaurus*, Allain et al. 2004; *Shunosaurus*, Zhang 1988). This pattern extends to the sacrum in macronarians (Wilson and Sereno 1998).

Procoelous anterior caudal vertebrae (Fig. 3.1C) evolved independently three or four times in sauropods, according to our current understanding of their interrelationships: (1) in the Late Jurassic basal eusauropod *Mamenchisaurus* (Young 1954; Xing et al. 2015); (2) within the diplodocoids (Calvo and Salgado 1995); (3) within the titanosaurs (McIntosh 1990; Wilson and Sereno 1998; Upchurch et al. 2004); and (4) in a tail of uncertain taxonomic position from the Late Jurassic of Tanzania (Bonaparte et al. 2000). In some Late Cretaceous titanosaurs, procoely extends to middle and distal caudal vertebrae (McIntosh 1990; Wilson 2002; Upchurch et al. 2004). Opisthocoelous anterior caudal vertebrae are known in only one sauropod, the titanosaur

Opisthocoelicaudia (Borsuk-Bialynicka 1977). Other patterns occurring in the first caudal vertebra and the distal caudal vertebrae are summarized in Fronimos and Wilson (in review).

Opisthocoelous cervical centra also occur in some theropod and ornithopod dinosaurs and many ungulates, and procoelous caudal vertebrae occur in crocodylians, squamates, and a few other reptiles. Cervical opisthocoely and caudal procoely occur together only in sauropods (see Nopcsa 1930: p. 19; Fronimos and Wilson in review; Table 2.1) and trionychid turtles (Williams 1950; Hoffstetter and Gasc 1969). Sauropods are distinct from the other taxa listed in that both the neck and tail are long, heavy cantilevers.

Although cervical opisthocoely and caudal procoely have the opposite anatomical orientation, they are mechanically equivalent; that is, in each case the concave articulation faces towards the body and the convex articulation faces away (Fig. 3.1C). In the intervertebral joints of the sauropod neck and tail, the forces of weight support are transferred proximally from cotyle to condyle, not from condyle to cotyle (with the exception of *Opisthocoelicaudia* mentioned above).

Previous Functional Studies of Concavo-Convex Joints.—The consistent mechanical polarity of concavo-convex joints in the sauropod neck and tail suggests there is a functional advantage for centra that are concave towards the body compared to the opposite polarity. Several previous studies sought to identify the factors that determine concavo-convex joint polarity. Early proposals by L. Fick (1845) and Henke and Reyher (1874) assumed that muscles play an active role in developing joint shape during ontogeny, leading those authors to the conclusion that the location of muscle insertion sites on the more mobile bone (i.e., the one further from the body) determines whether its articular surface is convex or concave. This was

expanded upon by R. Fick (1890), who, like his predecessors, focused predominately on the concavo-convex joints of the human appendicular skeleton. Summarizing Henke and Reyher (1874), Fick (1890: p. 392) wrote that, “the one articular surface where the muscles insert near the joint will always be ground concave, the joint end with distant muscle attachments, in contrast, will be convex” (translated from the German by JAF and J. Fahlke). In other words, when muscle insertion sites on the free element are located close to the joint, the free element will develop a cotyle, whereas when insertion sites are distally located, it will develop a condyle instead (Fig. 3.2). The fixed element of the joint will develop a corresponding condyle or cotyle, respectively.

Fick (1890) predicted the relationship between muscle insertion site and joint polarity based on his reconstruction of the forces acting on the free element in each scenario (Fig. 3.2). He decomposed the applied muscular force (F_m) into a rotational component (R) that moves the free element and a compressional component parallel to the free element (C_{fr}). At the joint surface, the compressional force acts oblique to the fixed element, and so can be further decomposed into compression acting on the fixed element (C_{fx}) and a shear component (S) acting along the joint surface. When the site of force application is far from the joint (Fig. 3.2A, t1), the opposing rotational and shear components are widely spaced, and there is a center of rotation in between them within the free element; as the distal end rotates laterally, the proximal end rotates medially. Although not clearly stated by Fick (1890), if the muscle originates from the fixed element, its pull will have a greater medial component the farther distally it inserts on the free element, which will also contribute to the described movement. Given the assumption that muscular action determines joint shape, Fick (1890) concluded that the pressure of this movement would abrade or inhibit bone growth at the corners of the free element, eventually

rounding its end into a condyle (Fig. 3.2A, t2); the corresponding pressure on the central part of the fixed element would generate the cotyle. In contrast, when muscles insert on the free element near the joint, the rotational component of the applied force acts close to the articular surface (Fig. 3.2B, t1). With the rotational force more directly opposed to the shear component, the center of rotation is located at the joint surface, and the proximal end of the free element must rotate laterally, along with the rest of the bone. The pulling muscle may also have a lesser medial component and a shorter moment arm, reducing the magnitude of the shear. As the free element is pulled laterally over the edge of the fixed element, the corners of the fixed element would be rounded off into a condyle, and the free element would bear the cotyle (Fig. 3.2B, t2). To test his hypothesis, Fick created flat-ended elements in plaster and attached strings to the free element at insertion sites near to or far from the joint. When the strings were repeatedly pulled side-to-side by a motor, the articular surfaces were ground into a condyle and cotyle in accordance with the predictions above (see Fick 1890: Fig. 5).

Although the mechanics described by Fick (1890) are plausible, the hypothesis presented does not explain the distribution of opisthocoely and procoely in the sauropod spine. Sauropod cervical vertebrae are hyperelongated, displacing the ligament and muscle insertions of the neural spine, transverse process, and cervical rib distally. According to the hypothesis, this should result in the formation of proximal condyles, that is, procoelous cervical vertebrae, which is opposite the observed pattern. By the same logic, the shorter caudal vertebrae would be more likely to be opisthocoelous. In the only case of opisthocoelous anterior caudal vertebrae among sauropods, *Opisthocoelicaudia*, the neural arch morphology closely resembles that of other titanosaurs, showing no evidence for distal displacement of insertion sites (Borsuk-Bialynicka

1977). In light of this, it is unlikely that intervertebral joint polarity in sauropods is predominately mediated by the position of muscle insertions.

Although the hypothesis that muscle insertion location determines joint polarity does not explain the patterns observed in sauropods, the observation that a free element with distal muscle insertion sites will experience medial rotation of the proximal end is significant. Medial rotation is potentially destabilizing because the proximal end of the vertebra rotates out and away from the joint. As discussed above, any tendency towards dislocation of an intervertebral joint is disadvantageous. We hypothesize that the polarity observed in sauropods is opposite to that predicted by the hypothesis of Fick (1890) in order to counteract medial rotation and thereby enhance joint stability.

Later investigations into the significance of concavo-convex joint polarity that specifically addressed opisthocoely and procoely were conducted by Troxell (1925) and Nopcsa (1930). Troxell (1925) sought to explain the presence of procoelous vertebrae in crocodylians using the observation that the center of rotation (COR) of a concavo-convex joint is invariably found in the condyle. Troxell (1925) hypothesized two advantages for proximally-concave vertebrae over proximally-convex ones. The first advantage is that the proximal displacement of the COR in proximally-concave vertebrae would increase the displacement of the vertebral column per unit of rotation. According to Troxell (1925), under these conditions, the free element has a greater functional length because it rotates about a point outside itself (Fig. 3.3, s). As a result, during rotation, the distal end of the vertebra is displaced farther from the midline for any given angle of rotation compared to the opposite polarity. In contrast, proximally-convex vertebrae rotate about an internal COR, so the functional length is less than the length of the centrum (Fig. 3.3, n) and displacement per unit of rotation is reduced. Troxell (1925) assumed

that the increase in functional length of crocodylian procoelous caudal vertebrae was additive serially. This means that a swimming crocodylian would generate significantly more displacement, and therefore more thrust, with its tail for a given energy input than would a hypothetical crocodylian with an opisthocoelous tail. This interpretation cannot be correct because it overlooks the effect of successive vertebrae on the functional length of one another. The functional length of a procoelous caudal vertebra must take into account both the gain from displacing the COR into the adjacent proximal vertebra and the loss from being the vertebra into which the COR of the adjacent distal vertebra is displaced. That these effects cancel out can be seen when model centra of equal size are articulated in series and rotated to a uniform angle (Fig. 3.3); series of proximally-concave (Fig. 3.3, top) and proximally-convex (Fig. 3.3, bottom) centra exhibit identical curvatures and nearly identical displacements from the midline. The displacement of the proximally-concave series is greater than that of the opposite polarity, but the displacement difference does not exceed the length of a single condyle regardless of the number of centra in series. The equivalence of the two polarities in terms of displacement was suggested by Gosnold and Slaughter (1977) and demonstrated by Fronimos and Wilson (2013). Therefore, the presence of cervical opisthocoely and caudal procoely in sauropods is not well-explained as increasing the displacement per unit rotation of the neck and tail.

The second advantage hypothesized by Troxell (1925), and also independently suggested by Nopcsa (1930), concerns the distribution of compressive force on a concavo-convex joint. Troxell (1925) declared that the thrust generated by the crocodylian tail during swimming must act parallel to the distal, free element in any given intervertebral joint, in the process always passing through the COR of the joint (Fig. 3.4). In the author's words (Troxell 1925: p. 607), "it must be clearly understood that the thrust through each vertebra is transmitted (lateral muscular

pull not considered) in the direction and along the line of the longer axis to the next vertebra in front." In this scenario, the force acts at an angle to the proximal, fixed vertebra. When the centra are proximally concave, the force acts upon the condyle of the more proximal centrum, which offers a greater thickness of bone to resist the force (Fig. 3.4, s). When the centra are proximally convex, the force acts upon the thinner bone of the cotylar rim (Fig. 3.4, n), presenting a greater risk of breakage. Nopcsa (1930: p. 23) presented a similar argument, stating, "In the one case unilateral pressure is taken on the center of the spherical articular surface, but in the other case it is taken on the thin edge of the socket. Now, since in the first case, the same possibility of movement is connected with a much greater mechanical strength than in the second, the first construction is obviously better; at the same time, this is the one in which the joint socket looks towards the fixed part" (translated from the German by JAF). Both authors presented the hypothesis only on the basis of geometric considerations, without experimental modeling. Gosnold and Slaughter (1977) reported an experiment in which alligator vertebrae were loaded according to Troxell's predictions by a hydraulic press and stressed to the point of failure. When the force was directed from the cotyle into the condyle, the force required to fracture the fixed centrum was three times greater than when it was directed into the cotylar rim; details of the experiment and quantitative results were not provided. Both Nopcsa (1930) and Gosnold and Slaughter (1977) recognized the applicability of this hypothesis to a variety of vertebrates, including sauropods, and Powell (2003) applied it specifically to procoelous caudal vertebrae in titanosaur sauropods. To date, the distribution of forces across a concavo-convex intervertebral joint has not been documented, so Troxell's assertion that the proximally-directed force acts parallel to the more mobile vertebra in a joint requires further assessment.

Functional Hypotheses Evaluated in this Study.—Two hypotheses for the functional advantage of proximally-concave over proximally-convex vertebrae are considered here: (1) proximally-concave centra exert stresses against a greater thickness of bone, the condyle, instead of the thin cotylar rim, reducing the risk of fracture; and (2) proximally-concave centra prevent the destabilizing rotation of the proximal end of the mobile centrum down and out of joint. The validity of each hypothesis is examined using physical experiments with models representing proximally-concave and proximally-convex centra in a jointed cantilever representing either a neck or a tail. The hypothesis that proximally-concave centra better resist fracture is tested using photoelastic models that allow direct observation of the magnitude and distribution of strain in joints of each polarity. If the hypothesis is correct, proximally-concave centra will exhibit lower strains that are more evenly distributed across the articular surface; the opposite polarity will show large strains concentrated in the cotylar rim. The rotational stability hypothesis is assessed by quantifying the relative stability of the two polarities under a variety of biologically plausible loading conditions. If proximally-concave centra confer greater rotational stability, then those models will require much greater forces to rotate out of joint, whereas proximally-convex centra will be easily dislocated. The results provide a framework for understanding the regional and phylogenetic distribution of opisthocoely and procoely in sauropods and other vertebrates. Implications for the polarity of concavo-convex joints in other skeletal regions, such as the appendicular skeleton, are discussed.

Materials and Methods

The hypotheses presented above were tested using simplified physical models of vertebral centra that were articulated under a variety of loading conditions. The centra were

modeled as schematic forms lacking neural arches that are concavo-convex in only one plane. Because both hypotheses make the same predictions in two-dimensional systems as they do in three-dimensions, the experiments could be constrained to a single plane without compromising the validity of the results. The models were first constructed digitally in Adobe Illustrator as two-dimensional concavo-convex shapes, 3 cm tall and 8 cm long in the longest model. Each model has one flat end for mounting to a base and one end that is either concave or convex. The models were designed so that the center of rotation is a uniform distance (6.5 cm) from the flat end, meaning that the elements do not have the same total length. The concavo-convex articular surfaces were created by the addition or subtraction of a semicircle from an initially rectangular shape. In order to permit a certain extent of rotation without impingement, the cotylar rim was truncated while maintaining the same radius of curvature. As the precise range of motion of sauropod intervertebral joints is not known, three biologically plausible maximum angles of rotation were chosen (15°, 25°, 35°), representing the approximate average presacral range of motion, total range of motion, and caudal range of motion, respectively, on the intervertebral joints of *Alligator mississippiensis* as measured by Fronimos and Wilson (in review). To shorten the cotylar rim the correct amount, the concave and convex models were placed in articulation in Illustrator and the concave element was rotated to a given angle. Then, the margins of the concavity were truncated at the point of impingement perpendicular to the length of the centrum. This resulted in three different models with concave articulations, characterized by a different depth of concavity (approximately 40%, 30%, and 20% of model height, respectively). The models were next imported into Autodesk 3ds Max, where the fit of the articulations was improved by enlarging the concave articulations slightly with a push modifier. The shapes were then extruded to a width of 3 cm to create three-dimensional forms.

The digital models were 3d printed in P430 acrylonitrile butadiene styrene (ABS) plastic on a Dimension Elite 3d printer. To create smooth surfaces, the gaps left by the 3d printing process were filled in with a thin layer of epoxy. A one-piece mold of each model was then produced in PolyGel Plat-Sil 73-25 RTV silicone molding rubber. These were used to cast the models in EPO-TEK 301 epoxy, a two-component epoxy that cures at low temperature and exhibits photoelastic properties. To conserve material and enhance optical clarity, casts were poured to a thickness of 1 cm rather than the 3 cm width of the ABS plastic models. Batches of epoxy were limited to 25 g at a time; mixing greater amounts resulted in cloudiness and anomalous birefringence under cross-polarized light, likely due to excess heat generation during the reaction between the two component phases. After pouring, the epoxy models were allowed to cure for a minimum of 24 hours at room temperature. Measurements of the models taken with digital calipers showed a variation in width from 0.82 cm to 1.07 cm, including a meniscus of not more than 0.10 cm.

To test each of the two hypotheses, the models first were suspended in articulation loaded as cantilevers, with a fixed proximal element and a free distal element that could be rotated relative to it. To do this, one model was fixed to a wooden testing rig at its flat end by two 0.62 cm (¼”) diameter wooden dowels; these were received by corresponding holes, 0.66 cm apart, drilled into the wooden frame and the flat end of the model. This modular setup allowed the proximal element to be switched out between the convex and concave elements to create either a proximally-concave or proximally-convex joint. To further stabilize the fixed element against rotation, a steel drawer handle with a clearance of 3.2 cm was attached below it, lined with foam to prevent damage to the epoxy of the model. The free element was suspended from the rig by a tensile element (either a wire or a string; see below) originating proximally on a metal hook. The

hook could be moved up and down to vary the angle of rotation of the free element and the insertion angle of the tensile element. To allow this, the hook was screwed into a separate wooden board bolted to the back of the wooden frame via a vertical slot. The board could be moved vertically when the bolts were loosened and, with the bolts tightened, stayed firmly in one position regardless of the load applied. This testing rig is shown in Figure 3.5, where it is configured for the rotational stability experiments.

The hypothesis that proximally-concave centra distribute forces more evenly across the articular surface than do proximally-convex centra was tested using photoelastic analysis. The principles and applications of photoelastic analysis are detailed by Post (1979) and are summarized only briefly here. Photoelastic materials are optically isotropic in an unstrained state, and therefore appear dark when viewed under cross-polarized light. The introduction of strain produces anisotropy in the index of refraction of the material, meaning that light travels through the material at a different speed depending on the direction in which the light vibrates. When viewed under cross-polarized light, rays passing through the material are out of phase and therefore interfere, resulting in birefringence. The greater the strain in the material is, the greater the difference in velocity between the rays will be, and the light observed will have a progressively higher-order interference color. Using this technique, the distribution of strain in a material can be observed and the relative magnitude of stress assessed. The EPO-TEK 301 epoxy used to create the models described above is a photoelastic material with a typical index of refraction of 1.519 at 23° C (Epoxy Technology Inc. 2012). The models, which were unstrained as a result of the molding and casting process, exhibited a slight biaxial anisotropy with first-order gray interference colors.

Strain visualization experiments were conducted using the wooden testing frame described above. The epoxy models were modified with the addition of a metal hook on the top and bottom surface, providing a strong attachment for the tensile element and heavy weights. In each model, a 1.1 cm-deep hole was drilled into the top and bottom surface, into which was placed a 1.6 cm metal cup hook. The hole was placed 2 cm from the flat end to prevent the strain associated with drilling the hole and applying forces to the hook from overprinting experimentally-induced strain at the articular surface. The hooks were set into the holes with epoxy, rather than screwed in, creating a strong bond to the epoxy model without introducing additional strain. For each test, the free element was supported by a tensile element consisting of twisted, 19-strand steel wire with 0.027 cm thick strands. A loop was made at each end of the wire by bending the wire back on itself twice; joining the overlapping segments with two copper crimp sleeves created a strong connection that resisted slipping. This setup being irreversible, a different wire was measured out for each test to provide the correct angle of insertion and angle of rotation, within a margin of error of 2° under the maximum load. The proximal end of the wire was attached to the wooden frame by the movable metal hook described previously. Weights were suspended from the hook on the bottom of the free element by a loop of wire held shut in the manner detailed above. Using iron dumbbell plates in increments of 1.13 kg (2.5 lb), weights of up to 4.54 kg (10 lb) were applied. For each of the two polarities, tests were conducted at two insertion angles (0°, 55°), two angles of rotation (15°, 25°), and four applied weights (0 kg, 1.13 kg, 2.27 kg, 4.54 kg). Two different cotyle depth-to-height ratios (0.3, 0.4) were used for the lower angle of rotation; only the shallower cotyle was used with the 25° angle. After the models were suspended and loaded, polarizing film was placed behind and in front of the models, with the polarization directions of the films perpendicular to one another. The models were backlit

with a light source behind and slightly to the left of the modeled joint. The results were photographed with a Nikon D810 DSLR digital camera and a 60 mm Micro Nikkor lens. The camera was placed at a distance of 26 cm from the models and manually focused, with a 1/1.6 second exposure time and an aperture of F22. For each configuration, the resulting strain distributions were compared to one another and to the predictions of the hypothesis put forward by Troxell (1925).

The hypothesis that joints between proximally-concave centra are significantly more resistant to failure by rotation was tested by measuring how much weight applied to the proximal end of the free element was necessary for joint failure (Figure 3.5). The experimental design had several additional parameters (Fig. 3.6) that were varied to determine how different combinations affected the joint integrity. The tensile element supporting the free centrum, representing ligament, tendon, and muscle was modeled as a piece of string, the length of which was varied to allow different insertion angles of the tensile element (20°, 45° to the horizontal; Fig. 3.6, α) and different angles of rotation of the free centrum (0°, 15°, 25°, 35°; Fig. 3.6, β). The insertion angles reflect uncertainty as to whether sauropods had a crocodylian-style supraspinal ligament that spanned each joint at a low angle (e.g., Schwarz et al. 2007) or an avian- or ungulate-style nuchal ligament spanning multiple segments at higher angles (e.g., Tsuihiji 2004). The tensile element was attached with tape to the free centrum at one of three possible insertion sites: proximal to the joint (0.50 cm from the COR; Fig. 3.6, P), middle (3.25 cm from the COR; Fig. 3.6, M), or distal to the joint (6.00 cm from the COR; Fig. 3.6, D). These permit assessment of the hypothesis that distal insertion sites result in medial rotation of the proximal end of the free element, as proposed by Fick (1890). Two different concavity depths were used (depth to height ratios of 0.2, 0.3; Fig. 3.6, c). The deepest concavity (depth to height ratio of 0.4) was not used

because it only permitted rotation up to 15°; the intermediate-depth concavity, though designed to permit rotation up to 25°, could be rotated to 35° with only a barely-visible opening of the joint space. For configurations using the less-stable shallow cotyle, an additional set of trials was conducted to determine whether the stabilizing effect of a distal load (e.g., an additional vertebra in series) would negate any stability difference between polarities. To do this, an additional 20 g (the approximate mass of an epoxy model) was suspended from the distal end of the free element at the position of the farthest insertion site from the joint.

To conduct each trial, the elements were first placed in articulation, and it was observed whether the free element stayed in joint or whether it disarticulated under its own weight. If the configuration was stable, more weight was suspended from a loop of string, affixed on the free element, for consistency of position, at the insertion site nearest the joint (Figure 3.5). Gram calibration weights were added in 5 g increments until disarticulation occurred or until 250 g had been applied, and the weight at which disarticulation occurred was recorded. When a 20 g weight was suspended from the distal end of the free element, the maximum weight applied to the proximal end was 230 g. When all measurements had been taken, comparisons were made between the results for each polarity, and the influence of each additional variable was compared between polarities. To determine whether a stability difference was significant (i.e., not attributable to model uncertainty), several trials were repeated at a later date; the weights recorded differed from the previous outcomes by up to 15 g. It was also noted that the convex model, bearing the additional weight of a condyle, weighed 11.8 g more than the lightest concave model. Therefore, a difference in stability between model configurations was considered significant only if the weight required for joint failure differed by more than 30 g.

Results

Stress Resistance.—As revealed by the photoelastic analysis, strain on the concavo-convex joints was consistently concentrated in the cotylar rim, regardless of joint polarity (Fig. 3.7). The distribution and magnitude of strain was dependent on the insertion angle of the tensile element. With a horizontal tensile element, strain was concentrated in the ventral cotylar rim for joints between proximally-convex centra (hereafter "proximally-convex joints"; Fig. 3.7A), as predicted. For joints between proximally-concave centra (hereafter "proximally-concave joints"), strain was not evenly distributed across the articular surface; instead, it was concentrated in the dorsal cotylar rim (Fig. 3.7B). Within the sensitivity of the analysis, the magnitude of strain was consistent between the two polarities (Fig. 3.7A', B'), with one exception. With the free element at a 25° angle of rotation, the strain magnitude was much greater in the proximally-convex joint (low third-order interference colors) than the proximally concave joint (middle first-order colors). With a steeply-angled tensile element (55° to the horizontal), no difference in strain magnitude was detected between the two polarities. Joints with a shallow cotyle exhibited a strain distribution as described above, but the magnitude of strain was much lower, barely exceeding the first-order gray colors of unstrained epoxy. The strain distribution differed with a deeper cotyle, as the proximally-concave joint exhibited strain in both the dorsal and the ventral cotylar rim, and the strain magnitude was nearer to that of joints with a horizontal insertion.

Rotational Stability—For any given combination of parameter states, proximally-concave centra always required more weight for joint failure to occur than did proximally-convex centra, except when both polarities were stable at the greatest weight applied (Fig. 3.8; Table 3.1). The stability difference between the two polarities was significant (i.e., it exceeded the model

uncertainty) for greater than 80% of the parameter state combinations (Fig. 3.8). Proximally-concave joints were always stable without applied weight, and an applied weight significantly greater than zero was required for joint failure in all but three of the 72 variable combinations (Table 3.1). Proximally-convex joints were stable in an unloaded state for most variable combinations, but for exactly half of the combinations, the weight at which joint failure occurred was not significantly greater than zero (Table 3.1). In a majority of the combinations with proximally-concave joints, joint failure did not occur at the maximum applied weight, whereas this was true in only four combinations with proximally-convex joints (Table 3.1). Note that, as a result, the stability differences shown in Figure 3.8 are minima whenever the weight required for failure of the proximally-concave joint remains unknown.

All five additional parameters examined (Fig. 3.6) were found to significantly influence joint stability (Table 3.1). Deeper cotyles, tensile element insertion sites nearer to the joint, and the presence of additional weight at the end of the free element increased stability for both joint polarities. The difference in stability between the two polarities was generally higher in the more stable combinations (Fig. 3.8), most likely because joint failure imposed an absolute lower limit on the stability range, whereas no such upper limit exists. The other two variables had opposite effects depending on the joint polarity (Table 3.1). Increasing the angle of rotation of the free element increased stability in proximally-concave joints but decreased stability in proximally-convex joints. As a result, the stability difference between joint polarities was least at the lowest angle of rotation (Fig. 3.8, β). Higher angles of tensile element insertion most often resulted in greater stability in proximally-convex joints and lower stability in proximally-concave joints, but counterexamples also occurred, and the difference was often less than the model uncertainty. The

polarities were generally more similar in stability with a 45° angle of insertion, but the effect was smaller and less consistent than that of the angle of rotation (Fig. 3.8, α).

Discussion

Stress Resistance.—The results of this analysis do not support the hypothesis of Troxell (1925) that proximally-concave (sauropod-type) centra distribute stress more evenly across the joint surface than do proximally-convex centra. As seen in the epoxy models (Fig. 3.7), the cotylar rim is strained regardless of joint polarity, and no significant difference in the magnitude or distribution of strain is detected within the sensitivity of the photoelastic analysis. Troxell (1925) assumed that forces acting along a series of procoelous caudal vertebrae would be parallel to the distal element in any given joint, and this assumption guided the experiment of Gosnold and Slaughter (1977). The observed strain distribution in joints loaded as cantilevers indicates that forces act oblique to the free element, rather than parallel to it. This orientation is consistent with the resultant vector of the applied forces (i.e., gravity and tensile support). When the tensile element is horizontal, the resultant vector has a 45° angle to the ground. This is approximately orthogonal to the joint surface of the ventral cotylar rim for proximally-convex centra and of the dorsal cotylar rim for proximally-concave centra. When the tensile element is steeply angled, the resultant vector will have a shallower angle and a smaller magnitude, hence the lower observed strain in the models. Therefore, the strongly conserved pattern of cervical opisthocoely and caudal procoely in sauropods is not well explained by a differential vulnerability to cotylar rim fractures.

The only instance in which the strain magnitude differed between joint polarities occurred with a high angle of rotation, a horizontal insertion, and a shallow cotyle; in this case,

the proximally-convex joint experienced much greater strain. Observation of this joint revealed that the joint surfaces had lost contact with each other dorsally, creating a narrow gape. This gape appears to have resulted from the distal and ventral rotation and translation of the condyle, as discussed with regard to rotational instability. This outcome is unsurprising in a proximally-convex joint having this angle of rotation, insertion angle, and cotyle depth, as this combination of parameter states is particularly unstable (see Results). As the condyle was pulled out of joint, the surface area of contact was reduced, increasing stress and, therefore, strain. It is plausible that proximally-convex joints are more susceptible to cotylar rim fractures than the opposite polarity in the event of a partial joint failure.

The models are a simplification of real intervertebral joints; the only tensile support in the models represents the supraspinal or nuchal ligament. The consequences of the presence of other soft tissues must, therefore, be considered. In the living animal, it is possible that the action of the epaxial muscles would have redirected the resultant vector so that the free element was loaded only in compression. As described by Crisco and Panjabi (1991), the human lumbar region requires active muscular stabilization to prevent buckling. In order to be effective for stabilization, the muscular force must be a “follower load”; that is, one that conforms to the lordotic curvature of the lumbar vertebrae rather than acting vertically on the column (Patwardhan et al. 1999). The orientation of the follower load, however, is not parallel to either vertebra participating in a joint; instead, the angle is intermediate between the orientations of the two vertebrae, such that the compressive force acts oblique to each centrum. In addition, the human vertebral column is habitually held upright, such that the long axis of the vertebral column at any point is subparallel to the direction of gravity. In a cantilevered sauropod neck or tail, the vertebrae would have a higher angle to the direction of gravity, so the force necessary to

load the vertebral column with a compressive follower load would have been much greater. Thus, although the stress on the cotylar rim in sauropod vertebrae could likely have been reduced by the action of the epaxial musculature, there is no basis to conclude that the stress would be preferentially eliminated from one joint polarity and not the other.

Rotational Stability.—Proximally-concave vertebral centra, such as the opisthocoelous cervical and procoelous caudal vertebrae of sauropods, are significantly more resistant to joint failure than proximally-convex centra. The difference in stability between the joint polarities can be explained by the position of the center of rotation, which, as noted by Troxell (1925), is always within the condyle. In a proximally-concave joint (Fig. 3.9A), the center of rotation is constrained to lie within the condyle of the more proximal, and therefore less mobile, element. As a result, the free element rotates about a point outside itself. The tensional force that supports the free element pulls it dorsally and proximally, holding the cotyle in joint with the condyle. A force directed towards the ground that is applied at the proximal end of the free element will tend to rotate the entire vertebra ventrally, a movement that is opposed by the tensile element. As demonstrated in the experiments, it is possible for a sufficiently large force acting close to the joint to pull the cotyle away from the condyle, causing joint failure. However, the forces required to do this are typically much greater than those causing joint failure in an equivalent proximally-convex joint. In a proximally-convex joint (Fig. 3.9B), the free element rotates about a point within itself. Consistent with the observations of Fick (1890), any dorsiflexion of the distal end of the free element will have the consequence of rotating the condyle ventrally and distally; that is, out and away from the cotyle. Conversely, if a force acts to rotate the condyle out of joint, the

distal end of the centrum will rotate dorsally, and the tension in the supporting tensile element will be reduced.

It is possible to compensate for joint instability with particular morphologies and orientations of the vertebrae and tensile elements. Three of the parameters examined in our experiments bore the same relationship to stability for both joint polarities. Proximal tensile element insertion sites, distal loading of the free vertebra, and deeper cotyles conferred greater stability. A configuration of these parameter states that provides stability to proximally-convex joints would increase stability as much or more for proximally-concave joints (Fig. 3.8). The first two variables also involve tradeoffs between joint stability and mechanical advantage, as proximal insertion sites decrease the leverage with which the tensile element supports the increasing distal load. Deeper cotyles could decrease joint mobility due to impingement, although a previous study of *Alligator* did not find a relationship between intervertebral joint morphology and range of motion (Fronimos and Wilson in review). The angle of rotation of the free element and the angle of insertion of the tensile element affect the two joint polarities differently, although the insertion angle has an inconsistent influence. The two polarities are generally comparable in stability when the vertebrae are oriented horizontally, but the sauropod-type joints become more stable at higher angles of rotation, whereas the opposite type become less stable. The sauropod-type joints therefore permit a greater mobility to be maintained without sacrificing stability. Some uncertainty surrounds the insertion angle of the supraspinal or nuchal ligament in sauropod cervical vertebrae (e.g., Tsuihiji 2004; Schwarz et al. 2007); high insertion angles are associated with an avian- or ungulate-type nuchal ligament that spans multiple segments (Tsuihiji 2004; see also Dimery et al. 1985). Insertion angles would be steepest in posterior cervical vertebrae, especially in taxa with anterior dorsal neural spines that are much

taller than the cervical spines (e.g., *Giraffatitan*, Janensch 1950). Osteological evidence led Tsuihiji (2004) to conclude that the sauropod nuchal ligament did not extend to the anterior cervical vertebrae; even if it did, the length of the neck would cause the insertion angles to be much lower than at the base of the neck. Proximally-concave joints, which are generally more stable with lower insertion angles, would be most advantageous in longer necks. A final mechanism for stabilizing proximally-convex joints is active contraction of the epaxial muscles, but this is a less energetically-efficient solution than the passive support provided by proximally-concave joints. Thus, the strongly conservative pattern of cervical opisthocoely and caudal procoely in sauropods would have conferred greater intervertebral joint stability than the opposite polarity without sacrificing mobility, mechanical advantage, or energetic efficiency.

Exceptions to the Predominant Sauropod Pattern.—Given the advantages of proximally-concave intervertebral joints, the existence of exceptions to the dominant pattern requires explanation. These exceptions include the opisthocoelous caudal vertebrae of the titanosaur sauropod *Opisthocoelicaudia* (Borsuk-Bialynicka 1977) and the procoelous cervical vertebrae of crocodylians (e.g., Owen 1859a) and pterosaurs (e.g., Owen 1859b). How these joints were stabilized is more easily conjectured than what advantage they conferred. For *Opisthocoelicaudia*, it is possible that the tail was held in a consistently near-horizontal posture with a limited range of motion, as proposed by Borsuk-Bialynicka (1977). Additionally, Borsuk-Bialynicka (1977) noted that the cotyles of caudal centra in *Opisthocoelicaudia* are consistently deeper than the condyles are long. It should be noted that the sacricaudal joint in titanosaurs and crocodylians is also proximally-convex. In *Alligator*, this joint is nearly immobile, but the cotyle depth is highly variable among crocodylians (Fronimos and Wilson in review). Posture and

mobility cannot explain cervical procoely in crocodylians, as the crocodylian neck has an intrinsic curvature (Virchow 1914; Fronimos and Wilson in review) with joint mobility typical of the presacral spine (Fronimos and Wilson in review). In *Alligator*, cotyle depth is consistently less than condyle length (Fronimos and Wilson in review). Procoelous cervical vertebrae in crocodylians might be stabilized by the combination of a short neck and a large, heavy skull. The short cervical centra result in more proximal insertion sites than in sauropods. The heavy terminal load of the skull might serve to hold the procoelous cervical vertebrae in articulation, a tendency that could also have facilitated cervical procoely in pterosaurs. These factors do not explain the condition in *Opisthocoelicaudia*. In *Opisthocoelicaudia*, the caudal neural arches resemble those of other titanosaurs, which have procoelous caudal vertebrae. The caudofemoralis longus muscle, which would have imparted shear across the intervertebral joints, also had a similar extent in *Opisthocoelicaudia* to other titanosaurs, as evidenced by the serial extent of the transverse processes (see Gatesy 1991). Thus, there does not appear to be a particular configuration of ligaments and/or muscles that provided additional stabilization. In addition, although the tail of *Opisthocoelicaudia* is short, there is no heavy terminal load at the distal end (Borsuk-Bialynicka 1977), and this morphology is shared by other titanosaurs for which we have complete tail sequences (e.g., *Alamosaurus*; Wilson 2002). Apart from the potential for active muscular stabilization, it appears that proximally-convex cervical or caudal centra have been stabilized in different ways by different taxa.

Opisthocoelous caudal vertebrae and procoelous cervical vertebrae were also derived from different ancestral states in different taxa. *Opisthocoelicaudia* is nested phylogenetically among titanosaurs with procoelous caudal vertebrae (e.g., Salgado et al. 1997; Wilson 2002), indicating that the joint polarity in the tail underwent an anatomical reversal. In contrast, the

procoelous cervical vertebrae of crocodylians were derived from an amphicoelous ancestral condition (Salisbury and Frey 2001); this seems also to be the case in pterosaurs, although the transition is less well understood (Sereno 1991). The repeated evolution of a seemingly suboptimal joint polarity in distinct taxa, from different functional precursors, suggests that such joints must confer some offsetting advantage under particular conditions. As noted by Borsuk-Bialynicka (1977), a change in joint polarity can be explained if the fixed end and free end of a vertebral series are reversed. For example, if a sauropod adopted a tripodal posture during feeding or reproduction, the distal end of the tail would be braced against the ground and immobilized relative to the trunk. In this case, caudal opisthocoely would be the stable configuration and procoely comparatively unstable. Although this interpretation is mechanically plausible, there is no anatomical evidence to suggest that *Opisthocoelicaudia* was more likely to adopt a tripodal stance than other titanosaurs. Apart from caudal opisthocoely, the skeletal characteristics used to suggest a tripodal stance for *Opisthocoelicaudia* are shared with other titanosaurs, which have procoelous caudal vertebrae (Powell 2003). Nopcsa (1930) similarly applied the concept of a reversal of forces to explain presacral procoely in crocodylians and squamates. He reasoned that the sprawling posture and hind limb driven locomotion of these animals would create forces acting from posterior to anterior. As a result, the head and shoulders would act as the fixed end of the vertebral column, and procoely would be favored. This hypothesis does not account for the diversity of locomotor patterns utilized by crocodylians (e.g., Renous et al. 2002) and squamates (e.g., Russell and Bauer 1992). It might, however, offer an explanation for cervical procoely in crocodylians and pterosaurs. During crocodylian swimming and pterosaur flight, propulsion is generated posterior to the neck, by the tail or the wings. Thus, the forces acting on the neck should be oriented as proposed by Nopcsa (1930). These

explanations remain conjectural in the absence of empirical data on how forces are distributed in the reptilian vertebral column during each of the different locomotor behaviors.

Rotational Stability in the Appendicular Skeleton.—The earliest research into concavo-convex joint polarity (e.g., Fick 1845; Henke and Reyher 1874; Fick 1890) was motivated to explain the patterns present in the human appendicular skeleton. If the polarity of concavo-convex intervertebral joints determines their rotational stability, it must be considered whether the same is true of appendicular joints. The tetrapod glenohumeral and femoro-acetabular joints exhibit a strong preferential joint polarity; in each, the stylopodium (viz. humerus, femur) bears a proximally-facing condyle that fits into a socket on one or more girdle elements. That the cotyle in these joints faces away from the body seems, at first, to be at odds with the pattern found in the sauropod neck and tail. However, during standing and in the stance phase of locomotion, the limb is braced against the ground, and the body is free to rotate about it. Thus, the weight-bearing autopodium in contact with the ground is the fixed element and the body, which is the more mobile element, bears the concavity. This is mechanically equivalent to the condition in the sauropod neck and tail, in which the distal vertebra in each joint is more mobile and bears the cotyle.

Phylogenetic evidence supports the interpretation that the tetrapod glenohumeral and femoro-acetabular joint polarity provides stability when the limbs are braced against the ground, supporting the body. In the extant outgroups of Tetrapoda, the lungfishes and coelacanths, the glenoid and acetabulum are convex (Rosen et al. 1981; Janvier 1996), indicating that the tetrapod condition evolved via a reversal of joint polarity. This reversal can be explained by the changing forces associated with the transition from fins to limbs. The non-tetrapod polarity would be more

favorable in a swimming animal because the distal end of the fin is mobile relative to the body; it is this mobile element that bears the cotyle. This also explains why the shoulder girdle bears a convexity in the basal actinopterygian *Polypterus*, another aquatic vertebrate with monobasal fins (Pollard 1892). As tetrapodomorphs began to use their fins in weight support and for terrestrial locomotion, a switch to the "tetrapod-type" joint polarity would have been necessary to maintain joint stability. This interpretation does not explain the retention of the concave glenoid in secondarily aquatic tetrapods. Nonetheless, further investigation of the functional significance of appendicular joint polarity in sarcopterygian evolution is merited.

The polarity of the human glenohumeral joint is sometimes altered surgically with the implantation of a reverse shoulder prosthesis. This structure is intended to compensate for rotator cuff injury by medializing the center of rotation, increasing the mechanical advantage of the deltoid (Grammont 1979). To accomplish this, the glenoid fossa is replaced with a convex element and the humeral head with a concave element. Grammont (1979) was inspired to invent this procedure by the evolutionary transition of human ancestors from quadrupedality to bipedality. As described by Baulot et al. (2011: p. 2426), "the freeing of the human upper limb resulted in a functional reversal of the roles of the humerus and the glenoid." In humans, the hand is not involved in weight support and represents the free end of the forelimb under most conditions. The results of the present analysis suggest that a reverse shoulder joint should be capable of greater rotational stability than the normal anatomical orientation in humans. Conversely, it is expected that a comparable reversal applied to the human femoro-acetabular joint, if such a prosthesis existed, would have a destabilizing influence.

Conclusions

The functional significance of concavo-convex joint polarity has been a source of lingering uncertainty, including with regard to opisthocoelous and procoelous vertebrae. Physical modeling of concavo-convex joints reveals that proximally-concave joints are significantly more resistant to joint failure. The strongly conserved pattern of cervical opisthocoely and caudal procoely in sauropod dinosaurs is, therefore, best explained as providing greater passive stabilization of the intervertebral joints than the opposite polarity. The sauropod configuration also would have permitted greater mobility, mechanical advantage of the supporting ligaments and muscles, and distal loading (i.e., a longer neck or tail) without sacrificing stability. The universal condition of cervical opisthocoely in sauropods may have been necessary for the evolution of large body size and neck hyperelongation. Among vertebrates, exceptions to the sauropod-type pattern may be dependent on limited mobility, short necks with large, heavy heads, or energetically-costly muscular activity for stabilization. Cervical procoely and caudal opisthocoely could be advantageous if the loading direction of the intervertebral joints was reversed, as during the adoption of a tripodal stance or, perhaps, during particular forms of locomotion. Further research into the loading regimes of intervertebral joints during these behaviors is needed. The concept that concavo-convex joint polarity reflects particular loading regimes may prove useful for explaining polarity in the appendicular skeleton, as in the case of the tetrapod glenohumeral and femoro-acetabular joints, and for exploring the functional evolution of these joints.

Literature Cited

Alexander, R. M. 1989. Dynamics of dinosaurs and other extinct giants. Columbia University Press, New York.

Allain, R., N. Aquesbi, J. Dejax, C. Meyer, M. Monbaron, C. Montenat, P. Richir, M. Rochdy, D. Russell, and P. Taquet. 2004. A basal sauropod dinosaur from the Early Jurassic of Morocco. Comptes Rendus Palevol 3:199–208.

Baulot, E., F. Sirveaux, and P. Boileau. 2011. Grammont's idea: the story of Paul Grammont's functional surgery concept and the development of the reverse principle. Clinical Orthopaedics and Related Research 469:2425–2431.

Bonaparte, J. F., W.-D. Heinrich, and R. Wild. 2000. Review of *Janenschia* Wild, with the description of a new sauropod from the Tendaguru beds of Tanzania and a discussion on the systematic value of procoelous caudal vertebrae in the sauropoda. Palaeontographica Abteilung A 256:25–76.

Borsuk-Bialynicka, M. 1977. A new camarasaurid sauropod *Opisthocoelicaudia skarzynskii* gen. n., sp. n. from the Upper Cretaceous of Mongolia. Acta Palaeontologica Polonica 37:1–64.

Calvo, J. O., and L. Salgado. 1995. *Rebbachisaurus tessonei* sp. nov. a new Sauropoda from the Albian-Cenomanian of Argentina; new evidence on the origin of the Diplodocidae. Gaia 11:13–33.

Coombs, W. P. 1975. Sauropod habits and habitats. Palaeogeography, Palaeoclimatology, Palaeoecology 17:1–33.

Crisco, J. J., and M. M. Panjabi. 1991. The intersegmental and multisegmental muscles of the lumbar spine: a biomechanical model comparing lateral stabilizing potential. Spine 16:793–799.

Dimery, N., R. M. Alexander, and K. A. Deyst. 1985. Mechanics of the ligamentum nuchae of some artiodactyls. Journal of Zoology 206:341–351.

Epoxy Technology, Inc. 2012. EPO-TEK® 301 Technical Data Sheet.

Fick, L. 1845. Physiologische Anatomie des Menschen. Christian Ernst Kollman, Leipzig.

Fick, R. 1890. Ueber die Form der Gelenkflächen. Archiv für Anatomie und Physiologie, Anatomische Abteilung 1890:391–402.

Fronimos, J. A., and J. A. Wilson. 2013. Function and polarity of concavo-convex articulations in the vertebral centra of sauropod dinosaurs with implications for other vertebrates. Journal of Vertebrate Paleontology, SVP Program and Abstracts Book 2013:131.

———. In review. Concavo-convex intervertebral joints stabilize the vertebral column in sauropod dinosaurs and crocodylians. Paleobiology.

Gatesy, S. M. 1991. Caudofemoral musculature and the evolution of theropod locomotion. Paleobiology 16:170–186.

Gosnold, W. D., and R. H. Slaughter. 1977. Procoelus versus opisthocoelus vertebrae. Texas Journal of Science 28:355–356.

Grammont, P. 1979. Place de l'ostéotomie de l'épine de l'omoplate avec translation, rotation, élévation de l'acromion dans les ruptures chroniques de la coiffe des rotateurs. Lyon Chirurgical 75:327–329.

Henke, W., and C. Reyher. 1874. Studien über die Entwickelung der Extremitäten des Menschen, inbesondere der Gelenkflächen. Sitzungsberichte der Kaiserlichen Akademie der Wissenschaften 70:217–273.

Hoffstetter, R., and J.-P. Gasc. 1969. Vertebrae and ribs of modern reptiles. Pp. 201–310 *in* C. Gans, A. d. A. Bellairs, and T. S. parsons, eds. Biology of the Reptilia Volume 1 Morphology A. Academic Press, London.

Janensch, W. 1950. Die Wirbelsäule von *Brachiosaurus brancai*. Palaeontographica 1:27–93.

Janvier, P. 1996. Early vertebrates. Clarendon, Oxford, U.K.
McIntosh, J. S. 1990. Species determination in sauropod dinosaurs with tentative suggestions for their classification. Pp. 53–69 *in* K. Carpenter and P. J. Currie, eds. Dinosaur systematics: approaches and perspectives. Cambridge University Press, U.K.
Nopcsa, F. 1930. Über prozöle und opisthozöle Wirbel. Anatomische Anzeiger 69:19–25.
Owen, R. 1859a. On the orders of fossil and recent Reptilia, and their distribution in time. Report of the British Association for the Advancement of Science 29:153–166.
———. 1859b. On the vertebral characters of the order Pterosauria, as exemplified in the genera *Pterodactylus* (Cuvier) and *Dimorphodon* (Owen). Philosophical Transactions of the Royal Society of London 149:161–169.
Patwardhan, A. G., R. M. Havey, K. P. Meade, B. Lee, and B. Dunlap. 1999. A follower load increases the load-carrying capacity of the lumbar spine in compression. Spine 24:1003–1009.
Pollard, H. B. 1892. On the anatomy and phylogenetic position of *Polypterus*. Zoologische Jahrbücher. Abteilung für Anatomie und Ontogenie der Tiere 5:387–428.
Post, D. 1979. Photoelasticity. Pp. 176–192 *in* A. S. Kobayashi, ed. Manual on experimental stress analysis, 3rd ed. Society for Experimental Stress Analysis, Westport, Conn.
Powell, J. E. 2003. Revision of South American titanosaurid dinosaurs: palaeobiological, palaeobiogeographical and phylogenetic aspects. Records of the Queen Victoria Museum 111:1–173.
Renous, S., J.-P. Gasc, V. L. Bels, and R. Wicker. 2002. Asymmetric gaits of juvenile *Crocodylus johnstoni*, galloping Australian crocodiles. Journal of Zoology 256:311–325.
Rosen, D. E., P. L. Forey, B. G. Gardiner, and C. Patterson. 1981. Lungfishes, tetrapods, paleontology, and plesiomorphy. Bulletin of the American Museum of Natural History 167:159–276.
Salgado, L., R. A. Coria, and J. O. Calvo. 1997. Evolution of titanosaurid sauropods. I: phylogenetic analysis based on the postcranial evidence. Ameghiniana 34:3–32.
Salisbury, S. W., and E. Frey. 2001. A biomechanical transformation model for the evolution of semi-spheroidal articulations between adjoining vertebral bodies in crocodilians. Pp. 85–134 *in* G. C. Grigg, F. Seebacher, and C. E. Franklin, eds. Crocodilian biology and evolution. Surrey Beatty & Sons, Chipping Norton, U.K.
Schwarz, D., E. Frey, and C. A. Meyer. 2007. Pneumaticity and soft-tissue reconstructions in the neck of diplodocid and dicraeosaurid sauropods. Acta Palaeontologica Polonica 52:167–188.
Sereno, P. C. 1991. Basal archosaurs: phylogenetic relationships and functional implications. Society of Vertebrate Paleontology Memoir 2:1–53.
Slijper, E. J. 1946. Comparative biologic-anatomical investigations of the vertebral column and spinal musculature of mammals. Verhandelingen der Koninklijke Nederlandsche Akademie van Wetenschappen, Afdeling Natuurkunde, Tweede Sectie 2:1–128.
Taylor, M. P., and M. J. Wedel. 2013. Why sauropods had long necks; and why giraffes have short necks. PeerJ 1:e36.
Troxell, E. L. 1925. Mechanics of crocodile vertebrae. Bulletin of the Geological Society of America 36:605–614.
Tsuihiji, T. 2004. The ligament system in the neck of *Rhea americana* and its implications for the bifurcated neural spines of sauropod dinosaurs. Journal of Vertebrate Paleontology 24:165–172.

Upchurch, P., P. M. Barrett, and P. Dodson. 2004. Sauropoda. Pp. 259–322 *in* D. B. Weishampel, P. Dodson, and H. Osmólska, eds. The Dinosauria, 2nd ed. University of California Press, Berkeley.
Virchow, H. 1914. Über die Alligatorwirbelsäule. Archiv für Anatomie und Physiologie Anatomische Abteilung 1914:103–142.
Williams, E. E. 1950. Variation and selection in the cervical centra articulations of living turtles. Bulletin of the American Museum of Natural History 94:505–562.
Wilson, J. A. 2002. Sauropod dinosaur phylogeny: critique and cladistics analysis. Zoological Journal of the Linnean Society 136:217–276.
Wilson, J. A., and P. C. Sereno. 1998. Early evolution and higher-level phylogeny of sauropod dinosaurs. Society of Vertebrate Paleontology Memoir 5:1–68.
Xing, L., T. Miyashita, J. Zhang, D. Li, Y. Ye, T. Sekiya, F. Wang, and P. J. Currie. 2015. A new sauropod dinosaur from the Late Jurassic of China and the diversity, distribution, and relationships of mamenchisaurids. Journal of Vertebrate Paleontology 35:1–17.
Young, C.-C. 1954. On a new sauropod from Yiping, Szechuan, China. Scientia Sinica 3:491–504.
Zhang, Y. 1988. The Middle Jurassic dinosaur fauna from Dashanpu, Zigong, Szechuan. Vol I. Sauropod dinosaur (I). *Shunosaurus*. Journal of the Chengdu College of Geology 3:1–89.

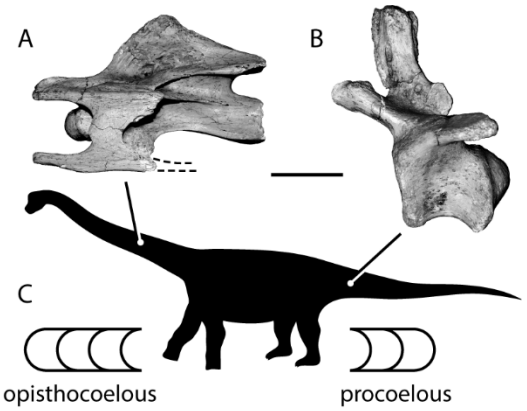

Figure 3.1. Sauropod centrum articular morphology and the anatomical distribution of centrum types. **A**, opisthocoelous cervical vertebra of the titanosaur *Trigonosaurus*. **B**, procoelous caudal vertebra of the titanosaur *Trigonosaurus*. The serial distribution of opisthocoely and procoely is depicted on a sauropod silhouette, **C**, with schematic representations of the two concavo-convex joint polarities. In both the neck and the tail, the concave articular surfaces of the centra face towards the body. Vertebrae are shown in left lateral view. Dashed lines indicate missing regions of vertebrae. Scale bar equals 10 cm for **A** and 6 cm for **B**. Silhouette modified from Wilson and Sereno (1998).

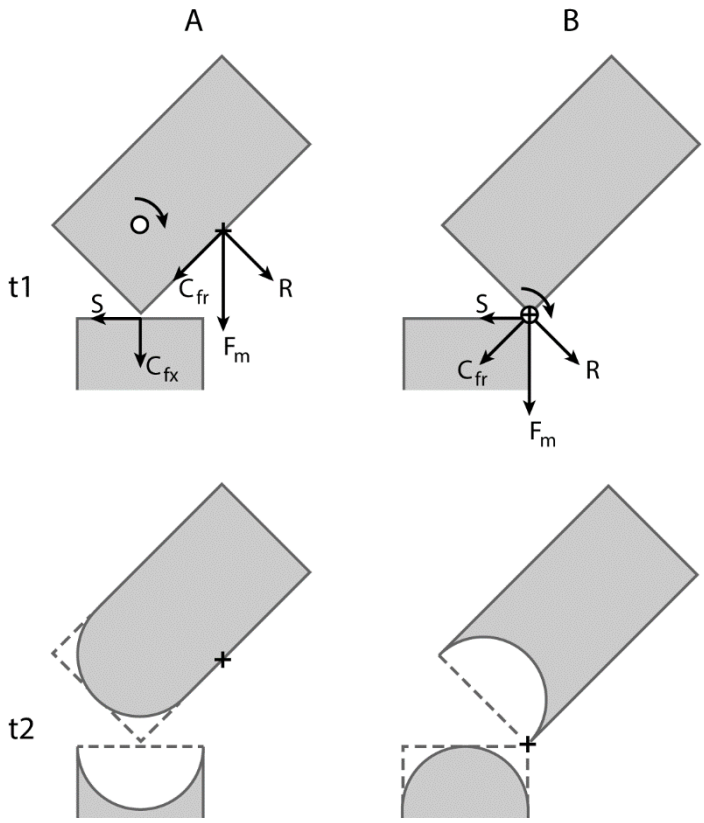

Figure 3.2. Schematic depiction of the forces interpreted to act on two articulated vertebrae when the muscle insertion site on the free element is located far from the joint surface, **A**, and close to the joint surface, **B**. Fick (1890) proposed that the location of the muscle insertion site on a moving bone determines which joint surface is convex and which is concave. The applied muscular force (**F_m**) has a rotational component (**R**) and a compressional component (**C_{fr}**). At the joint surface, the compressional component can be further decomposed into compression acting on the fixed element (**C_{fx}**) and shear acting along the joint (**S**). When the muscle insertion site (black cross) is located far from the joint, the rotational and shear components are widely separated, and the center of rotation (white circle) lies between them in the free element. When the distal end of the free element rotates laterally, the proximal end rotates medially (curved arrow). According to Fick (1890), over time the edges of the proximal end would be ground down, producing a condyle. When the muscle insertion site is located near the joint, the rotational component of force directly counteracts the shear component. As a result, the center of rotation is at the joint surface and the entire free element rotates laterally. In this case, Fick (1890) believed the proximal end would be ground into a cotyle over time. Adapted from Fick (1890: Fig. 2). Other abbreviations: **t1**, starting time; **t2**, time later in ontogeny.

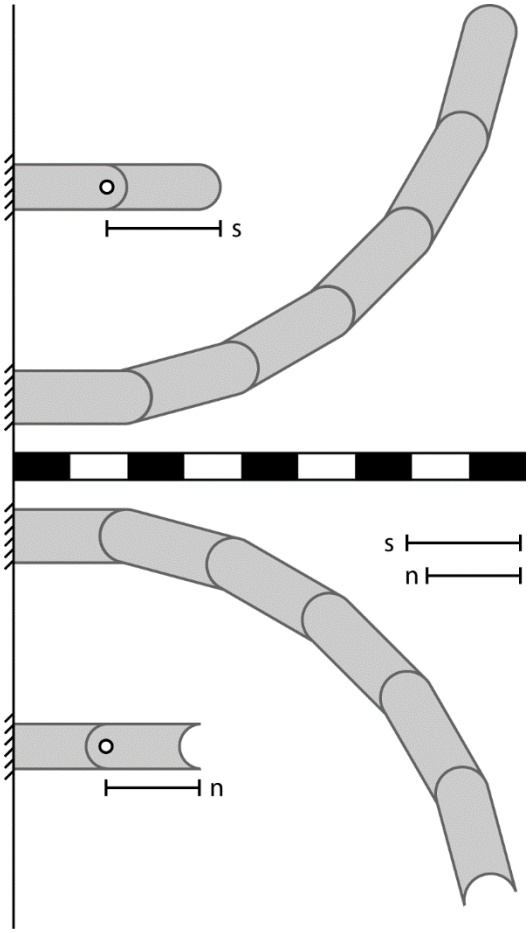

Figure 3.3. Influence of the position of the center of rotation (COR) of a concavo-convex joint on the total displacement of the free element, shown with schematic concavo-convex centra. Proximally-concave joints (top), such as those of sauropods, have the COR within the fixed element, resulting in a longer functional length (**s**) and a greater displacement per unit rotation. Proximally-convex joints (bottom) have the COR within the free element, resulting in a shorter functional length (**n**) and a lower displacement per unit rotation. Troxell (1925) proposed that this effect is additive serially, such that the sauropod-type joint will yield a much greater deflection from the midline. In practice, for a given angle of rotation, the two joint polarities yield nearly identical curvatures. Proximally-concave joints have a greater displacement only by the length of a single condyle regardless of the number of vertebrae in series. Abbreviations: **n**, non-sauropod type joint polarity; **s**, sauropod-type joint polarity.

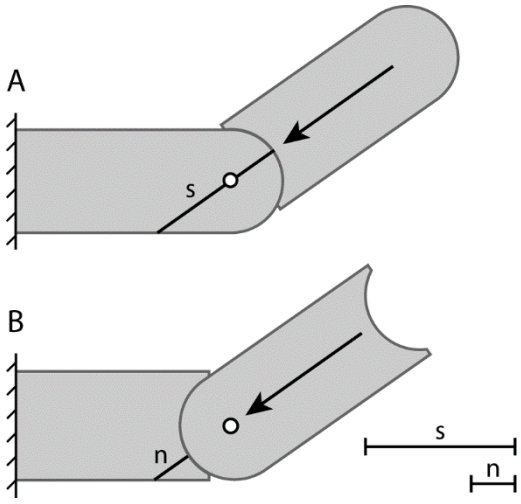

Figure 3.4. Resistance of centrum articular surfaces to stress when forces are directed parallel to the free element of a concavo-convex joint, as predicted by Troxell (1925). If compressional forces act parallel to the free element, proximally-concave centra result in a greater resistance to stress. A proximally-concave centrum (**A**) directs forces into the thicker condyle (**s**). A proximally-convex centrum (**B**) directs forces into the thinner cotylar rim (**n**), increasing the risk of fracture. Arrows indicate the presumed direction of compression. White circles represent the center of rotation. The labeled black lines indicate the thickness of bone in the fixed element resisting the applied compressive force. Modified from Troxell (1925). Abbreviations: **n**, non-sauropod type joint polarity; **s**, sauropod-type joint polarity.

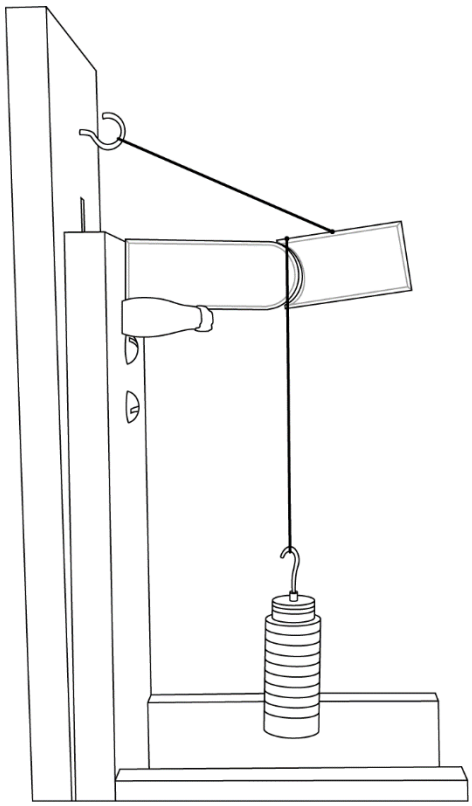

Figure 3.5. Model setup for testing concavo-convex joint rotational stability. Model is depicted with proximally-concave (sauropod-type) polarity and maximum applied load (250 g).

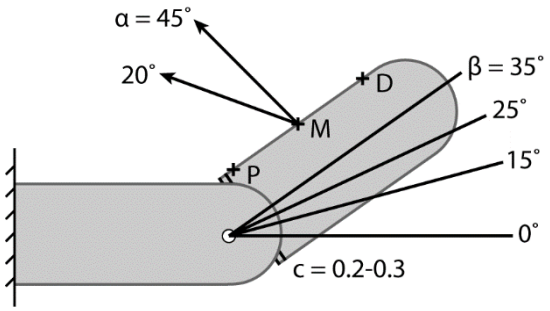

Figure 3.6. Model parameters that were varied during the rotational stability experiments, depicted on a schematic proximally-concave joint with the free centrum supported by a tensile element. The alternative, proximally-convex polarity is not pictured. The parameters are the insertion angle of the tensile element (**α**), the angle of rotation of the free element (**β**), the depth of the cotyle relative to its height (**c**), and the insertion site of the tensile element (black crosses). Another variable, the addition of weight to the distal end of the free element, is not shown. The white circle represents the center of rotation. Abbreviations: **D**, distal to the joint; **M**, middle; **P**, proximal to the joint.

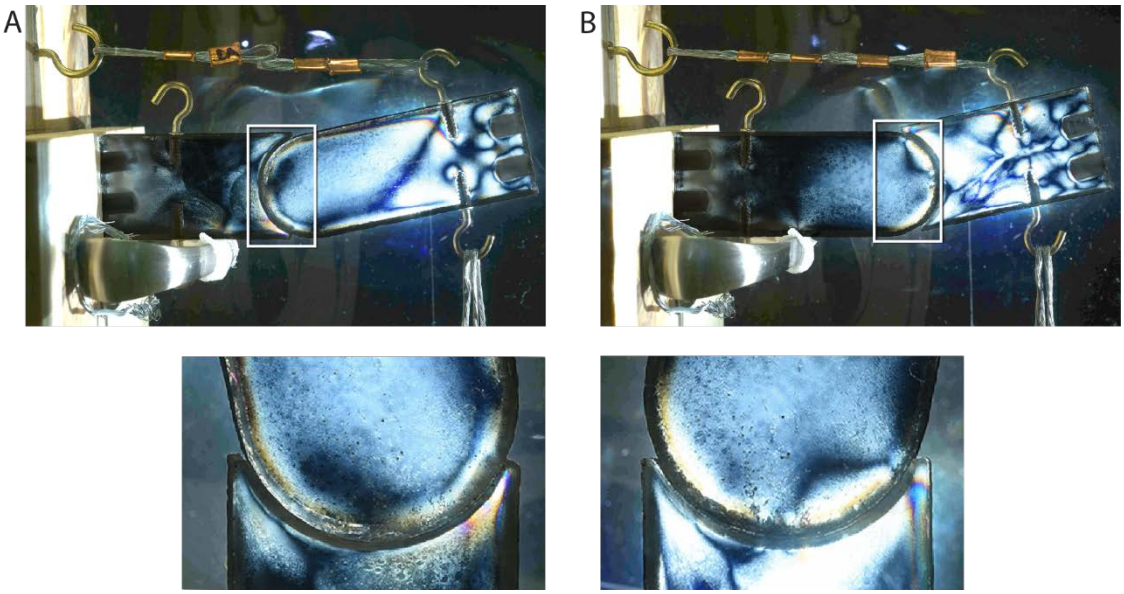

Figure 3.7. Stress distribution on modeled concavo-convex joints, as visualized using photoelasticity. Proximally-convex joints concentrate stress in the ventral cotylar rim (**A**). Proximally-concave joints concentrate stress in the dorsal cotylar rim (**B**). When compared side-by-side (lower panels), the two polarities exhibit the same magnitude of strain, as indicated by the order of the interference colors observed. In the lower panels, the joints have been rotated to allow direct comparison of the stressed region of the cotylar rim.

	β	0°			15°			25°			35°		
	c → / α	0.3	0.2	0.2+	0.3	0.2	0.2+	0.3	0.2	0.2+	0.3	0.2	0.2+
Proximal	20°	≥0	> 140	≥0	> 130	> 155	> 75	> 160	> 170	> 85	> 185	> 175	> 95
	45°	> 0	> 95	≥0	> 85	> 120	≥0	> 125	> 145	≥0	> 130	> 170	> 50
Middle	20°	> 190	20	130	> 215	115	70	> 225	130	140	> 230	> 225	> 180
	45°	160	25	65	225	60	170	> 230	145	> 175	> 235	180	> 195
Distal	20°	40	25	25	95	45	> 200	> 245	75	> 220	> 250	170	> 220
	45°	20	5	15	140	30	70	> 250	40	120	> 250	80	> 230

Figure 3.8. Stability differences between proximally-concave and proximally-convex joints across a range of biologically-plausible loading conditions. Each cell indicates how much more weight (in grams) was required for joint failure to occur in the proximally-concave joint than the proximally-convex one. Warm colors indicate differences that exceeded the model uncertainty, and cool colors indicate differences that did not exceed the model uncertainty. The columns and rows indicate five additional variables: the insertion site of the tensile element (**proximal**, **middle**, **distal**), the insertion angle of the tensile element (**α**), the angle of rotation of the free element (**β**), the depth of the concavity relative to its height (**c**), and the addition of weight to the distal end of the free element (+). A > sign indicates that the measured value is a minimum because the proximally-concave joint did not fail at the maximum applied weight (250 g with no distal loading or 230 g with distal loading). Values that are ≥ 0 are those for which neither polarity failed at the maximum load. Abbreviations: **c**, concavity.

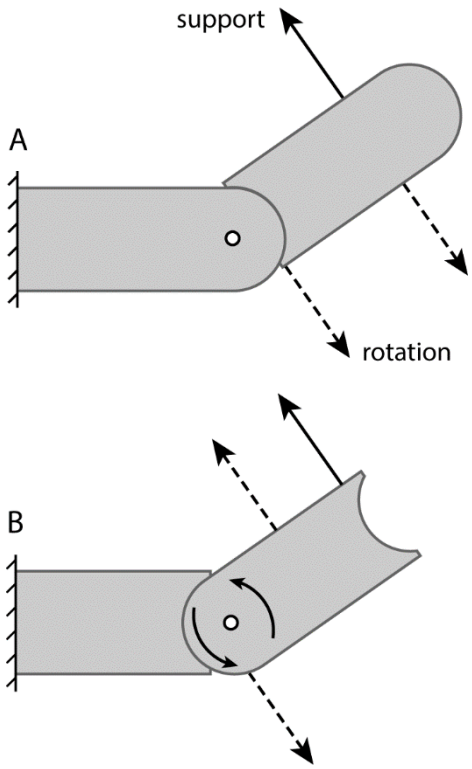

Figure 3.9. Influence of the position of the center of rotation of a concavo-convex joint on rotational stability. In a proximally-concave joint (**A**), the center of rotation (white circle) is within the fixed element, and the free element rotates about a point outside itself. For a force to pull the free element out of joint (dashed arrows), it must rotate both ends of the free element ventrally, which is directly opposed by the supporting tensile element (solid arrow). In a proximally-convex joint (**B**), the center of rotation is within the free element. If a force pulls the proximal end down and out of joint, the distal end rotates dorsally, which is unopposed by the tensile element. As a result, sauropod-type proximally-concave joints are less susceptible to joint failure by rotation.

Table 3.1. Measured rotational stability of concavo-convex joints, given by the weight applied near the joint necessary to cause joint failure. Variables at left are the joint polarity, muscle insertion site, and muscle insertion angle. Variables at top are the rotation angle of the free element and the cotyle depth-to-height ratio. All weights are in grams. Abbreviations: **+**, additional weight at the distal end of the free element (20 g).

		Rotation angle	**0°**			**15°**			**25°**			**35°**		
		Cotyle depth-height ratio	**0.3**	**0.2**	**0.2 +**	**0.3**	**0.2**	**0.2 +**	**0.3**	**0.2**	**0.2 +**	**0.3**	**0.2**	**0.2 +**
Proximally concave	**Proximal**	**20° muscle insertion**	> 250	> 250	> 230	> 250	> 250	> 230	> 250	> 250	> 230	> 250	> 250	> 230
		45° muscle insertion	> 250	> 250	> 230	> 250	> 250	> 230	> 250	> 250	> 230	> 250	> 250	> 230
	Middle	**20° muscle insertion**	> 250	60	215	> 250	135	> 230	> 250	140	> 230	> 250	> 250	> 230
		45° muscle insertion	190	45	145	245	75	230	> 250	155	> 230	> 250	190	> 230
	Distal	**20° muscle insertion**	65	35	85	110	45	135	> 250	75	195	> 250	170	> 230
		45° muscle insertion	25	5	35	140	30	80	> 250	40	130	> 250	80	> 230
Proximally convex	**Proximal**	**20° muscle insertion**	> 250	110	> 230	120	95	155	90	80	145	65	75	135
		45° muscle insertion	250	155	> 230	165	130	> 230	125	105	> 230	120	80	180
	Middle	**20° muscle insertion**	60	40	85	35	20	65	25	10	55	20	5	50
		45° muscle insertion	30	20	80	20	15	60	20	10	55	15	10	35
	Distal	**20° muscle insertion**	25	10	60	15	0	30	5	0	10	0	0	10
		45° muscle insertion	5	0	20	0	0	10	0	0	10	0	0	0

CHAPTER 4

NEUROCENTRAL SUTURE COMPLEXITY AND STRESS DISTRIBUTION IN THE VERTEBRAL COLUMN OF A SAUROPOD DINOSAUR

Abstract.—Sauropod dinosaurs achieved extreme body sizes via rapid and sustained growth, permitted in part by the delayed fusion of the neurocentral sutures. Unfused sutures are joined by cartilage, which is more susceptible to dislocation than the bone that replaces it. In sauropods, the competing interests of growth and strength were balanced by the presence of complex, interdigitated neurocentral sutures. Sutural complexity is correlated with the magnitude of stress the suture must resist. To better understand this relationship in sauropods, sutural complexity was measured from the articulated presacral vertebrae of *Spinophorosaurus nigerensis*. Complexity was calculated as a length ratio and as the fractal dimension of the suture, and patterns of gross morphology were observed. The complexity pattern indicates that stress increased proximally along the neck, was greatest in the anterior dorsal vertebrae, and decreased towards the sacrum. This stress distribution would result from supporting the weight of the neck and the ribcage. The sutural structures in cervical vertebrae are oriented to resist anteroposterior translation of the neural arch; in dorsal vertebrae, resistance to lateral rotation of the neural arch is greater. This pattern could result from the greater mechanical advantage of an elongate cervical centrum in resisting torsion relative to a short dorsal centrum, and the greater mechanical advantage of wide dorsal transverse processes in generating torsion. The patterns and

structures described are similar to those of *Alligator*. Complex neurocentral sutures may represent an archosauriform adaptation that facilitated rapid growth rates and large adult body sizes.

Introduction

Sauropod dinosaurs represent an extreme condition in the history of vertebrate biomechanics, having achieved the largest body sizes (Alexander 1989) and longest necks (Taylor and Wedel 2013) of any terrestrial vertebrates. Their highly elongate necks and tails acted as opposed cantilevers, supported only at the proximal end (i.e., the body). The considerable weight of the neck and tail was transferred to the body via compressive stress on the vertebral centra and tensile stress in the muscles and ligaments inserting on the neural arches, as in extant mammals (Slijper 1946) and reptiles (Hoffstetter and Gasc 1969), as well as shear stresses acting across the intervertebral joints (Salisbury and Frey 2001; Fronimos and Wilson in review). It has long been recognized, in particular from histological evidence (e.g., Rimblot-Baly et al. 1995; Curry 1999; Sander 2000), that sauropods achieved their extreme dimensions via growth that was both rapid and sustained. Studies suggest that they achieved growth rates exceeding those of modern non-avian reptiles (e.g., Lehman and Woodward 2008; Grady et al. 2014) and perhaps even approaching those of placental mammals (D'Emic 2015). In the vertebral column, this growth would have been facilitated by the delayed closure of the neurocentral junction, which is an important zone of growth for both the neural arch and the centrum (Vital et al. 1989).

The neurocentral junction is a synchondrosis (a joint connected by cartilage) between two separately-ossified elements in juvenile vertebrates (Ikejiri 2012) that is typically fused by the

ossification of cartilage at or before the time of maturity (Romer 1956). In archosaurs, however, the neurocentral suture commonly remains patent in at least part of the vertebral column long after sexual maturity (Ikejiri 2010, 2012). The capacity for continued growth comes at a cost, as the cartilage holding the joints together is more susceptible to dislocation than the bone that replaces it after fusion (Moss, 1958; Herring, 1972; Jaslow 1990). Therefore, in the neurocentral sutures of immature sauropods, the demands of a rapid growth rate were in competition with the need to resist stresses resulting from increasingly large body size.

One way in which sauropods and other archosaurs appear to have balanced these competing demands is through the development of complex, interdigitated neurocentral sutures (Ikejiri 2010; Fig. 4.1). It has been previously remarked that cranial sutures that fuse late in ontogeny are typically more highly interdigitated than those that fuse earlier (e.g., Washburn 1947; Herring 1972). However, delayed fusion alone does not provide a consistent explanation for sutural interdigitation; as noted by Herring (1972: p. 244), "growth alone is not sufficient to cause interdigitation, and some other factor (for example, stress) is also necessary." Studies of stress in cranial sutures (e.g., Moss 1957; Herring 1972) have demonstrated that the complexity of interdigitation is linked to the magnitude and type of stresses acting upon the suture. Interdigitated sutures generally provide a greater strength than straight sutures because they increase the area of contact between bones without increasing the total volume of the bones (Long 1985). This is consistent with in situ measurements of the stress distribution on variably interdigitated sutures in the skulls of mammals (e.g., Jaslow 1989; Herring and Mucci 1991; Byron et al. 2004) and fish (Markey et al. 2006). Sutural complexity is greatest in areas of predominately compressive stress and least in areas where tensile stress dominates (Herring and

Mucci 1991; Raffery and Herring 1999). Greater sutural complexity is also correlated with greater bending strength (Jaslow 1990).

Interdigitated neurocentral sutures characterize many archosauriforms (Ikejiri 2010) and may be seen in a diverse range of sauropods (e.g., *Rapetosaurus*, Curry Rogers 2009; *Spinophorosaurus*, Remes et al. 2009; *Europasaurus*, Carballido and Sander 2014; *Bonitasaura*, Gallina and Apesteguía 2015). Ikejiri (2010) proposed that these complex sutures are functionally similar to cranial sutures in the relationship between complexity and stress. In addition, Ikejiri (2010) noted that interdigitations in crocodylian neurocentral sutures often take the form of transverse ridges (Fig. 4.1.2) that may resist shear stresses and oppose lateral rotation of the neural arch relative to the centrum; similar transverse ridges occur in the sauropod taxa listed above. Therefore, it is plausible that neurocentral sutural complexity in sauropods and other archosauriforms represents a means to resist stresses acting on the spine while maintaining an active zone of growth within the vertebra.

To better understand the relationship between sutural complexity and stress distribution in sauropod dinosaurs, we present a quantitative description of neurocentral suture morphology in the basal eusauropod *Spinophorosaurus nigerensis*. Sutural complexity was calculated for an articulated series of presacral vertebrae, and patterns of variation between and within vertebrae were compared to the expected stress distributions. The results reveal regional variation in how the neurocentral junction was loaded and suggest relationships between distinctive morphological features and specific loading regimes.

Institutional Abbreviations.—**GCP**: Grupo Cultural Paleontológico de Elche, Spain; **NMB**: Staatlisches Naturhistorisches Museum Braunschweig, Germany; **UMMZ**: University of Michigan Museum of Zoology, USA.

Materials and Methods

Material Examined.—The holotypic specimen of *Spinophorosaurus nigerensis* includes the majority of the vertebral column, which was found in articulation from the second cervical vertebra to the 37th caudal vertebra (Remes et al. 2009). The centra of the second and ninth dorsal vertebrae were not preserved. Part of the holotype (NMB-1699-R) is reposited in Braunschweig, Germany, including the second and third cervical vertebrae; the remainder of the holotype (GCP-CV-4229), including the fourth through twelfth cervical vertebrae and all preserved dorsal, sacral, and caudal vertebrae, is held in the Museo Paleontológico de Elche. Only GCP-CV-4229 was examined for this study. The neurocentral suture is observable in all the presacral vertebrae. In certain cervical vertebrae, it was partially obscured by the diapophysis, which crosses the neurocentral junction. The sacral and caudal vertebrae were not included in this study because the neurocentral sutures are obscured by the attachment of the sacral ribs and caudal transverse processes, respectively. The neural arch and centrum remain in articulation in all of the vertebrae examined, so only the two-dimensional surface trace of the suture is visible. Although a study of cranial sutures in the actinopterygian fish *Polypterus* by Markey and Marshall (2007) found cross-sectional interdigitation to be more functionally informative than the interdigitation of the surface trace, we consider the surface trace of the neurocentral suture to be more representative of the internal structure than it is for cranial sutures. As described above, in sauropods and crocodylians, the interdigitations visible on the lateral surface trace of the neurocentral suture (Fig. 4.1.1) correspond to transverse ridges that continue medially into the interior of the element, in many cases all the way to the neural canal (Fig. 4.1.2). Additionally, several large-scale structures observed in the surface traces of *Spinophorosaurus* were found to

be serially-persistent, suggesting that the morphology of the surface trace is functionally significant (see Results).

Data Collection.—To capture the surface trace of each neurocentral suture, the presacral vertebrae were photographed in left lateral view with a Canon EOS and a Fujifilm XF1 digital camera. Images were taken on manual focus with an ISO of 100–2000, an aperture of 1.8–22.0, and a shutter speed of 1/4–1/200s, depending on the size, position, and lighting conditions of the specimen. The cervical vertebrae were photographed in groups of three to five in articulation and at a lower magnification than the dorsal vertebrae. The dorsal vertebrae, as well as the fourth and tenth cervical vertebrae, were photographed individually, with the exception of the 13th dorsal vertebra, which was photographed in articulation with the sacral series. For each vertebra, the photograph that most clearly captured the neurocentral suture was selected for digitization.

The sutural traces were digitized in Adobe Illustrator CS6 using a WACOM intuos tablet. Repeated trials at different pencil fidelities (0.5, 1.0, 2.0 pixels) indicated that a fidelity of one pixel best captured the detail of the sutural trace without introducing noise from subtle and/or accidental hand movements. All digitization was done by the same investigator (JAF). Because the photographs were taken at different magnifications, it was necessary to assess whether complexity variation was confounded by magnification. To do this, each sutural trace was digitized twice, once with the image of the suture filling the screen, another time with the image zoomed in until no further gain in resolution could be achieved. The scale bar in each image was measured on the monitor to calculate the magnification for every measurement. To test for error due to the investigator, one specimen, the fifth dorsal vertebra, was traced at both scales three times, at the beginning, middle, and end of data collection, and the results were compared.

To digitize each sutural trace, the dorsal margin of the suture (i.e., the neural arch component) was followed except in cases where the dorsal margin was unequivocally broken and the adjoining ventral margin was intact enough to follow instead. Only the left lateral aspect of the sutural trace was digitized, with the end points defined by where the sutural trace curved medially towards the neural canal; reference to multiple photographs was used to verify the location of this point in three dimensions. Each digitized trace represents a two-dimensional projection of a three-dimensional structure; the selection of the end points restricts the digitized portion of the suture to the nearly two-dimensional lateral aspect of the suture. In some specimens (the fourth cervical vertebra and the first, fifth, seventh, and eleventh dorsal vertebrae), damage to the neural arch pedicle truncated one end of the sutural trace. In such cases, complexity was estimated from the preserved part of the suture. In the fourth cervical vertebra, a photograph of the right side of the vertebra allowed the missing end of the suture to be estimated; the trace of the right side was flipped, rescaled, and aligned to the left side using the ends of the centrum for reference, then the two traces were joined at an area of overlap. In cervical vertebrae 4–10 and 12, the diapophysis obscured an anterior segment of the suture in lateral view. Additionally, in the ninth cervical vertebra, a fracture through the posterior centrodiapophyseal lamina removed a posterior segment of the suture. In these cases, the missing region was bridged with a straight line segment, providing a minimum estimate for the total complexity of the suture. In two other cases (cervical nine, dorsal seven), a fracture displaced part of the centrum relative to the rest. These were digitally restored to the correct position in Adobe Photoshop before the suture was digitized.

Complexity Metrics.—To compute the complexity of each sutural trace, two different commonly-used metrics were calculated. The first metric is the ratio of the total length of the surface trace of a suture to the straight-line length from one end point of the suture to the other (see Fig. 4.2, inset). Originally proposed by Jaslow (1989: p. 275) and termed "sutural complexity," the metric has been frequently used (e.g., Anton et al. 1992; Nicolay and Vaders 2006; Markey and Marshall 2007) under a variety of names. Here, the name "length ratio" is used, following Nicolay and Vaders (2006: p. 843), to distinguish the metric from other measures of complexity. Nicolay and Vaders (2006: p. 845) favored the length ratio as a metric because it captures complexity "at the gross morphological level," which is of interest in the analysis of stress resistance, and because it directly reflects increases in the amount of cartilage present within the joint.

To compute the length ratio, the total length and straight-line length between end points of each neurocentral suture were measured in Adobe Illustrator using the Object Info window. This window provides the object length scaled to document size rather than actual size, so the measurements were rescaled relative to the object length of a 1 cm line on the scale bar in the photograph. The total length of each suture was taken from the digitized trace, and the straight-line length was measured by connecting the end points of the suture trace with a straight line segment. The ratio of the two measurements for each trace was then calculated to yield a whole-suture length ratio. To evaluate how complexity varies along the length of the suture, length ratios were also calculated for segments. This was done by dividing the straight-line length of each trace into ten equal-length segments. The segments were marked by guidelines in Adobe Illustrator oriented orthogonal to the straight-line length. Where each guideline intersected the sutural trace, an anchor point was added, allowing each part of the trace to be selected

independently with the direct selection tool and duplicated as separate objects. In some places, the sutural trace curved back and forth between adjacent segments; in these cases, all parts of the suture within a given segment were counted towards that segment, even if they were not contiguous. The resulting ten segments were aligned at their end points to confirm that no anchor points were missed. For each segment, the length ratio was calculated using one tenth of the original straight-line length as the denominator. For additional insight into the relationship between sutural morphology and the length ratio, the height of the highest peak in each suture was taken using the Object Info window, as described above. This was measured orthogonal to the straight-line between the end points, which also served as the baseline for the height.

The other commonly employed metric of sutural complexity is the fractal dimension (e.g., Long 1985; Masuda and Yohro 1987). The concept of fractal dimensions is summarized by Mandelbrot (1967) and is only briefly reviewed here. For a sufficiently complex or self-similar line such as a suture, the measured total length of the line increases exponentially as the measurement scale is made finer. The relationship is described by an exponent, *D*, that ranges from a value of one for a straight line to two for a plane; the non-integer values of complex lines represent fractional dimensionality. In biology, the fractal dimension *D* is often used as a measure of how fully a complex line occupies the space in which it occurs (Cross 1997). Although the fractal dimension is often thought of in terms of self-similarity, a line need not be a true fractal (i.e., self-similar) to provide a value of *D* (Long and Long 1992), making it applicable to a broad range of biological structures.

The fractal dimension of the sutural traces was calculated using the FracLac v. 2.5 plugin (Karperien 1999–2013) for ImageJ version 1.48v (Rasband 1997–2014). This plugin determines *D* using a box-counting algorithm, which superimposes grids of different spacing over the sutural

trace and counts the number of boxes that are occupied. When the logarithm of the grid spacing is plotted against the logarithm of the box count, the slope found by linear regression gives an estimate of the fractal dimension, *D* (Morse et al. 1985). Each sutural trace was saved in a separate file, oriented with the end points aligned horizontally. To create a binary raster image suitable for the box-counting algorithm, each trace was converted to grayscale and saved as a TIFF file without anti-aliasing at 150 dpi, which provided the closest resolution to that of the original photographs. In FracLac, the minimum box size was set at 5 pixels to avoid boxes smaller than the smallest data point, which result in an underestimation of *D* (Górski and Skrzat 2006). The maximum box size was set at 45% of image size, and the number of box sizes between the maximum and minimum was determined automatically by the program. The algorithm was run four times with different starting grid positions, and the outcomes of each were averaged to yield a final value of *D* for each trace.

Results

General Description of Neurocentral Suture Morphology.—In every presacral vertebra of *Spinophorosaurus* observed, the neurocentral suture has its lateral aspect dorsal to the pleurocoel and ventral to the floor of the neural canal. At its anterior and posterior ends, the suture curves dorsally and medially to follow the base of the neural arch pedicle a short distance above the floor of the neural canal. In the third and fourth dorsal vertebrae (hereafter D3–4), the parapophysis spans the neurocentral junction and is cut across by the neurocentral suture. Two large-scale structures of the suture persist serially through much of the presacral column. The first is a prominent dorsally-directed peak that occurs in every vertebra studied with the exception of D12–13 (Fig. 4.2, inset). In the cervical vertebrae and D1–3, this peak is located in

the anterior half of the suture, and in D4–11 it is located at approximately mid-length along the suture. The position of the peak coincides approximately with the position of the diapophysis. In the dorsal region, the peak is sometimes composed of multiple large-scale interdigitations, with a single peak occurring in D1, D3, and D5, three peaks in D4, D6, D10, and D11, and two distinct areas containing multiple peaks in D7–8. The second serially-persistent structure is a prominent interdigitation or spike near the posterior end of the centrum (Fig. 4.2, inset). In cervical vertebrae four through 11 (hereafter C4–11), the structure is a long, slender, posteriorly directed process. From C12 to D4, the process is stout and directed posteroventrally. In D6 and possibly D7, there is a short, ventrally-directed process in the same location. The structure is absent in D8–13.

Quantification of Experimental Error.—Complexity calculated using the length ratio method shows a weak positive correlation with image magnification. When the cervical and dorsal vertebrae are considered separately, this relationship disappears and complexity is uncorrelated with magnification. Complexity represented by the fractal dimension is uncorrelated regardless of whether the results are compared in the aggregate or divided up by region. Therefore, complexity differences between cervical and dorsal vertebrae are regarded as genuine biological patterns, rather than artifacts of image resolution. Sutural traces digitized from the same image at two different magnifications afford an additional test for error due to differences in image magnification. The average difference in the length ratio between the higher magnification and lower magnification trace of the same image is 3.0 percentage points, and the maximum difference observed is 12.1 percentage points. For the fractal dimension, the average difference is 0.004 and the maximum difference is 0.015. Replicate measurements of D5 taken at

different times yielded a maximum difference in length ratio of 9.7 percentage points and in fractal dimension of 0.018. Therefore, only differences between vertebrae that exceed the maximum error values are regarded as significant.

Length Ratio Results.—Measured neurocentral suture length ratios (Fig. 4.2; Table 4.1) range from 113.1% to 179.3%. The length ratio generally increases proximally along the neck, reaching the highest values in the anterior to middle dorsal region, and decreasing in the posterior dorsal vertebrae. In C4–6, values are among the lowest measured, remaining near 120%. Posteriorly, these values generally increase to C12, which has a length ratio of almost 160%. Measured complexity for C4–10 represents the minimum values because the diapophysis obscured part of the sutural trace from view. The complexity of C9 and C11 is significantly lower than expected based on the adjacent vertebrae. This appears to be genuine; although there is some damage to C9, the preserved regions exhibit generally lower complexity than the corresponding regions of C8 and C10 (see below and in Fig. 4.4), and C11 is undamaged. Complexity is also significantly lower at D1, but the possibility that this is due only to the relatively complex posterior end of the suture being broken off cannot be excluded. The most complex suture occurs in D3, and the values of D5–7 are not significantly different from D3, lying within the range of 170–180%. A significant decrease at D4, which is not attributable to damage, overlaps the highest measured cervical values. From D7 to D12 there is a continuous decline in complexity; D12 is closely comparable to the anterior cervical vertebrae. D13 has a more intermediate value, similar to D4 and D10.

The observed complexity patterns are closely matched by the variation in height of the highest peak in the suture, except in the region from C8 to D1 (Fig. 4.3; Table 4.1). The peaks of

C9 and D1 are taller relative to the overall length ratio than in most vertebrae, whereas the other vertebrae in this region have lower peaks relative to the length ratio. The variation in the length ratio within each suture (Fig. 4.4; Table 4.2) further indicates that gross morphological features, the mid-length peak and posterior spike, are major influences on the total complexity of a vertebra. The vertebrae present distinct regional patterns in how complexity is distributed within sutures, although the transitions between regions are usually gradational. In C4–9 (see Fig. 4.4, C7), complexity is highest at the ends of the suture where the sutural trace turns dorsally, especially near the posterior end where the elongate spike structure is present. The length ratio near the peak, when known, does not exceed 150%, and elsewhere the ratio remains near value of a straight line (100%). In C10–D1 (see Fig. 4.4, C10), the length ratio increases in all parts of the suture; the greatest increase is in the anterior half, where values may exceed 200%. The posterior spike persists, associated with values above 200%. In D3–5 (see Fig. 4.4, D3), high complexity is more broadly distributed in the anterior half of the suture than in cervical vertebrae, and the posterior spike continues to make a large contribution to total complexity. In the most complex suture, that of D3, the high overall complexity can be attributed to very high length ratios (> 300%) near both the mid-length peak and the posterior spike. In D6–11 (see Fig. 4.4, D8), the pattern characteristic of anterior cervical vertebrae has been reversed: high complexity values are broadly distributed throughout the middle portion of the suture, and low values occur at the ends. The reduced posterior spike makes little contribution to total complexity; from D8 onward, it is lost altogether. The pattern of decreasing total complexity from D8–12 is linked to decreasing complexity throughout the suture. In D12–13 (see Fig. 4.4, D13), the mid-length peak and associated high complexity values in the middle of the suture are

lost and the complexity pattern becomes more irregular, with slightly higher values posteriorly. Length ratios in this region do not exceed 200%.

Fractal Dimension Results.—The fractal dimension of the neurocentral sutures ranges from 1.060 to 1.174 (Fig. 4.5; Table 4.1) and is poorly correlated with the length ratio. The highest values occur in the middle cervical vertebrae, reaching a maximum in C10 that is significantly higher than in all other vertebrae. Dorsal values show a general increase from D1, comparable to the lowest anterior cervical values, to D7, which is not significantly different from most middle cervical vertebrae. The fractal dimension and length ratio results are similar in having increasing values from the anterior to middle cervical vertebrae and in the general pattern of the dorsal values. Both metrics indicate lower values for C9, D1, D4, and D12 relative to the adjacent vertebrae, but for the fractal dimension, the differences for D4 and D12 are not significant. Serial variation in the fractal dimension does not correspond to changes in the large-scale morphological features of the suture, the mid-length peak and the posterior spike.

Discussion

The observed variation in the neurocentral suture complexity of *Spinophorosaurus* greatly exceeds the magnitude of error in data collection. The two metrics used here, the length ratio and the fractal dimension, present different patterns of complexity. The length ratio is particularly sensitive to large-scale morphological features (Nicolay and Vaders 2006). The fractal dimension measures how complexity increases at finer scales and is, therefore, less sensitive to large-scale features. These results indicate that, in the neurocentral sutures of *Spinophorosaurus*, the development of large-scale structures within sutures is not closely

coupled to the fractal elaboration of fine-scale interdigitations. This stands in contrast to studies of mammalian cranial sutures that have found agreement between length ratios and fractal dimensions (Byron et al. 2004; Nicolay and Vaders 2006). Mammalian cranial sutures do not exhibit large-scale structures within the length of a single sutural segment, so complexity is entirely a function of the amplitude and elaboration of the interdigitations. Therefore, the two metrics will be more closely correlated. It is noteworthy that the fractal dimensions measured in this study (1.047–1.174) are lower than those typical of mammalian cranial sutures (e.g., approximately 1.2–1.5 in humans, Masuda and Yohro 1987, and in deer, Nicolay and Vaders 2006), overlapping with the relatively simple interfrontal suture in juvenile deer. It is possible that the large-scale morphological structures represent an alternative stabilizing mechanism to the fractal elaboration of interdigitations. However, it remains to be determined whether the two modes of stabilization are functionally equivalent, or whether they are instead adaptations to different loading regimes. We also cannot rule out the possibility that the lower fractal dimensions in *Spinophorosaurus* are a phylogenetic signal, as fractal dimension values measured for cranial sutures in *Caiman* are similarly low (approximately 1.12–1.29, Monteiro and Lessa 2000). The question of what drives the serial variation in the fractal dimension of the neurocentral sutures independent of gross morphology remains an open one.

The length ratio, as a measure of complexity, offers the clearest insight into the stress distribution because its variation corresponds to distinct regional transitions in other aspects of vertebral morphology, and because it captures variation in the surface area of the neurocentral junction (Nicolay and Vaders 2006). In *Spinophorosaurus*, the length ratio increases proximally along the neck, reaches its maximum in the anterior-middle dorsal vertebrae, and decreases posteriorly towards the sacrum. The same pattern is also present in *Alligator* (Ikejiri 2010). The

pattern in the cervical and anterior dorsal vertebrae is consistent with the expected distribution of compressive stress, of which sutural complexity is a known indicator (e.g., Herring and Mucci 1991; Rafferty and Herring 1999). The weight of a cantilevered neck increases proximally and is borne most heavily by the anterior dorsal vertebrae. Conversely, the lower sutural complexity of the cervical region may indicate that the neurocentral sutures of the neck were loaded primarily in tension by the interspinal ligaments and epaxial muscles.

Several factors could explain the reduction in complexity in the posterior dorsal region. First, these vertebrae do not support the weight of the neck. Second, the dorsal ribs, which bear the weight of the viscera, decrease in size and lose their connection to the sternum posteriorly (Romer 1956). In *Spinophorosaurus*, this reduction begins at D6; no ribs were reported for D12–13 (Remes et al. 2009). This offers an explanation for why the highly-complex peak in *Spinophorosaurus* neurocentral sutures is generally positioned close to the diapophysis, and why the peak is lost in the last two dorsal vertebrae. This interpretation is also consistent with the patterns in *Alligator*, which has a distinct lumbar region (i.e., lacking dorsal ribs; see Reese 1915). The lumbar vertebrae of *Alligator* exhibit the lowest complexity values in the dorsal column, and the mid-length peak in this region is reduced in height (Ikejiri 2010). Finally, the posterior dorsal region is subject to additional stabilization. In non-titanosaur sauropods such as *Spinophorosaurus*, the posterior dorsal vertebrae bear accessory articulations, the hyposphene-hypantrum complex (Gauthier 1986; Wilson and Sereno 1998), and there is a general trend in the clade for the incorporation of posterior dorsal vertebrae into the sacrum (Wilson and Sereno 1998). However, in *Spinophorosaurus*, the hyposphene-hypantrum is present from the D4–5 joint onward (pers. obs.), which does not coincide with where complexity begins to decrease. In at least some crocodylians, the posterior dorsal region is an area of low flexibility (Molnar et al.

2014), and the posteriormost dorsal vertebra is braced by the sacral ribs (Reese 1915; Fronimos and Wilson in review). However, the hypothesis that the posteriormost dorsal vertebra has extra stabilization, and is perhaps incipiently sacralized, does not explain why, in both taxa, this vertebra has a higher complexity than one or more preceding dorsal vertebrae.

As noted by Ikejiri (2010), interdigitated neurocentral sutures also provide resistance to shear stress and rotation of the neural arch relative to the centrum. We reconstruct these stresses by examining the distribution of complexity within sutures as well as the large-scale morphological structures present. In the cervical vertebrae, complexity is greatest at the ends of the sutures, due in large part to the presence of the posteriorly directed spike (Fig. 4.4; Table 4.2). This arrangement would provide resistance to the posterior translation of the neural arch relative to the centrum, as might result from the proximally directed pull of the interspinal ligaments and epaxial muscles supporting the neck.

Additional evidence for significant anteroposterior loading in sauropod cervical vertebrae is provided by the morphology of the neurocentral junction in the titanosaur *Rapetosaurus* (e.g., C3; Curry Rogers 2009: Fig. 7). Internally, the surface of the neurocentral junction is spanned by numerous ridges that show a strong transverse alignment. This orientation would resist anteroposterior translation and provide some resistance to lateral rotation, but it would not oppose lateral translation caused by unidirectional contraction of the epaxial muscles. The forces involved in supporting the sauropod neck were likely the greatest loads acting on the neurocentral junctions, resulting in greater stabilization against anteroposterior movement than lateral movement. It is also possible that the suture morphology reflects predominately dorsoventral mobility of the neck, as Christian and Dzemski (2007) proposed for *Giraffatitan*. A third interpretation is that the morphology of sauropod cervical vertebrae conferred intrinsic

resistance to lateral rotation of the neural arch. The length of the neurocentral junction would provide a long moment arm to resist rotation, and the short transverse processes would provide a shorter moment arm to the muscles involved in lateral flexion. Thus, the risk of neurocentral joint failure in cervical vertebrae due to lateral flexion may have been reduced relative to dorsiflexion.

In the posterior cervical and dorsal vertebrae of *Spinophorosaurus*, the contribution of the posterior spike to total complexity diminishes, and the spike becomes shorter and more dorsoventrally oriented (Figure 4.4; Table 4.2). The peak near mid-length becomes taller and, often, more highly interdigitated. This suggests a reduction in the importance of anteroposterior translation relative to compression and/or rotation. In *Rapetosaurus*, the neurocentral junctions of posterior cervical and dorsal vertebrae exhibit ridges that are oriented anterolaterally and posterolaterally at the ends of the vertebra and transversely in the middle, forming an overall radial pattern (e.g., D4; Curry Rogers 2009: Fig. 17). This arrangement would provide resistance to lateral rotation of the neural arch relative to the centrum. The same arrangement of ridges is seen throughout the presacral column of *Alligator* (e.g., Ikejiri 2010: Fig. 3-4). In sauropods, the posterior cervical and anterior dorsal regions could be a region of increased lateral flexion relative to dorsiflexion, as suggested by Christian and Dzemski (2007). Although this is plausible, the suture morphology in this region can also be explained without increased lateral flexibility. The short centra of posterior cervical and dorsal vertebrae would provide a mechanical disadvantage in resisting lateral rotation of the neural arch, and the broad transverse processes would provide a long moment arm for the generation of torque at the neurocentral junction. Thus, additional stabilization against rotation may have been necessary even without much lateral flexibility. This accords with the condition in *Alligator*, in which the presacral

column exhibits only modest lateral flexibility and the cervical centra are not elongated (Fronimos and Wilson in review).

Many questions remain regarding the function of complex neurocentral sutures. Further study of sutural morphology in sauropods is needed to assess whether the patterns described here are general to the clade or specific to the taxa discussed. If variations exist among taxa, we predict that sutures should be more complex in larger-bodied and longer-necked taxa. Additionally, the morphology of ridges and other sutural structures should vary with the proportions of vertebral centra and transverse processes, and perhaps also with joint mobility. As noted by Ikejiri (2010), complex, interdigitated neurocentral sutures may be synapomorphic for Archosauriformes. Placing sutural morphology in a phylogenetic framework would help to illuminate the relationships between complexity, the timing of fusion, growth rate, and adult body size in this clade.

Conclusions

The extended period of rapid growth experienced by sauropod dinosaurs required that the neurocentral junctions remain unfused even as the animals attained very large body sizes. As a result, the increasingly heavy loading of the neurocentral junctions was borne by cartilage, which is more susceptible to dislocation than solid bone (Moss, 1958; Herring, 1972; Jaslow 1990). The presence of complex, interdigitated neurocentral sutures may represent an adaptation to strengthen the joints against dislocation (Ikejiri 2010). The results of this study indicate that the neurocentral suture morphology in *Spinophorosaurus* is consistent with a role in resisting stresses acting on the neurocentral junction. Total sutural complexity reflects the distribution of stress resulting from the weight of the neck and the ribcage. The distribution of complexity

within a single suture, combined with the orientation of internal ridges, confers resistance to anteroposterior translation in the neck and to lateral rotation in the trunk. Complexity in these vertebrae results primarily from large-scale morphological structures that can be linked to particular stress regimes. The fine-scale elaboration of interdigitations appears to have been less significant for resisting these stresses. We conclude that the presence of complex, interdigitated neurocentral sutures in sauropods and other archosaurs enabled vertebral growth to continue to an advanced ontogenetic stage while resisting the stresses associated with large body size.

Literature Cited

Alexander, R. M. 1989. Dynamics of dinosaurs and other extinct giants. Columbia University Press, New York.

Anton, S. C., C. R. Jaslow, and S. M. Swartz. 1992. Sutural complexity in artificially deformed human (*Homo sapiens*) crania. Journal of Morphology 214:321–332.

Byron, C. D., J. Borke, J. Yu, D. Pashley, C. J. Wingard, and M. Hamrick. 2004. Effects of increased muscle mass on mouse sagittal suture morphology and mechanics. The Anatomical Record 279A:676–684.

Carballido, J. L., and P. M. Sander. 2014. Postcranial axial skeleton of *Europasaurus holgeri* (Dinosauria, Sauropoda) from the Upper Jurassic of Germany: implications for sauropod ontogeny and phylogenetic relationships of basal Macronaria. Journal of Systematic Palaeontology 12:335–387.

Christian, A., and G. Dzemski. 2007. Reconstruction of the cervical skeleton posture of *Brachiosaurus brancai* Janensch, 1914 by an analysis of the intervertebral stress along the neck and a comparison with the results of different approaches. Fossil Record 10:38–49.

Cross, S. S. 1997. Fractals in pathology. Journal of Pathology 182:1–8.

Curry, K. A. 1999. Ontogenetic histology of *Apatosaurus* (Dinosauria: Sauropoda): new insights on growth rates and longevity. Journal of Vertebrate Paleontology 19:654–665.

Curry Rogers, K. 2009. The postcranial osteology of *Rapetosaurus krausei* (Sauropoda: Titanosauria) from the Late Cretaceous of Madagascar. Journal of Vertebrate Paleontology 29:1046–1086.

D'Emic, M. D. 2015. Comment on "Evidence for mesothermy in dinosaurs." Science 348:982.

Fronimos, J. A., and J. A. Wilson. In review. Concavo-convex intervertebral joints stabilize the vertebral column in sauropod dinosaurs and crocodylians. Paleobiology.

Gallina, P. A., and S. Apesteguía. 2015. Postcranial anatomy of *Bonitasaura salgadoi* (Sauropoda, Titanosauria) from the Late Cretaceous of Patagonia. Journal of Vertebrate Paleontology 35: e924957-1–22.

Gauthier, J. 1986. Saurischian monophyly and the origin of birds. *In* K. Padian, ed. The origin of birds and the evolution of flight. Memoirs of the California Academy of Sciences 8:1–55.
Górski, A. Z., and J. Skrzat. 2006. Error estimation of the fractal dimension measurements of cranial sutures. Journal of Anatomy 208:353–359.
Grady, J. M., B. J. Enquist, E. Dettweiler-Robinson, N. A. Wright, and F. A. Smith. 2014. Evidence for mesothermy in dinosaurs. Science 344:1268–1272.
Herring, S. W. 1972. Sutures – a tool in functional cranial analysis. Acta Anatomica 83:222–247.
Herring, S. W., and R. J. Mucci. 1991. In vivo strain in cranial sutures: the zygomatic arch. Journal of Morphology 207:225–239.
Hoffstetter, R., and J.-P. Gasc. 1969. Vertebrae and ribs of modern reptiles. *In* C. Gans, A. d. A. Bellairs, and T. S. Parsons, eds. Biology of the Reptilia Volume 1 Morphology A:201–310. Academic Press, London.
Ikejiri, T. 2010. Morphology of the neurocentral junction during postnatal growth of *Alligator* (Reptilia, Crocodylia). Doctoral thesis, Department of Geological Sciences, University of Michigan, Ann Arbor, 182 p. Unpublished.
———. 2012. Histology-based morphology of the neurocentral synchondrosis in *Alligator mississippiensis* (Archosauria, Crocodylia). The Anatomical Record 295:18–31.
Jaslow, C. R. 1989. Sexual dimorphism of cranial suture complexity in wild sheep (*Ovis orientalis*). Zoological Journal of the Linnean Society 95:273–284.
———. 1990. Mechanical properties of cranial sutures. Journal of Biomechanics 23:313–321.
Karperien, A. 1999–2013. FracLac for ImageJ. http://rsb.info.nih.gov/ij/plugins/fraclac/FLHelp/Introduction.htm.
Lehman, T. M., and H. N. Woodward. 2008. Modeling growth rates for sauropod dinosaurs. Paleobiology 34:264–281.
Long, C. A. 1985. Intricate sutures as fractal curves. Journal of Morphology 185:285–295.
Long, C. A., and J. E. Long. 1992. Fractal dimensions of cranial sutures and waveforms. Acta Anatomica 145:201–206.
Mandelbrot, B. 1967. How long is the coast of Britain? Statistical self-similarity and fractional dimension. Science 156:636–638.
Markey, M. J., R. P. Main, and C. R. Marshall. 2006. *In vivo* cranial suture function and suture morphology in the extant fish *Polypterus*: implications for inferring skull function in living and fossil fish. Journal of Experimental Biology 209:2085–2102.
Markey, M. J., and C. R. Marshall. 2007. Linking form and function of the fibrous joints in the skull: a new quantification scheme for cranial sutures using the extant fish *Polypterus endlicherii*. Journal of Morphology 268:89–102.
Masuda, Y., and T. Yohro. 1987. Are there any regularities in cranial sutures? Okaijimas Folia Anatomica Japonica 64:39–46.
Molnar, J. L., S. E. Pierce, and J. R. Hutchinson. 2014. An experimental and morphometric test of the relationship between vertebral morphology and joint stiffness in Nile crocodiles (*Crocodylus niloticus*). Journal of Experimental Biology 217:758–768.
Monteiro, L. R., and L. G. Lessa. 2000. Comparative analysis of cranial suture complexity in the genus *Caiman* (Crocodylia, Alligatoridae). Revista Brasileira de Biologia 60:689–694.
Morse, D. R., J. H. Lawton, M. M. Dodson, and M. H. Williamson. 1985. Fractal dimension of vegetation and the distribution of arthropod body lengths. Nature 314:731–733.
Moss, M. L. 1957. Experimental alteration of sutural area morphology. The Anatomical Record 127:569–589.

Nicolay, C. W., and M. J. Vaders. 2006. Cranial suture complexity in white-tailed deer (*Odocoileus virginianus*). Journal of Morphology 267:841–849.
Rafferty, K. L., and S. W. Herring. 1999. Craniofacial sutures: morphology, growth, and in vivo masticatory strains. Journal of Morphology 242:167–179.
Rasband, W. S. 1997–2014. ImageJ. US National Institutes of Health, Bethesda, Md.
Reese, A. M. 1915. The alligator and its allies. G. P. Putnam's Sons, New York.
Remes, J., F. Ortega, I. Fierro, U. Joger, R. Kosma, J. M. M. Ferrer, Project PALDES, Niger Project SNHM, O. A. Ide, and A. Maga. 2009. A new basal sauropod dinosaur from the Middle Jurassic of Niger and the early evolution of Sauropoda. PLoS ONE 4:1–13.
Rimblot-Baly, F., A. de Ricqles, and L. Zylberberg. 1995. Analyse paléohistologique d'une série de croissance partielle chez *Lapparentosaurus madagascariensis* (Jurassique Moyen): essai sur la dynamique de croissance d'un dinosaur sauropode. Annales de Palèontologie 81:49–86.
Romer, A. S. 1956. Osteology of the reptiles. University of Chicago Press.
Salisbury, S. W., and E. Frey. 2001. A biomechanical transformation model for the evolution of semi-spheroidal articulations between adjoining vertebral bodies in crocodilians. Pp. 85–134 i*n* G. C. Grigg, F. Seebacher, and C. E. Franklin, eds. Crocodilian biology and evolution. Surrey Beatty & Sons, Chipping Norton, U.K.
Sander, P. M. 2000. Longbone histology of the Tendaguru sauropods: implications for growth and biology. Paleobiology 26:466–488.
Slijper, E. J. 1946. Comparative biologic-anatomical investigations on the vertebral column and spinal musculature of mammals. Verhandelingen der Koninklijke Nederlandsche Akademie van Wetenschappen, Afdeling Natuurkunde, Tweede Sectie 2:1–128.
Taylor, M. P., and M. J. Wedel. 2013. Why sauropods had long necks; and why giraffes have short necks. PeerJ 1:e36.
Vital, J. M., J. L. Beguiristain, C. Algara, C. Villas, B. Lavignolle, N. Grenier, and J. Sénégas. 1989. The neurocentral vertebral cartilage: anatomy, physiology and physiopathology. Surgical and Radiologic Anatomy 11:323–328.
Washburn, S. L. 1947. The relation of the temporal muscle to the form of the skull. The Anatomical Record 99:239–248.
Wilson, J. A., and P. C. Sereno. 1998. Early evolution and higher-level phylogeny of sauropod dinosaurs. Society of Vertebrate Paleontology Memoir 5:1–68.

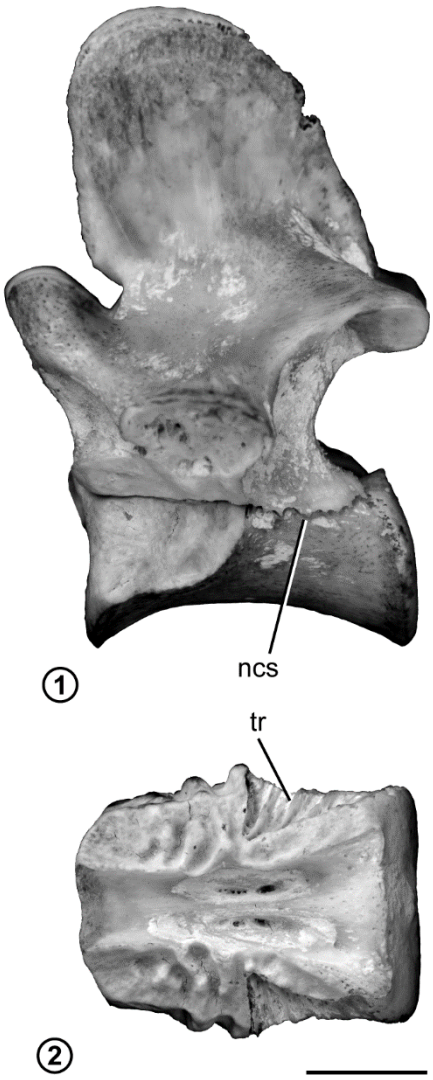

Fig. 4.1. First sacral vertebra of *Alligator mississippiensis* (UMMZ 238959) showing a patent neurocentral suture in **1**, left lateral view; **2**, dorsal view, with the neural arch removed to expose the surface of the neurocentral junction. Scale bar equals 0.5 cm. Abbreviations: **ncs**, neurocentral suture; **tr**, transverse ridge.

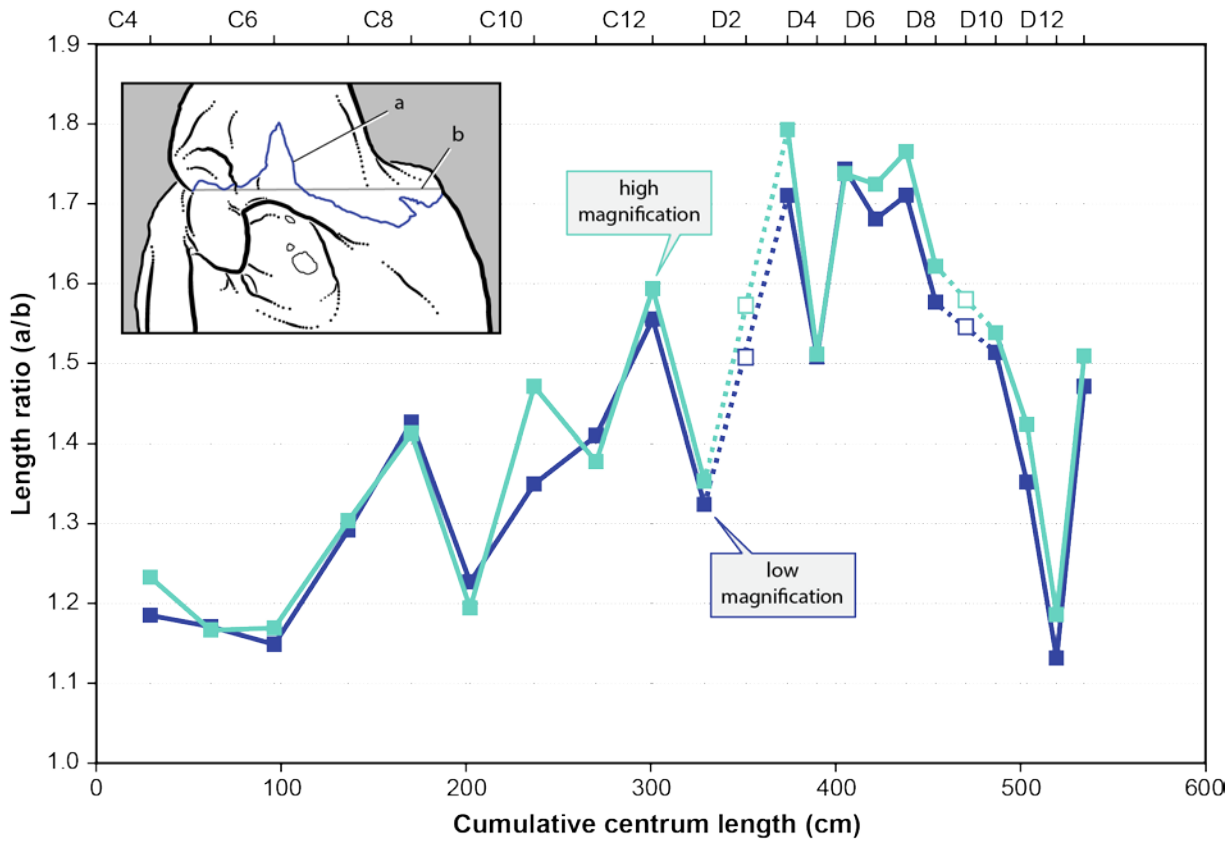

Fig. 4.2. Serial variation in neurocentral suture complexity in the presacral vertebrae of *Spinophorosaurus nigerensis* (GCP-CV-4229), calculated using the length ratio method. The x-axis depicts serial position in the vertebral column using cumulative centrum length; the boxes at top indicate vertebral position and are scaled by centrum length. Hollow squares and dashed lines indicate vertebrae for which the neurocentral junction was not preserved. Each suture was measured at two different image magnifications. Inset depicts the measurements used to calculate the length ratio (actual length of suture / straight-line length), shown on the suture of the third dorsal vertebra in left lateral view. Abbreviations: **a**, actual length of suture; **b**, straight-line length of suture; **C**, cervical; **D**, dorsal.

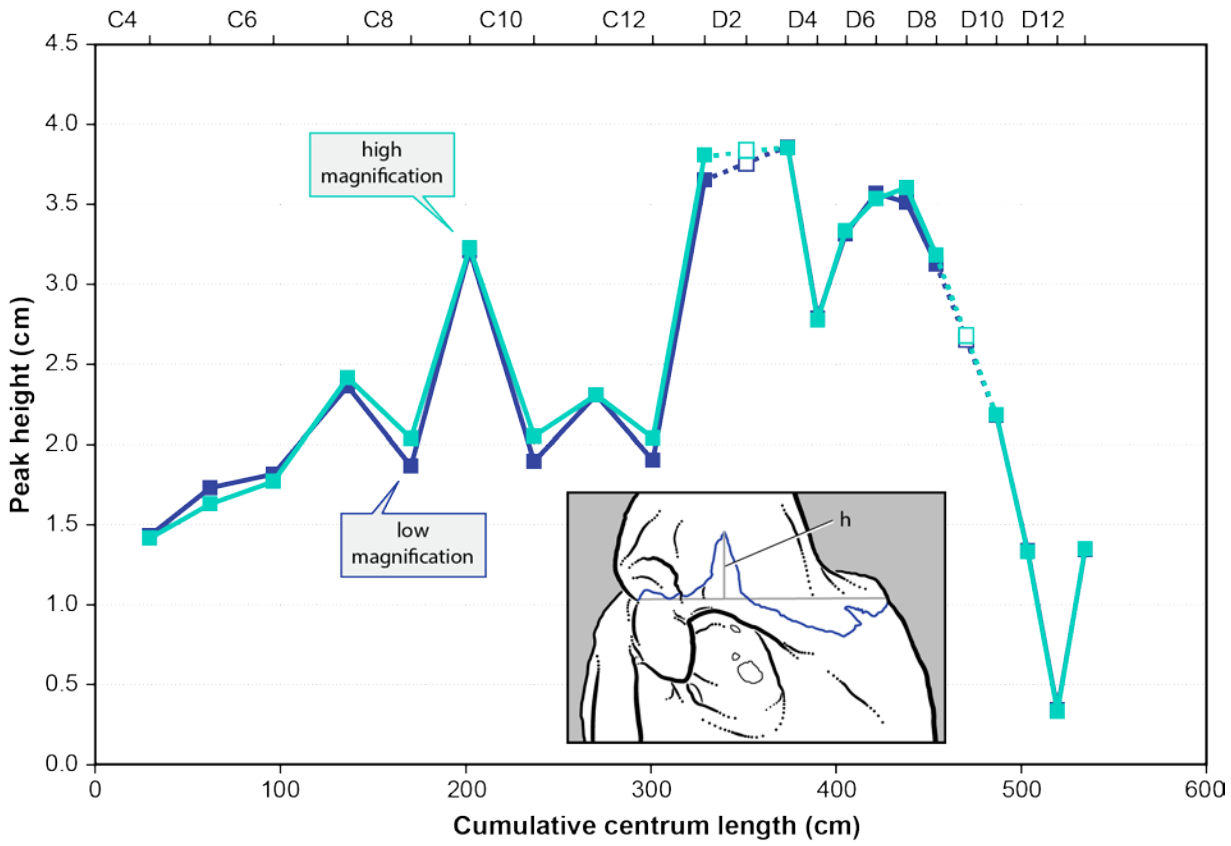

Fig. 4.3. Serial variation in the height of the highest peak in the presacral neurocentral sutures of *Spinophorosaurus nigerensis* (GCP-CV-4229), measured relative to a straight line connecting the end points of the sutural trace. The x-axis depicts serial position in the vertebral column using cumulative centrum length; the boxes at top indicate vertebral position and are scaled by centrum length. Hollow squares and dashed lines indicate vertebrae for which the neurocentral junction was not preserved. Each suture was measured at two different image magnifications. Inset depicts the measurement taken for peak height, shown on the suture of the third dorsal vertebra left lateral view. Abbreviations: **C**, cervical; **D**, dorsal; **h**, peak height

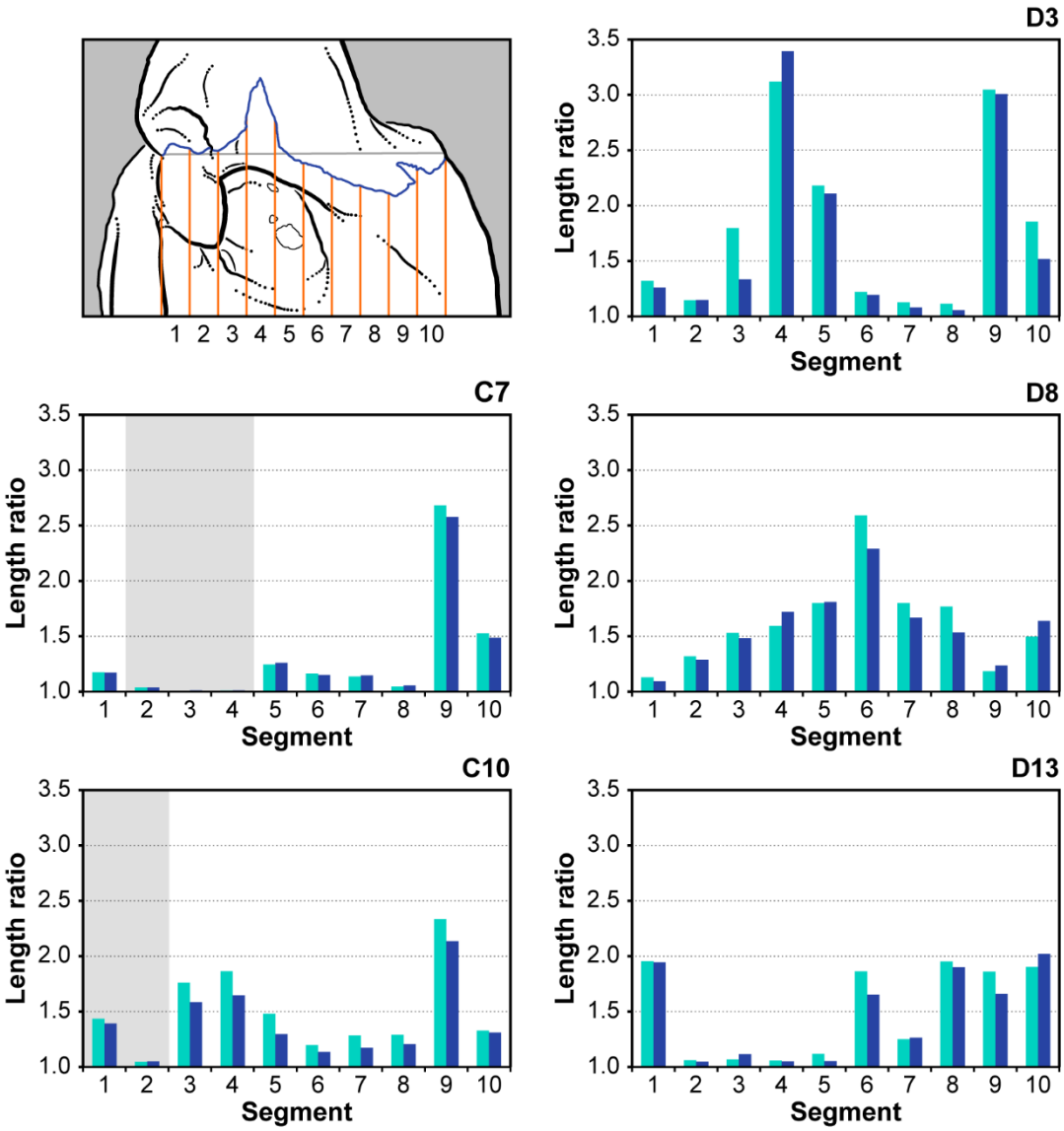

Fig. 4.4. Variation in complexity within individual neurocentral sutures of *Spinophorosaurus nigerensis* (GCP-CV-4229), calculated using the length ratio method. The length ratio was measured for each of ten equal segments along the straight-line length of the suture (upper left). Plots depict the length ratio of the ten segments for representative vertebrae from five anatomical regions: a middle cervical vertebra (**C7**); a posterior cervical vertebra (**C10**); an anterior dorsal vertebra (**D3**); a middle dorsal vertebra (**D8**); and a posterior dorsal vertebra (**D13**). Note that complexity is greatest near the ends of the centrum in cervical vertebrae and near the middle of the suture in dorsal vertebrae. Color scheme follows figure 4.2. Shaded segments represent regions that were obscured by the diapophysis, making the length ratio a minimum value. Abbreviations: **C**, cervical; **D**, dorsal.

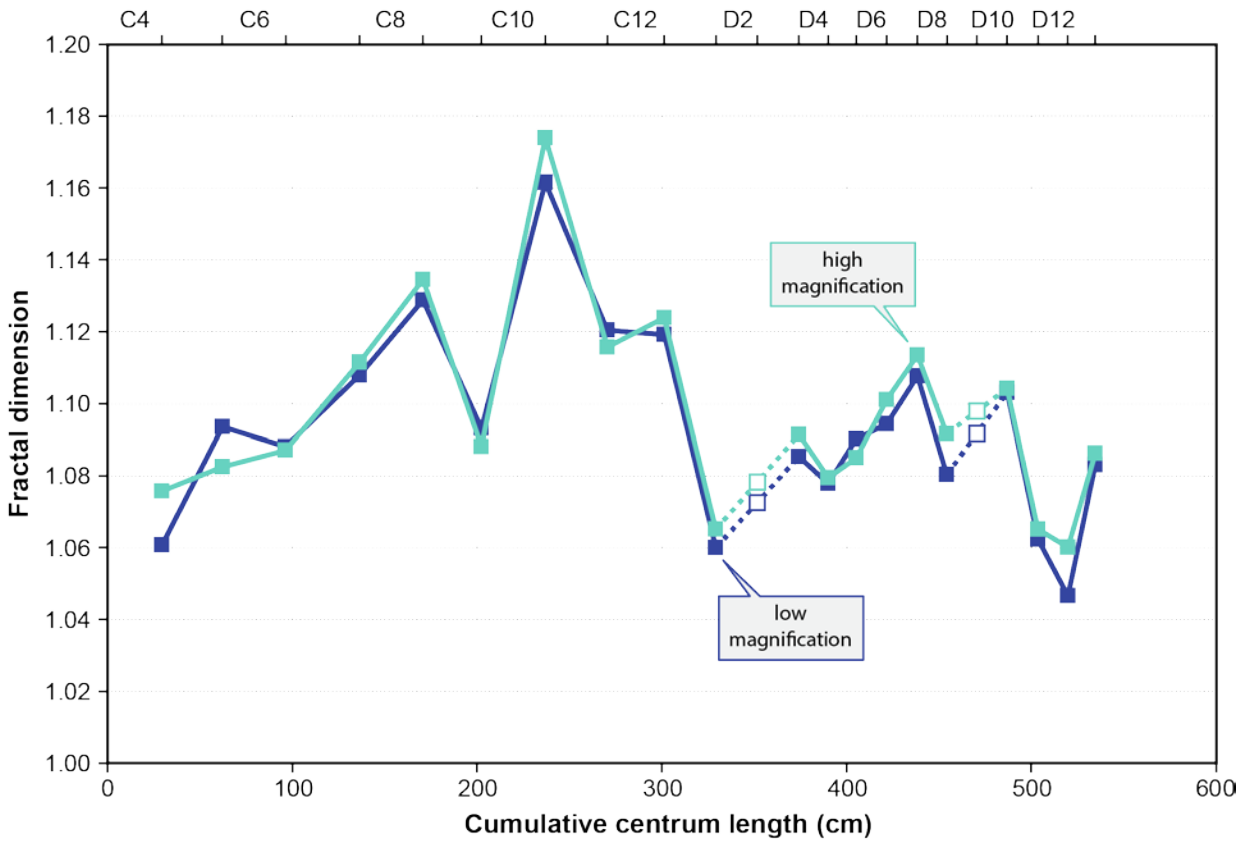

Fig. 4.5. Serial variation in neurocentral suture complexity in the presacral vertebrae of *Spinophorosaurus nigerensis* (GCP-CV-4229), calculated as the fractal dimension of the suture. The x-axis depicts serial position in the vertebral column using cumulative centrum length; the boxes at top indicate vertebral position and are scaled by centrum length. Hollow squares and dashed lines indicate vertebrae for which the neurocentral junction was not preserved. Abbreviations: **C**, cervical; **D**, dorsal.

Table 4.1. Neurocentral suture complexity in the presacral vertebrae of *Spinophorosaurus nigerensis* (holotype, GCP-CV-4229). Measurements were taken at two different magnifications to test for error due to variable image resolution. All lengths and heights are in cm; other values are unitless. Measurements were taken from the left side of the vertebra unless otherwise specified. Abbreviations: **C**, cervical; **D**, dorsal; **frac**, fractal; **mag**, magnification.

Position		Straight length	Actual length	Length ratio	Peak height
C4	zoom out	23.68	27.09	1.14	>=1.856
	zoom in	23.65	27.85	1.18	>=1.890
	zoom out	23.32	27.05	1.16	>=1.342
	zoom in	23.31	27.58	1.18	>=1.301
	zoom out	26.76	31.71	1.18	>=1.430
	zoom in	26.77	33.00	1.23	>=1.414
C5	zoom out	29.33	34.34	1.17	>=1.730
	zoom in	29.36	34.25	1.17	>=1.629
C6	zoom out	32.15	36.93	1.15	>=1.815
	zoom in	32.07	37.50	1.17	>=1.769
C7	zoom out	35.52	45.88	1.29	>=2.361
	zoom in	35.51	46.29	1.30	>=2.415
C8	zoom out	34.27	48.87	1.43	1.866
	zoom in	34.44	48.65	1.41	2.036
C9	zoom out	31.06	38.10	1.23	3.209
	zoom in	30.98	37.00	1.19	3.227
C10	zoom out	35.88	47.61	1.33	1.894
	zoom in	35.75	51.38	1.44	2.050
C11	zoom out	34.18	48.19	1.41	2.306
	zoom in	34.21	47.12	1.38	2.308
C12	zoom out	27.88	43.36	1.56	1.902
	zoom in	27.78	44.28	1.59	2.039
D1	zoom out	15.66	20.73	1.32	3.651
	zoom in	15.60	21.10	1.35	3.808
D2	-	-	-	-	-

Table 4.1. (cont.)

Position		Straight length	Actual length	Length ratio	Peak height
D3	zoom out	14.40	24.62	1.71	3.858
	zoom in	14.32	25.66	1.79	3.851
D4	zoom out	14.24	21.42	1.50	2.788
	zoom in	14.30	21.61	1.51	2.774
D5	zoom out	12.10	22.14	1.83	3.321
	zoom in	12.12	22.09	1.82	3.325
D5 (2nd)	zoom out	12.15	21.06	1.73	3.342
	zoom in	12.17	21.32	1.75	3.360
D5 (3rd)	zoom out	12.03	20.98	1.74	3.314
	zoom in	12.07	20.97	1.74	3.335
D6	zoom out	16.21	27.25	1.68	3.568
	zoom in	16.14	27.83	1.72	3.534
D7	zoom out	15.37	26.29	1.71	>=3.510
	zoom in	15.39	27.16	1.76	>=3.604
D8	zoom out	15.46	24.38	1.58	3.124
	zoom in	15.50	25.13	1.62	3.183
D9					
D10	zoom out	15.12	22.88	1.51	2.178
	zoom in	15.13	23.28	1.54	2.183
D11	zoom out	14.51	19.60	1.35	1.336
	zoom in	14.57	20.63	1.42	1.328
D12	zoom out	14.56	16.50	1.13	0.341
	zoom in	14.46	17.15	1.19	0.329
D13	zoom out	11.87	17.47	1.47	1.341
	zoom in	11.82	17.83	1.51	1.348

Table 4.1. (cont.)

Position	Frac dimension	Zoom	Mag	Notes
C4	1.0580	162%	1.89	Right side; peak obscured
	1.0737	300%	3.50	
	1.0767	400%	1.97	Left side; incomplete
	1.0900	600%	2.95	
	1.0607	-	1.89	Composite
	1.0758	-	3.50	
C5	1.0936	300%	1.35	Peak obscured
	1.0825	600%	2.70	
C6	1.0881	300%	1.25	Peak obscured
	1.0871	600%	2.50	
C7	1.1079	300%	1.41	Peak obscured
	1.1114	500%	2.35	
C8	1.1288	162%	0.81	
	1.1345	300%	1.50	
C9	1.0931	200%	1.08	Offset at fracture
	1.0880	400%	2.15	
C10	1.1615	50%	1.15	Peak obscured
	1.1740	200%	4.60	
C11	1.1204	300%	1.60	
	1.1157	450%	2.40	
C12	1.1192	300%	1.25	Posterior spike shorter and stouter
	1.1239	600%	2.50	
D1	1.0600	150%	3.10	Posterior end broken off
	1.0652	300%	6.20	
D2	-	-	-	Centrum not preserved

Table 4.1. (cont.)

Position	Frac dimension	Zoom	Mag	Notes
D3	1.0853	162%	3.48	
	1.0914	300%	6.45	
D4	1.0779	200%	3.98	D4-5 is first joint with hyposphene-hypantrum
	1.0794	400%	7.95	
D5	1.1006	162%	3.21	Triplicate measurements to assess error
	1.1028	300%	5.95	Last dorsal with parapophysis partly on centrum
D5 (2nd)	1.0890	162%	3.21	Anterior end broken
	1.0916	300%	5.95	
D5 (3rd)	1.0902	162%	3.21	
	1.0850	300%	5.95	
D6	1.0944	162%	3.40	Posterior spike directed ventrally
	1.1010	300%	6.30	Followed ventral margin in anterior 2/3rds
D7	1.1077	125%	2.96	Posterior spike directed ventrally
	1.1135	300%	7.10	Two peaks; measured height of taller one
D8	1.0803	150%	3.58	Posterior spike absent
	1.0917	300%	7.15	
D9				Centrum not preserved
D10	1.1031	66.67%	3.47	
	1.1042	150%	7.80	
D11	1.0624	66.67%	2.42	Minor damage to posterior end
	1.0651	150%	5.45	Margins of suture less clearly visible
D12	1.0466	100%	3.75	Mid-length peak absent; measured highest point
	1.0601	200%	7.50	Greater uncertainty in anterior region
D13	1.0831	300%	3.27	Mid-length peak absent; measured highest point
	1.0863	500%	5.45	Greater uncertainty in anterior region

Table 4.2. Variation in complexity within individual neurocentral sutures of *Spinophorosaurus nigerensis* (holotype, GCP-CV-4229). Complexity was calculated using the length-ratio method. Only the composite measurement was used for C4, and only one measurement was used for D5. Yellow indicates regions that are partially or fully obstructed from view in the photographs. Abbreviations: **C**, cervical; **D**, dorsal.

			Complexity by segment									
Position	Zoom	Segment length (cm)	1	2	3	4	5	6	7	8	9	10
C4	in	2.68	1.88	1.14	1.11	1.04	1.12	1.18	1.04	1.03	1.03	1.75
	out	2.68	1.81	1.12	1.07	1.03	1.06	1.08	1.04	1.03	1.02	1.59
C5	in	2.94	1.49	1.11	1.01	1.01	1.03	1.11	1.02	1.07	1.02	1.80
	out	2.93	1.52	1.13	1.01	1.01	1.03	1.08	1.02	1.09	1.02	1.78
C6	in	3.21	1.33	1.11	1.01	1.04	1.05	1.01	1.03	1.04	1.09	1.98
	out	3.22	1.27	1.10	1.01	1.05	1.05	1.01	1.04	1.04	1.12	1.81
C7	in	3.55	1.18	1.04	1.01	1.01	1.25	1.16	1.14	1.05	2.68	1.53
	out	3.55	1.17	1.04	1.01	1.01	1.26	1.15	1.15	1.06	2.58	1.49
C8	in	3.45	1.13	1.05	1.00	1.47	1.14	1.12	1.12	1.46	3.35	1.29
	out	3.43	1.19	1.02	1.00	1.43	1.23	1.19	1.14	1.23	3.33	1.51
C9	in	3.10	1.21	1.08	1.01	1.19	1.19	1.08	1.03	1.08	1.03	2.03
	out	3.11	1.18	1.09	1.01	1.34	1.25	1.11	1.02	1.06	1.06	2.16
C10	in	3.42	1.44	1.05	1.76	1.86	1.48	1.20	1.28	1.29	2.33	1.33
	out	3.42	1.39	1.05	1.59	1.65	1.30	1.14	1.17	1.21	2.14	1.31
C11	in	3.42	1.42	1.75	1.69	1.53	1.10	1.12	1.06	1.03	1.38	1.68
	out	3.42	1.46	1.90	1.82	1.60	1.10	1.12	1.06	1.03	1.40	1.63
C12	in	2.78	1.36	2.72	2.03	1.45	1.12	1.10	1.09	1.08	1.10	2.88
	out	2.79	1.34	2.49	1.90	1.46	1.14	1.10	1.09	1.10	1.10	2.83
D1	in	1.56	1.12	1.15	2.02	2.24	1.54	1.10	1.08	1.07	1.14	1.07
	out	1.57	1.11	1.18	1.85	2.22	1.48	1.08	1.09	1.05	1.09	1.08
D2	-	-	-	-	-	-	-	-	-	-	-	-

Table 4.2. (cont.)

			Complexity by segment									
Position	Zoom	Segment length (cm)	1	2	3	4	5	6	7	8	9	10
D3	in	1.43	1.32	1.15	1.80	3.12	2.18	1.22	1.13	1.11	3.05	1.86
	out	1.44	1.26	1.15	1.33	3.39	2.11	1.19	1.08	1.06	3.01	1.52
D4	in	1.43	1.65	1.08	1.36	1.74	1.54	1.58	1.24	1.30	1.15	2.48
	out	1.42	1.61	1.08	1.39	1.69	1.60	1.57	1.24	1.30	1.15	2.40
D5	in	1.21	1.54	2.27	2.56	1.81	1.91	1.71	1.20	1.07	1.17	2.13
	out	1.20	1.61	2.32	2.51	1.79	1.73	1.69	1.14	1.25	1.14	2.25
D6	in	1.61	1.03	1.43	2.37	2.20	1.97	1.95	1.74	1.66	1.57	1.31
	out	1.62	1.05	1.39	2.31	2.13	1.94	1.95	1.79	1.56	1.42	1.26
D7	in	1.54	1.52	1.61	2.28	2.63	2.37	2.29	1.29	1.35	1.16	1.15
	out	1.54	1.52	1.52	2.27	2.54	2.21	2.35	1.14	1.32	1.12	1.12
D8	in	1.55	1.13	1.32	1.53	1.59	1.80	2.59	1.80	1.77	1.18	1.50
	out	1.55	1.09	1.29	1.48	1.72	1.81	2.29	1.67	1.53	1.24	1.64
D9	-	-	-	-	-	-	-	-	-	-	-	-
D10	in	1.51	1.30	1.10	1.82	2.10	2.01	2.07	1.34	1.37	1.13	1.16
	out	1.51	1.21	1.11	1.84	2.03	1.96	2.05	1.32	1.38	1.11	1.13
D11	in	1.45	1.24	1.05	1.36	1.56	1.98	1.86	1.69	1.17	1.19	1.11
	out	1.45	1.23	1.04	1.19	1.46	1.84	1.81	1.59	1.16	1.13	1.05
D12	in	1.45	1.07	1.26	1.04	1.01	1.12	1.18	1.36	1.29	1.28	1.25
	out	1.46	1.07	1.28	1.03	1.04	1.13	1.12	1.28	1.14	1.13	1.12
D13	in	1.18	1.96	1.06	1.07	1.06	1.12	1.86	1.25	1.95	1.86	1.90
	out	1.19	1.94	1.05	1.12	1.05	1.05	1.65	1.26	1.90	1.66	2.02

CHAPTER 5

CONCLUSIONS

This work integrated fossil evidence, data from an extant analog taxon, and experiments comparing real and theoretical morphology to test hypotheses about vertebral joint function in sauropod dinosaurs. The results suggest that vertebral joint morphology plays an important role in stabilizing the vertebral column. Morphological specializations of the sauropod intercentral and neurocentral joints would have conferred stability without compromising mobility, mechanical advantage, or the potential for sustained growth. This may have facilitated the acquisition of the long, heavy necks and tails characteristic of the clade.

Chapter 2 rejected the prevalent hypothesis that the presence of concavo-convex joints between vertebral centra provides greater flexibility than does the ancestral planar condition. The most strongly convex articular surfaces in *Alligator* occur in the less-flexible presacral column, and planar articular surfaces occur in the highly flexible distal tail. The weak negative correlation between convexity and flexibility suggests that strongly convex joints do not inherently limit flexibility. The regions of greatest convexity are those that should experience the greatest shear stress during terrestrial locomotion. This supports the hypothesis that concavo-convex joints serve to resist the translation of one centrum relative to another. It is likely that the

opisthocoelous cervical and procoelous caudal vertebrae of sauropods provided extra stability to the cantilevered neck and tail without sacrificing mobility.

Chapter 3 tested several hypotheses for the functional advantage of vertebral centra with the concavity facing towards the body (the sauropod condition) over the opposite polarity. Most hypotheses examined were found to be implausible or did not match the observed pattern in sauropods. Photoelastic strain visualization revealed that the two joint polarities have comparable stress distributions when loaded as cantilevers. Joint stability experiments demonstrated that sauropod-type joints are significantly more resistant to failure by rotation than the opposite polarity. This difference is most pronounced with greater mobility, more mechanically advantageous ligament and muscle insertion sites, and greater distal loading. The strongly conserved pattern of cervical opisthocoely and caudal procoely in sauropods is best explained as providing greater passive stabilization of the vertebral column than its opposite with fewer functional sacrifices. The need to maintain rotational stability provides a compelling explanation for the observed intervertebral joint polarity in many vertebrate groups. Other cases, such as the opisthocoelous caudal vertebrae of the sauropod *Opisthocoelicaudia*, remain enigmatic, but this study provides a framework for future investigations of those taxa. Rotational stability also explains the consistent polarity of the tetrapod shoulder and hip joints; the tetrapod polarity should be more stable than its opposite in terrestrial quadrupeds.

Chapter 4 found support for the hypothesis that complex, interdigitated neurocentral sutures strengthen the unfused neurocentral junction in archosaurs, providing stability throughout a protracted growth period. The serial variation in sutural complexity in *Spinophorosaurus*, measured with the length-ratio method, is consistent with the expected distribution of stress on the vertebral column. Complexity increases proximally along the neck, as neck mass would in

life, and decreases posteriorly in the trunk with the decreasing size of the ribs, which support the weight of the viscera. Large-scale sutural structures are oriented to resist anteroposterior translation in the neck and lateral rotation in the trunk. Sutural complexity in *Spinophorosaurus* appears to result primarily from large-scale morphological structures rather than the fine-scale fractal elaboration of interdigitations, unlike the condition in cranial sutures.

The results of this dissertation indicate that the morphology of intervertebral joints and neurocentral sutures in sauropods provided a greater surface area to resist joint failure under extreme loading. Patterns of serial variation in joint surface convexity and sutural complexity are in good agreement, indicating a common loading regime influencing both morphological parameters. Sutural complexity increases proximally along the neck, reaching a maximum among the anterior dorsal vertebrae, and is lower in the posterior dorsal region. Unpublished measurements of condylar convexity in sauropod vertebrae reveal that convexity generally also increases proximally along the neck, and is almost always at a maximum among the anterior dorsal vertebrae. The posterior dorsal vertebrae exhibit lower convexity, being amphiplatyan in many taxa. This stress regime appears to be widespread among sauropods. Whether similar stress distributions occur in other taxa remains to be assessed, and in some cases will require indicators of stress other than convexity (e.g., basal sauropodomorphs, which have only amphiplatyan vertebrae).

Given the relationship between the forces acting on vertebrae and the morphology of the centrum articular surfaces and neurocentral sutures, it may be possible to use vertebral measurements as predictors of the forces acting on the vertebral column. To date, no quantitative relationship between vertebral measurements and stress magnitude has been developed. To do so will require in situ stress measurements in living animals or cadaveric specimens, which would

also make it possible to determine how strongly correlated the variables are. In situ measurements would be especially useful in the problematic dorsal region, in which the relative contributions to loading of neck weight, the weight of the ribcage and viscera, the pull of the limbs, and bending during locomotion must all be accounted for.

One of the ultimate objectives of stress reconstruction in extinct taxa is to evaluate hypotheses of organismal function and behavior. For instance, there is persistent uncertainty regarding the habitual neck posture and browsing height of some sauropods. A high-browsing sauropod that typically held its neck at a high angle to the ground would experience a different loading regime than a low-browsing sauropod that maintained a horizontal or subhorizontal neck posture. If predictive models can be developed for how vertebral morphology should vary with different loading regimes, then vertebral measurements will provide a useful test of this sort of functional hypothesis.

The present research opens up several additional avenues of future inquiry. First, if joint convexity and sutural interdigitation increase with stress magnitude, we predict that both parameters will be positively correlated with body size and, for cervical and anterior dorsal vertebrae, neck length. Similarly, both parameters are expected to increase ontogenetically. Unpublished measurements of joint convexity in sauropods are consistent with these expectations; broader sampling of neurocentral sutures in sauropods and of both parameters in non-sauropod taxa will afford further evidence.

Second, some sauropod vertebrae observed exhibit deviations from the idealized morphology presented in the studies above. Most notably, many sauropod vertebrae exhibit a broad, flat attachment for the annulus fibrosus surrounding the convex region of the condyle. Some condyles are also dorsoventrally asymmetrical, with the anteriormost point of the condyle

nearer to the dorsal margin than the ventral margin. Future research aims to assess the functional significance of such structures. Are they alike in the magnitude of stress that can be resisted? How does the position of the center of rotation vary from one to another? Is the phylogenetic distribution of these morphologies a product of differences in body plan or behavior?

Third, as noted in Chapter 3, some taxa, living and extinct, exhibit patterns of concavo-convex joint polarity that our results suggest are disadvantageous. Examples include the opisthocoelous caudal vertebrae of the titanosaur sauropod *Opisthocoelicaudia* and the procoelous cervical vertebrae of crocodylians, squamates, and pterosaurs. The hypothesis that these examples of seemingly suboptimal polarity are the product of a reversal in loading direction is an intriguing possibility that requires experimental assessment. Direct measurements of loads in living animals during behaviors such as swimming and flight may offer the necessary insight. Alternatively, digital modeling of vertebral series with different polarities that can be loaded in a variety of ways could be used. If this hypothesis is not supported, there must be some other factor, as yet unidentified, that can control joint polarity in addition to rotational stability.

Fourth, the patterns and relationships detailed in this dissertation are not unique to vertebrae. Concavo-convex joints occur in the appendicular skeleton, jaw joint, and atlanto-occipital joint of vertebrates. Future research can investigate whether joint convexity is similarly linked to the loading on joints; what effects the absence of structures such as zygapophyses, neural spines, and ribs have on joint mechanics; and how the mechanics of concavo-convex joints translate to other joint types, such as the planar-convex structure of the knee joint. Some of these joints, such as the jaw joint and the atlanto-occipital joint, also exhibit the opposite polarity from that predicted by the need for rotational stability, as discussed above. Interdigitated sutures occur between cranial bones and at epiphyses in mammalian limbs. Our results are generally

consistent with studies of cranial sutures, but differences in large-scale morphology and the fractal dimension remain to be explained. Epiphyseal sutures offer another test for the hypothesis that sutural complexity is linked to stress magnitude and timing of fusion. A sample of multiple taxa with different body sizes across ontogeny would indicate whether this is the case.

Finally, careful documentation of patterns of serial variation in well-preserved specimens of diverse taxa offers a potential tool for identifying the serial position of isolated fossil vertebrae. For instance, a centrum with a strongly convex anterior condyle and a highly interdigitated suture with a mid-length peak would be best reconstructed as a posterior cervical or anterior dorsal vertebra based on the present results. In order for these interpretations to be precise and reliable, a large sample size representing all major sauropod lineages is needed. As more specimens are studied, and as more extensive datasets of different aspects of vertebral morphology are assembled, serial identifications can be further refined and taxonomic differences accounted for.

This dissertation and similar studies highlight the importance of an empirical approach to biomechanical questions. The synthesis of fossil and modern data with experimental modeling yields functional insights that cannot be obtained from any one method in isolation. In this way, a new perspective can be gained on both the study taxon and vertebrates more generally. The study of extinct animals such as sauropod dinosaurs thereby illuminates even ourselves.